HAL
archives-ouvertes.fr

Sharp algebraic and total a posteriori error bounds for h and p finite elements via a multilevel approach. Recovering mass balance in any situation

Jan Papež, Ulrich Rüde, Martin Vohralík, Barbara Wohlmuth

▶ **To cite this version:**

Jan Papež, Ulrich Rüde, Martin Vohralík, Barbara Wohlmuth. Sharp algebraic and total a posteriori error bounds for h and p finite elements via a multilevel approach. Recovering mass balance in any situation. Computer Methods in Applied Mechanics and Engineering, Elsevier, 2020, 371, pp.113243. hal-01662944v5

HAL Id: hal-01662944
https://hal.inria.fr/hal-01662944v5

Submitted on 1 Sep 2020

HAL is a multi-disciplinary open access archive for the deposit and dissemination of scientific research documents, whether they are published or not. The documents may come from teaching and research institutions in France or abroad, or from public or private research centers.

L'archive ouverte pluridisciplinaire **HAL**, est destinée au dépôt et à la diffusion de documents scientifiques de niveau recherche, publiés ou non, émanant des établissements d'enseignement et de recherche français ou étrangers, des laboratoires publics ou privés.

Sharp algebraic and total a posteriori error bounds for h and p finite elements via a multilevel approach. *Recovering mass balance in any situation*[*]

Jan Papež[†§] Ulrich Rüde[‡] Martin Vohralík[†§] Barbara Wohlmuth[¶]

September 1, 2020

Abstract

We present novel $\boldsymbol{H}(\mathrm{div})$ and H^1 liftings of given piecewise polynomials over a hierarchy of simplicial meshes, based on a global solve on the coarsest mesh and on local solves on patches of mesh elements around vertices on subsequent mesh levels. This in particular allows to lift a given algebraic residual. In connection with approaches lifting the total residual, we show how to obtain guaranteed, fully computable, and constant-free upper and lower a posteriori bounds on the algebraic, total, and discretization errors; here we consider the model Poisson equation discretized by the conforming finite element method of arbitrary order and including an arbitrary iterative solver. We next formulate safe stopping criteria ensuring that the algebraic error does not dominate the total error. We also prove efficiency, i.e., equivalence of our upper total and algebraic estimates with the total and algebraic errors, respectively, up to a generic constant; this constant is polynomial-degree-independent for the total error. Numerical experiments illustrate sharp control of all error components and accurate prediction of their spatial distribution in several test problems, including cases where some classical estimators fail. The $\boldsymbol{H}(\mathrm{div})$-liftings at the same time allow to recover mass balance for any problem, any numerical discretization, and any situation such as inexact solution of (nonlinear) algebraic systems or algorithm failure, which we believe is of independent interest. We demonstrate this mass balance recovery in a simulation of immiscible incompressible two-phase flow in porous media.

Key words: finite element method, finite volume method, iterative algebraic solver, discretization error, algebraic error, a posteriori error estimate, stopping criterion, p-robustness, hierarchical splitting, mass balance, porous media flow

1 Introduction

Numerical discretizations of partial differential equations typically give rise to large sparse systems of linear algebraic equations. Their efficient solution is then often achieved by iterative solvers. Many are based on a hierarchy of nested meshes such as, e.g., multilevel and multigrid methods, see [22, 50] for optimal convergence results on uniformly refined meshes, [88, 51, 89, 29] for graded meshes, and [47, 90, 48, 64] for massively-parallel large-scale simulations on modern architectures. In many cases, however, other techniques like preconditioned Krylov solvers remain a vital and widely used alternative, see, e.g., [57, 65] and the references therein.

Numerical schemes and algebraic solvers are often treated separately, both in theoretical analysis and in practical algorithms, but numerous intriguing questions signal that they actually rather need to be treated together. Two important questions are namely: what is the *total error* in a *given step* of the iterative solver

[*]This project has received funding from the European Research Council (ERC) under the European Union's Horizon 2020 research and innovation program (grant agreement No 647134 GATIPOR) and by the German Research Foundation (DFG) through WO 671/11-1 and WO 671/15-1 (within the Priority Programme SPP 1748, "Reliable Simulation Techniques in Solid Mechanics. Development of Non-standard Discretisation Methods, Mechanical and Mathematical Analysis"). It was also supported by the ERC-CZ project LL1202 financed by the MŠMT of the Czech Republic.

[†]Inria Paris, 2 rue Simone Iff, 75589 Paris, France (jan@papez.org, martin.vohralik@inria.fr).

[§]Université Paris-Est, CERMICS (ENPC), 77455 Marne-la-Vallée, France.

[‡]Informatik 10, System Simulation, Friedrich-Alexander-Universität Erlangen-Nürnberg, 91058 Erlangen, Germany (ulrich.ruede@fau.de).

[¶]Fakultät für Mathematik, Lehrstuhl für Numerische Mathematik, Boltzmannstrasse 3, 85748 Garching bei München, Germany (wohlmuth@ma.tum.de).

and how to realize adaptive *stopping criteria* which *balance* algebraic and discretization error *components*? Pioneering answers were proposed by Brandt [21], Bank and Sherman [12], Bai and Brandt [11], Bank and Smith [13], Rüde [75, 76, 77], or Oswald [66], or more recently by, e.g., Janssen and Kanschat [52]. Rigorous upper a posteriori error estimates of the total error valid at each step of the geometric multigrid were designed in the work of Becker *et al.* [15]. The estimates are then decomposed into parts that are identified with the algebraic and discretization error components, though not necessarily their upper or lower bounds. Additionally, adaptive stopping criteria are proposed and numerical experiments show that numerous iterations may be saved with respect to classical stopping criteria. These estimates involve some generic constants that are not at disposal in practical computations. Later, the development of a posteriori error estimates including algebraic error continued, e.g., in Arioli *et al.* [8, 7], Meidner *et al.* [61], Jiránek *et al.* [53], Ern and Vohralík [43], or Papež *et al.* [69], see also the references therein. Typically, some limitations still appear: the estimates in [53, 43, 69] apply to an arbitrary iterative solver but additional iteration steps are required; the estimates in [8, 61, 7] provide a total bound which is not fully computable and/or the results only apply to one specific solver.

The present contribution develops a unified approach which seems rather flexible. Main results of our analysis for a model Poisson problem can be summarized as follows:

1. We provide *constant-free* fully computable *upper* and *lower* bounds for all the *algebraic*, *discretization*, and *total* errors, independent of the choice of the iterative solver and including arbitrary higher-order (conforming) finite elements. We also prove that our total upper bound is *efficient*, i.e., equivalent to the total error up to a generic constant that is, importantly, independent of the approximation polynomial degree. Moreover, we also prove efficiency of the algebraic upper bound and refer to a proof of efficiency of the algebraic lower bound.

2. The evaluation of the estimates is based on a *global coarse solve* and independent *local solves* associated with vertex patches, based on a hierarchy of nested meshes. Thus, it is obtained on the current iteration for a price that is linear in terms of the number of vertices and corresponds to one V-cycle multigrid step with a block-Jacobi smoother.

3. *Safe stopping criteria* for iterative solvers are proposed. They ensure that the algebraic system will neither be over-solved, nor under-solved.

Property 1 states that all total, algebraic, and discretization errors are fully certified (supposing that the coarse solve is exact and that the computer evaluation of the data oscillation term for total and discretization errors is possible). We derive the upper bounds on the algebraic and total errors in the spirit of Prager and Synge [73], relying on the a posteriori methodology of *equilibrated flux* reconstructions that can be seen as $\boldsymbol{H}(\mathrm{div},\Omega)$-liftings of the algebraic and total residuals. These have been proposed and studied for finite elements with an exact algebraic solve in Destuynder and Métivet [38], Luce and Wohlmuth [59], Braess and Schöberl [19], Nicaise *et al.* [63], Agouzal *et al.* [1], Ainsworth [3], Vohralík [85], and Ern and Vohralík [43, 44], or Kopteva [55], see also the references therein. Relying on the recent results of Braess *et al.* [18] and Ern and Vohralík [45], *p-robust* efficiency is shown which means that the derived total upper bound will be of the same quality for any order finite elements. Our lower bounds on the algebraic and total errors are then obtained via $H^1_0(\Omega)$-liftings of the algebraic and total residuals.

Property 2 improves the approaches of [53, Sec. 7.2] and [43, 69], where an a priori unknown number of additional steps of the iterative algebraic solver needs to be performed so as to evaluate the estimates. The construction of the estimates presented here rather involves a coarse solve followed by a sweep through all the vertices on all levels, where small *mixed finite element problems* on patches of elements are solved to obtain the $\boldsymbol{H}(\mathrm{div},\Omega)$-*liftings* and small *conforming finite element problems* on patches of elements are solved to obtain the $H^1_0(\Omega)$-*liftings*. Our hierarchical decomposition of the algebraic error shares some ideas with those of stable splittings [13, 67, 66, 76, 77, 49] for multigrid and multilevel methods. The key differences of our approach, though, seem to be: a) our estimates give guaranteed and computable bounds; b) no generic multiplicative constant appears; c) no regularity beyond $H^1(\Omega)$ of the weak solution is requested; d) the hierarchy of meshes needs to be neither structured nor uniformly refined; e) any polynomial degree $p \geq 1$ is allowed; f) the derived estimates hold true for any iterative solver. In contrast to the splitting techniques, however, our approach is typically more expensive. In this direction, we note that any solution of local patch problems (local matrices assembly and inversion) can be avoided by an explicit variant that we describe in Section 8.3 below and that we present in detail in the contribution [70].

Finally, the salient consequence of Property 3 is that it typically brings an important economy in terms of the number of algebraic solver iterations, while being sure that we do not stop too early.

Two important tools that are at the heart of the above results seem of independent interest:

(a) $\boldsymbol{H}(\mathrm{div},\Omega)$-*lifting of a given piecewise polynomial.* Given a piecewise p-degree polynomial r_h, the algebraic residual lifting $\boldsymbol{\sigma}_{h,\mathrm{alg}}$ of Concept 4.1 is a vector-valued piecewise polynomial belonging to $\boldsymbol{H}(\mathrm{div},\Omega)$ such that its divergence equals to r_h, $\nabla{\cdot}\boldsymbol{\sigma}_{h,\mathrm{alg}} = r_h$, and such that the norm of $\boldsymbol{\sigma}_{h,\mathrm{alg}}$ is locally minimized.

(b) *Mass-conservative total flux reconstruction in* $\boldsymbol{H}(\mathrm{div},\Omega)$. In Concept 4.2, we construct a total flux $\boldsymbol{\sigma}_{h,\mathrm{tot}}$ that lies in $\boldsymbol{H}(\mathrm{div},\Omega)$ and satisfies the target divergence, so that it allows to recover mass balance in any situation.

Tool (a) is related to the question of so-called finite element potentials, see, e.g., Alonso Rodríguez and Valli [5] and the references therein. Here, we additionally use local minimization to produce liftings helpful in a posteriori analysis. The applications include a posteriori estimates for challenging systems of time-dependent, nonlinear, and degenerate PDEs with *inexact solvers*: tool (a) can be, e.g., immediately used in the porous media applications in [86, equations (4.7) and (5.8)], [25, equation (A.9)], and [39, equation (4.14c) and Remark 4.3].

Tool (b) is probably of even more important independent interest: it allows to recover local mass balance for *any problem*, *any numerical discretization*, and *any situation* such as inexact solution of (nonlinear) algebraic systems or algorithm failure. It is related to postprocessing techniques designed to recover local mass conservation, important, e.g., in porous media simulations, see for example the discussion in Dawson *et al.* [37] and the references therein.

Local mass balance for numerical methods not locally conservative by construction has been traditionally achieved by a global (exact) solve as in Chippada *et al.* [31], Sun and Wheeler [80], or Cockburn *et al.* [33] (in the middle reference, an iterative procedure with local solves is also designed). From a posteriori error analysis, in turn, it has been understood that for a numerical solution with no algebraic error (when the associated algebraic system is solved exactly, or, more precisely, when orthogonality with respect to the lowest-order test functions is satisfied), a *local solve* is sufficient, see [38, 59, 19, 63, 3, 85, 43] and the references therein, as well as [44] for a unified framework covering *all standard numerical methods*. Local mass balance has also been achieved in the past on *each step* of carefully designed *algebraic solvers* for locally conservative methods, in particular in Ewing and Wang [46] for mixed finite elements and a multigrid solver, in Keilegavlen and Nordbotten [54] for (cell- or vertex-centered) finite volume methods and a multilevel preconditioner, and in Ali Hassan *et al.* [4] for mixed finite elements and a domain decomposition solver. Tool (b) is a generalization of these techniques and allows to achieve local mass balance for any numerical method (locally conservative or not) for the price of one multigrid step in any situation, namely when the lowest-order orthogonality is not satisfied because of an inexact solve.

The rest of this contribution is organized as follows. To motivate our developments, we start in Sec. 2 with two examples where some commonly used estimators on the algebraic error lead to significant overestimation/underestimation of the algebraic error. In Sec. 3, we introduce the hierarchy of meshes and piecewise polynomial spaces that we will rely on. The $\boldsymbol{H}(\mathrm{div},\Omega)$- and $H^1_0(\Omega)$-liftings are then presented in Secs. 4 and 5, respectively. These developments are presented in an abstract setting. In Secs. 6 and 7, we restrict our attention to the model Poisson equation discretized by conforming finite elements, where we first describe the problem and then present our main results, including short (instructive) proofs. We discuss in Sec. 8 efficient implementation of our reconstructions and estimates, as well as possible reductions of their computational cost. Numerical performance of the a posteriori estimates for the Poisson equation is then examined in Sec. 9 for the V- and full geometric multigrid methods as well as for the preconditioned conjugate gradient method. A concluding discussion is presented in Sec. 10. Appendices A and B present respectively the proofs of efficiencies of our upper algebraic and total estimates. Finally, Appendix C presents the application of our mass-conservative total flux reconstruction in $\boldsymbol{H}(\mathrm{div},\Omega)$ to a challenging two-phase porous media flow problem with a finite volume fully implict/iterative coupling discretization. Applications to other problems, namely when deriving guaranteed upper bounds on the total error in presence of inexact solvers, have already been considered in [34, 35] to steady and unsteady variational inequalities, in [26] to eigenvalue problems, in [60] to goal-oriented error estimates, and in [87, 2] to degenerate multiphase (multicompositional) flows.

2 Warning examples: overestimation/underestimation of the algebraic error by commonly used estimators

The purpose of this introductory section is to present two examples in which some commonly used estimators of the algebraic error fail importantly. In contrast, the rigorously justified upper and lower bounds on the algebraic error developed in this manuscript behave without flaw.

2.1 Algebraic error estimator based on the fine grid only for a model problem

In the first example, we consider the Poisson model problem of finding $u : \Omega \to \mathbb{R}$ such that

$$-\Delta u = f \qquad \text{in } \Omega, \tag{2.1a}$$

$$u = 0 \qquad \text{on } \partial\Omega. \tag{2.1b}$$

Let u_h^{ex} be the finite element discretization of (2.1) with an exact algebraic solver and u_h its approximation. The associated degrees of freedom in the standard nodal Lagrange basis on a simplicial mesh $\mathcal{T}_h$ are respectively denoted by U_h and $\mathrm{U}_h^{\mathrm{ex}}$, and the stiffness matrix on mesh $\mathcal{T}_h$ is named $\mathbb{A}_h$, so that the algebraic system reads as $\mathbb{A}_h\mathrm{U}_h^{\mathrm{ex}} = \mathrm{F}_h$ on $\mathcal{T}_h$. We compare the guaranteed lower bound on the algebraic error $\|\nabla(u_h^{\mathrm{ex}} - u_h)\| = \|\mathrm{U}_h^{\mathrm{ex}} - \mathrm{U}_h\|_{\mathbb{A}_h}$ based on a *lifting* of the algebraic residual on the *mesh* $\mathcal{T}_h$ *only* in the spirit of [10, Sec. 5.1], [74, Sec. 4.1.1], [44, Sec. 3.3], and [69, Sec. 5.4], see Remark 5.2 below, to the lifting of the algebraic residual on a *hierarchy of meshes* put forward in this paper in Concept 5.1 and Definition 5.1 below. The latter corresponds to one multigrid V-cycle step with zero pre-smoothing and one block-Jacobi (additive Schwarz) post-smoothing step, whereas in the former, only the finest level is employed.

We consider $d = 2$, an L-shape problem (see Sec. 9), and increasing condition number of the stiffness matrix $\mathbb{A}_h$ by either increasing the number of mesh elements in the mesh $\mathcal{T}_h$, or by increasing the finite element polynomial degree. More precisely, an initial triangular mesh with element size $h \approx 0.026$ is considered along with a mesh obtained by two uniform refinements (with mesh size $h/4$), whereas polynomial degrees 1 and 3 are employed. We focus on results in function of iterations of the Gauss–Seidel solver, where the initial approximation U_h^0 is chosen such that the initial algebraic error $\mathrm{U}_h^{\mathrm{ex}} - \mathrm{U}_h^0$ is a vector with random elements uniformly distributed in the interval $[-0.5, 0.5]\|\mathrm{U}_h^{\mathrm{ex}}\|_2$. After a fast reduction of oscillating components of the error in the initial iterations, the convergence is very slow. Fig. 1 presents the underestimation factor

$$\frac{\|\nabla(u_h^{\mathrm{ex}} - u_h)\|}{\underline{\eta}_{\mathrm{alg}}} \geq 1,$$

where $\underline{\eta}_{\mathrm{alg}}$ is given by (7.5a) for the two considered liftings $\underset{\sim}{\rho}_{h,\mathrm{alg}}$ of Remark 5.2 and $\rho_{h,\mathrm{alg}}$ of Definition 5.1. While the lower bound based on the finest-mesh only (one level) deteriorates considerably, we observe a robust behavior of the lower bound obtained with the hierarchically constructed lifting of this paper (hierarchical).

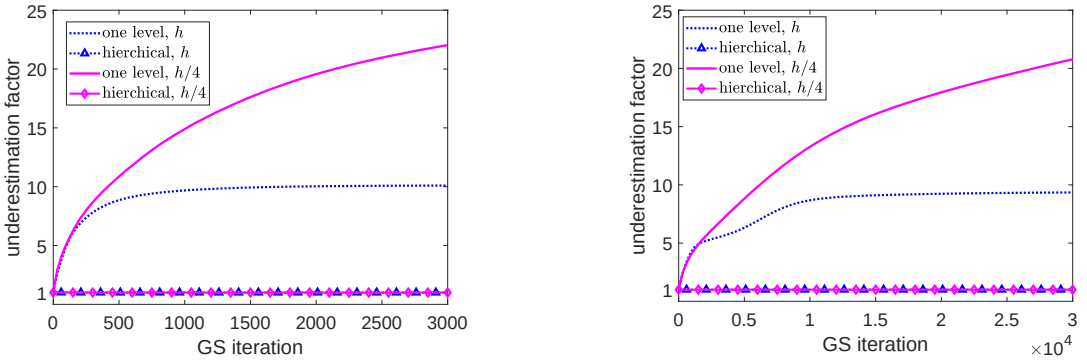

Figure 1: L-shape problem with random initial error and the Gauss–Seidel iterative solver. Underestimation of the guaranteed lower bound on the algebraic error $\underline{\eta}_{\mathrm{alg}}^i = (r_h^i, \rho_{h,\mathrm{alg}}^i)/\|\nabla\rho_{h,\mathrm{alg}}^i\|$ given by (7.5a) with the one-level algebraic residual lifting of Remark 5.2 and by the hierarchical algebraic residual lifting of Definition 5.1. Mesh sizes h and $h/4$, polynomial degrees $p = 1$ (left) and $p = 3$ (right). Optimal underestimation stays close to one.

2.2 Algebraic error estimator based on comparison of two consecutive iterates for a porous medium flow

In the second example, we consider the conjugate gradient solver with an incomplete Cholesky preconditioner for a linear system that arises from a finite element (vertex-centered finite volume) discretization of an unsteady nonlinear problem; more precisely, we consider the immiscible incompressible two-phase flow in porous media in an iterative coupling formulation. The problem reads: find the vector $P_{\mathrm{w}}^{n,k}$ such that

$$\mathbb{P}_{\mathrm{wn}}^{n,k-1} P_{\mathrm{w}}^{n,k} = D_{\mathrm{wn}}^{n,k-1}, \tag{2.2}$$

where $\mathbb{P}_{\mathrm{wn}}^{n,k-1}$ is a symmetric and positive definite matrix arising from diffusion with tensor $\boldsymbol{A}^{n,k-1}$ and $D_{\mathrm{wn}}^{n,k-1}$ is a right-hand side vector; both $\mathbb{P}_{\mathrm{wn}}^{n,k-1}$ and $D_{\mathrm{wn}}^{n,k-1}$ are obtained from [86, Section 6.2], describing a real-life problem. For reader's convenience, the setting leading to (2.2) is recalled in Appendix C.3 below, see (C.7).

We test three algebraic error estimates: 1) the popular estimator based on comparison of two consecutive iterates $P_{\mathrm{w}}^{n,k,i+1}$ and $P_{\mathrm{w}}^{n,k,i}$; 2) the guaranteed lower bound $\underline{\eta}_{\mathrm{alg}}^i = (r_h^i, \rho_{h,\mathrm{alg}}^i)/\|(\boldsymbol{A}^{n,k-1})^{\frac{1}{2}}\nabla\rho_{h,\mathrm{alg}}^i\|$ on the algebraic error proposed in this paper based on Concept 5.1 and Definition 5.1; and 3) the guaranteed upper bound $\overline{\eta}_{\mathrm{alg}}^i = \|(\boldsymbol{A}^{n,k-1})^{-\frac{1}{2}}\boldsymbol{\sigma}_{h,\mathrm{alg}}^i\|$ on the algebraic error proposed in this paper based on Concept 4.1 and Definition 4.3. The results are reported in Fig. 2. We can see that even though the comparison of two consecutive iterates may lead to quite tight estimate on the algebraic error at some iterations, it may importantly underestimate the algebraic error at other iterations. More importantly, its quality is severely impacted by mesh refinement, compare the effectivity indices in the right plots of Fig. 2. In contrast, the guaranteed upper and lower bounds presented herein lead to constantly very satisfactory results also for this challenging test case.

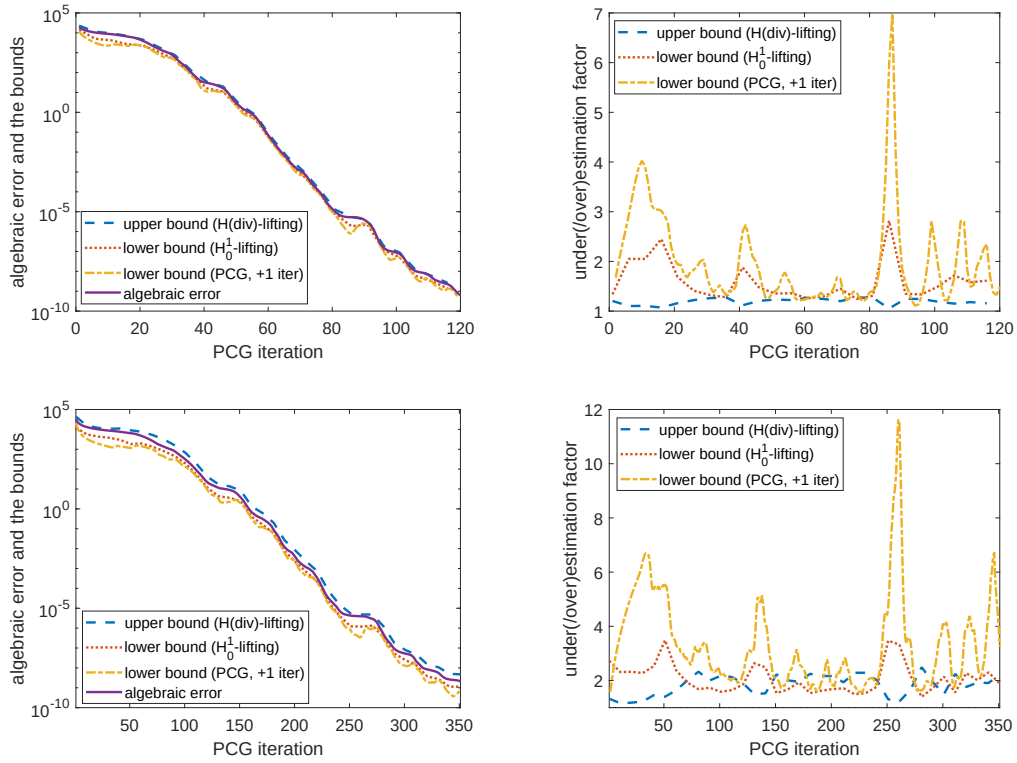

Figure 2: Porous medium flow (C.1) leading to (2.2). Conjugate gradient solver with incomplete Cholesky preconditioning. The algebraic error $\|P_{\mathrm{w}}^{n,k} - P_{\mathrm{w}}^{n,k,i}\|_{\mathbb{P}_{\mathrm{wn}}^{n,k-1}}$ on iteration i, the estimator (lower bound) based on comparison of two consecutive iterates $\|P_{\mathrm{w}}^{n,k,i+1} - P_{\mathrm{w}}^{n,k,i}\|_{\mathbb{P}_{\mathrm{wn}}^{n,k-1}}$, the guaranteed lower bound $\underline{\eta}_{\mathrm{alg}}^i = (r_h^i, \rho_{h,\mathrm{alg}}^i)/\|(\boldsymbol{A}^{n,k-1})^{\frac{1}{2}}\nabla\rho_{h,\mathrm{alg}}^i\|$ on the algebraic error proposed in this paper, and the guaranteed upper bound $\overline{\eta}_{\mathrm{alg}}^i = \|(\boldsymbol{A}^{n,k-1})^{-\frac{1}{2}}\boldsymbol{\sigma}_{h,\mathrm{alg}}^i\|$ on the algebraic error proposed in this paper (left). Corresponding under/overestimation factors (right). Setting of [86, Section 6.2], time step 260 (time $2.6\cdot10^6$s), first iterative coupling linearization, 45×45 mesh (top) and 137×137 mesh (bottom).

3 Setting

We introduce here the setting for our lifting and reconstruction procedures. Let $\Omega \subset \mathbb{R}^d$, $1 \le d \le 3$, be an open bounded polytope with a Lipschitz-continuous boundary.

3.1 Continuous-level notation

For a nonempty subset $\omega \subset \Omega$, we denote by $|\omega|$ its Lebesgue measure, by $(\cdot,\cdot)_\omega$ the $L^2(\omega)$ scalar product, and by $\|\cdot\|_\omega$ the $L^2(\omega)$ norm; when $\omega = \Omega$, the index is dropped. Same notation is used on $\boldsymbol{L}^2(\omega) :=$

$[L^2(\omega)]^d$. We let $H^1(\Omega)$ be the space of scalar-valued $L^2(\Omega)$ functions with weak gradients in $\boldsymbol{L}^2(\Omega)$, $H^1(\Omega) := \{v \in L^2(\Omega);\, \nabla v \in \boldsymbol{L}^2(\Omega)\}$; $H^1_0(\Omega)$ is its subspace formed by functions vanishing on $\partial\Omega$ in the sense of traces. We also let $\boldsymbol{H}(\mathrm{div},\Omega)$ be the space of vector-valued $\boldsymbol{L}^2(\Omega)$ functions with weak divergences in $L^2(\Omega)$, $\boldsymbol{H}(\mathrm{div},\Omega) := \{\boldsymbol{v} \in \boldsymbol{L}^2(\Omega);\, \nabla\cdot\boldsymbol{v} \in L^2(\Omega)\}$. We remark that we will be using the norms $\|\nabla(\cdot)\|$ and $\|\cdot\|$ on respectively $H^1_0(\Omega)$ and $\boldsymbol{H}(\mathrm{div},\Omega)$.

3.2 A hierarchy of meshes

Let $\mathcal{T}_h$ be a simplicial mesh of Ω, matching in the sense that for two distinct elements K of $\mathcal{T}_h$, their intersection is either an empty set or a common vertex, edge, or face. Associated with $\mathcal{T}_h$, let there be a hierarchy of meshes $\{\mathcal{T}_j\}_{0\le j\le J}$. These are again matching simplicial partitions of the domain Ω, *nested* in the sense that $\mathcal{T}_j$ is a refinement of $\mathcal{T}_{j-1}$, $1 \le j \le J$, and satisfying $\mathcal{T}_J = \mathcal{T}_h$. Below, we will suppose shape regularity in the sense that there exists a constant $\kappa_{\mathcal{T}} > 0$ such that $\max_{K\in\mathcal{T}_j} h_K/\rho_K \le \kappa_{\mathcal{T}}$ for all $0 \le j \le J$, where h_K is the diameter of K and ρ_K is the diameter of the largest ball contained in K. We will also request a bound on the refinement strength in the sense that the diameters of all sons of an element are comparable to the diameter of the father element up to a constant $\iota_{\mathcal{T}} > 0$. Highly graded meshes and mesh hierarchies where only some elements are refined are admitted. Affine quadrilateral/hexahedral meshes could easily be considered as well.

The set of vertices of $\mathcal{T}_j$, $0 \le j \le J$, is denoted by $\mathcal{V}_j$, and it is decomposed into interior vertices $\mathcal{V}_j^{\mathrm{int}}$ and boundary vertices $\mathcal{V}_j^{\mathrm{ext}}$. By $\psi_j^{\boldsymbol{a}}$ we denote the hat function associated with the vertex $\boldsymbol{a} \in \mathcal{V}_j$, i.e., the function that is piecewise affine with respect to the j-th level mesh $\mathcal{T}_j$, taking the value 1 at the vertex $\boldsymbol{a}$ and zero at all other j-th level vertices of $\mathcal{V}_j$. The support of $\psi_j^{\boldsymbol{a}}$ is denoted by $\omega_j^{\boldsymbol{a}}$ and it corresponds to the patch of elements of $\mathcal{T}_j$ which share the vertex $\boldsymbol{a} \in \mathcal{V}_j$. We identify $\omega_h^{\boldsymbol{a}} := \omega_J^{\boldsymbol{a}}$ and $\mathcal{V}_h := \mathcal{V}_J$, $\mathcal{V}_h^{\mathrm{int}} := \mathcal{V}_J^{\mathrm{int}}$, $\mathcal{V}_h^{\mathrm{ext}} := \mathcal{V}_J^{\mathrm{ext}}$.

3.3 Piecewise polynomial spaces

In the presentation, three types of piecewise polynomial spaces will be needed.

First, the space of discontinuous (piecewise) qth-order polynomials associated with the mesh $\mathcal{T}_j$ is

$$\mathbb{P}_j^q := \{v_h \in L^2(\Omega), v_h|_K \in \mathbb{P}^q(K) \quad \forall K \in \mathcal{T}_j\} \qquad 0 \le j \le J, \quad q \ge 0. \tag{3.1}$$

Here $\mathbb{P}^q(K)$ stands for polynomials of total degree less than or equal to q on the simplex K.

The space of continuous or trace-continuous, i.e., $H^1_0(\Omega)$-conforming, piecewise qth-order polynomials associated with the mesh $\mathcal{T}_j$ is denoted by V_j^q and defined as

$$V_j^q := \mathbb{P}_j^q \cap H^1_0(\Omega) \qquad 0 \le j \le J, \quad q \ge 1. \tag{3.2}$$

Below, we will often consider $u_h \in V_J^p$ for a fixed polynomial degree $p \ge 1$ as well as derive various $H^1_0(\Omega)$-conforming reconstructions in V_J^p; we will also sometimes treat the more general case $u_h \in \mathbb{P}_J^p$, $p \ge 0$.

Finally, we will need vector-valued piecewise polynomials with continuous normal trace, i.e., $\boldsymbol{H}(\mathrm{div},\Omega)$-conforming, Raviart–Thomas–Nédélec (RTN) mixed finite element spaces given by, see, e.g., Brezzi and Fortin [24],

$$\boldsymbol{V}_j^q := \{\boldsymbol{v}_j \in \boldsymbol{H}(\mathrm{div},\Omega); \boldsymbol{v}_j|_K \in [\mathbb{P}^q(K)]^d + \mathbb{P}^q(K)\boldsymbol{x} \quad \forall K \in \mathcal{T}_j\} \qquad 0 \le j \le J, \quad q \ge 0, \tag{3.3}$$

where various $\boldsymbol{H}(\mathrm{div},\Omega)$-conforming liftings/reconstructions will be performed.

Actually, in the sequel, all the liftings/reconstructions related to the *algebraic error* will use the entire *hierarchy* of the spaces, whereas those related to the *discretization error* will only use the *finest-level* spaces. Henceforth, the latter are denoted

$$\mathbb{P}_h^q := \mathbb{P}_J^q, \quad V_h^q := V_J^q, \quad \boldsymbol{V}_h^q := \boldsymbol{V}_J^q. \tag{3.4}$$

For a given space X defined over the entire domain Ω, we use $X|_\omega$ to denote its restriction to the subdomain $\omega \subset \Omega$. Finally, we denote the $L^2(\Omega)$-orthogonal projection onto $\mathbb{P}_j^q$ by Π_j^q and use the notation $\Pi_h^q := \Pi_J^q$. The choice of fixed polynomial degree is adopted for the simplicity of presentation; taking into account a variable polynomial degree is possible and was addressed in [36], see also the references therein.

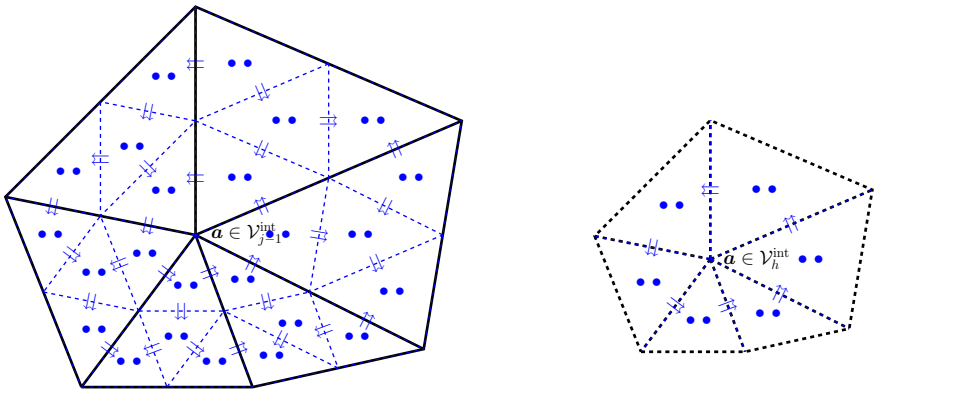

coarse patch $\omega_{j-1}^{\boldsymbol{a}}$ for $\boldsymbol{a} \in \mathcal{V}_{j-1}^{\mathrm{int}}$ (full line)
fine mesh $\mathcal{T}_j$ of $\omega_{j-1}^{\boldsymbol{a}}$ (dashed line)
degrees of freedom of $\boldsymbol{V}_j^p(\omega_{j-1}^{\boldsymbol{a}})$ (arrows and bullets)

fine patch $\omega_h^{\boldsymbol{a}}$ for $\boldsymbol{a} \in \mathcal{V}_h^{\mathrm{int}}$ (dashed line)
fine mesh $\mathcal{T}_h$ of $\omega_h^{\boldsymbol{a}}$ (dashed line)
degrees of freedom of $\boldsymbol{V}_h^{p'}(\omega_h^{\boldsymbol{a}})$ (arrows and bullets)

Figure 3: Degrees of freedom of the local Raviart–Thomas–Nédélec spaces $\boldsymbol{V}_j^p(\omega_{j-1}^{\boldsymbol{a}})$ for the residual liftings $\boldsymbol{\sigma}_{j,\mathrm{alg}}^{\boldsymbol{a}}$, $1 \le j \le J$, (left) and $\boldsymbol{V}_h^{p'}(\omega_h^{\boldsymbol{a}})$ for the discretization flux reconstruction $\boldsymbol{\sigma}_{h,\mathrm{dis}}^{\boldsymbol{a}}$ (right). Interior vertex $\boldsymbol{a}$, polynomial degree $p = 1$, and discretization flux reconstruction degree $p' = p = 1$.

4 $\boldsymbol{H}(\mathrm{div},\Omega)$-lifting of the algebraic residual and a mass-conservative total flux reconstruction in $\boldsymbol{H}(\mathrm{div},\Omega)$

We first show in this section how for an arbitrary discontinuous piecewise polynomial $r_h \in \mathbb{P}_h^p$, $p \ge 0$, a locally minimized vector-valued piecewise polynomial $\boldsymbol{\sigma}_{h,\mathrm{alg}} \in \boldsymbol{V}_h^p \subset \boldsymbol{H}(\mathrm{div},\Omega)$ such that $\nabla{\cdot}\boldsymbol{\sigma}_{h,\mathrm{alg}} = r_h$ can be constructed for the price proportional to one multigrid V-cycle step with block-Jacobi (additive Schwarz) smoothing. This involves a global solve and local solves on patches of vertices on each mesh level. The main lines of this construction are summarized in Concept 4.1, and the details are given in Sec. 4.1. We will term $\boldsymbol{\sigma}_{h,\mathrm{alg}}$ a *hierarchical* $\boldsymbol{H}(\mathrm{div},\Omega)$*-lifting* of the algebraic residual r_h.

Let $f \in L^2(\Omega)$ be the target divergence, $\boldsymbol{A} \in [\mathbb{P}_h^0]^{d\times d}$ be a uniformly bounded and positive definite diffusion tensor of the medium Ω, and let $u_h \in \mathbb{P}_h^p$, $p \ge 1$, be the (possibly discontinuous) numerical approximation for which r_h is the algebraic residual such that

$$(f - r_h, \psi_h^{\boldsymbol{a}})_{\omega_h^{\boldsymbol{a}}} - (\boldsymbol{A}\nabla u_h, \nabla\psi_h^{\boldsymbol{a}})_{\omega_h^{\boldsymbol{a}}} = 0 \qquad \forall \boldsymbol{a} \in \mathcal{V}_h^{\mathrm{int}}, \tag{4.1}$$

where ∇ stands for the elementwise (broken) gradient. Condition (4.1) actually typically determines r_h out of a given f, $\boldsymbol{A}$, and u_h. Then, employing existing flux equilibration techniques, cf. [18, 43], we construct $\boldsymbol{\sigma}_{h,\mathrm{dis}} \in \boldsymbol{V}_h^{p'} \subset \boldsymbol{H}(\mathrm{div},\Omega)$, $p' \in \{p, p+1\}$, locally close to $-\boldsymbol{A}\nabla u_h$ and such that $\nabla{\cdot}\boldsymbol{\sigma}_{h,\mathrm{dis}} = \Pi_h^{p'} f - r_h$, for the price of a local problem for each patch of the finest mesh $\mathcal{T}_h$. The main lines are presented in Concept 4.2 and details in Sec. 4.2.

Setting $\boldsymbol{\sigma}_{h,\mathrm{tot}} := \boldsymbol{\sigma}_{h,\mathrm{alg}} + \boldsymbol{\sigma}_{h,\mathrm{dis}}$, we obtain a *total flux reconstruction* which is *mass conservative* in that $\boldsymbol{\sigma}_{h,\mathrm{tot}} \in \boldsymbol{V}_h^{p'} \subset \boldsymbol{H}(\mathrm{div},\Omega)$ and $\nabla{\cdot}\boldsymbol{\sigma}_{h,\mathrm{tot}} = \Pi_h^{p'} f$.

4.1 Algebraic residual hierarchical $\boldsymbol{H}(\mathrm{div},\Omega)$-lifting

We detail here the construction of the *algebraic residual lifting* $\boldsymbol{\sigma}_{h,\mathrm{alg}}$ of Concept 4.1.

4.1.1 Coarse residual solve

The first, crucial, step for obtaining $\boldsymbol{\sigma}_{h,\mathrm{alg}}$ is to find the *coarsest-level Riesz representer* $\rho_{0,\mathrm{alg}}$ of the algebraic residual r_h given by: find $\rho_{0,\mathrm{alg}} \in V_0^1$ such that

$$(\boldsymbol{A}\nabla\rho_{0,\mathrm{alg}}, \nabla v_0) = (r_h, v_0) \qquad \forall v_0 \in V_0^1. \tag{4.4}$$

This is the coarsest-grid residual solve familiar from multigrid methods; it can only be realized with *lowest-order*, continuous and piecewise affine polynomials from the space V_0^1 of the coarsest mesh $\mathcal{T}_0$. It is of course also possible to replace the space V_0^1 by the (more expensive) V_0^p if $p \ge 1$.

Input:

algebraic residual $r_h \in \mathbb{P}_h^p$, $p \geq 0$,
diffusion tensor $\boldsymbol{A} \in [\mathbb{P}_h^0]^{d\times d}$.

Output:

$$\boldsymbol{\sigma}_{h,\mathrm{alg}} \in \boldsymbol{V}_h^p \subset \boldsymbol{H}(\mathrm{div},\Omega),$$
$$\nabla\cdot\boldsymbol{\sigma}_{h,\mathrm{alg}} = r_h,$$
$$\|\boldsymbol{A}^{-\frac{1}{2}}\boldsymbol{\sigma}_{h,\mathrm{alg}}\| \text{ locally minimized.}$$

Construction (Definition 4.3):

1. Solve the coarse problem (4.4).
2. Run through mesh levels $j = 1 \dots J$:
   (a) Run through all coarser vertices $\boldsymbol{a} \in \mathcal{V}_{j-1}$.
   (b) Assemble the RTN spaces $\boldsymbol{V}_j^p(\omega_{j-1}^{\boldsymbol{a}})$ and $\mathbb{P}_j^p(\omega_{j-1}^{\boldsymbol{a}})$, see (4.5) and Fig. 3, left.
   (c) Solve the local Neumann mixed finite element problems (4.7) for $j = 1$ and (4.11) for $j > 1$ to obtain $\boldsymbol{\sigma}_{j,\mathrm{alg}}^{\boldsymbol{a}} \in \boldsymbol{V}_j^p(\omega_{j-1}^{\boldsymbol{a}})$.
3. Combine

$$\boldsymbol{\sigma}_{h,\mathrm{alg}} := \sum_{j=1}^{J} \sum_{\boldsymbol{a}\in\mathcal{V}_{j-1}} \boldsymbol{\sigma}_{j,\mathrm{alg}}^{\boldsymbol{a}}.$$

Simplifications:

- Lowest-degree spaces $\boldsymbol{V}_j^0(\omega_{j-1}^{\boldsymbol{a}})$ instead of $\boldsymbol{V}_j^p(\omega_{j-1}^{\boldsymbol{a}})$ for all $j < J$: Sec. 8.3 and [70].
- Explicit construction avoiding local patchwise problems (4.7) or (4.11): Sec. 8.3 and [70].
- Computable bound avoiding physical construction of $\boldsymbol{\sigma}_{h,\mathrm{alg}}$: (A.1)–(A.2) in Appendix A below.

Concept 4.1: Algebraic residual $\boldsymbol{H}(\mathrm{div},\Omega)$-lifting

Input:

target divergence $f \in L^2(\Omega)$,
approximation $u_h \in \mathbb{P}_h^p$, $p \geq 1$,
diffusion tensor $\boldsymbol{A} \in [\mathbb{P}_h^0]^{d\times d}$,
algebraic residual $r_h \in \mathbb{P}_h^p$,
condition $(f - r_h, \psi_h^{\boldsymbol{a}})_{\omega_h^{\boldsymbol{a}}} - (\boldsymbol{A}\nabla u_h, \nabla\psi_h^{\boldsymbol{a}})_{\omega_h^{\boldsymbol{a}}} = 0$
$\forall \boldsymbol{a} \in \mathcal{V}_h^{\mathrm{int}}$.

Output:

$$\boldsymbol{\sigma}_{h,\mathrm{tot}} \in \boldsymbol{V}_h^{p'} \subset \boldsymbol{H}(\mathrm{div},\Omega), p' \in \{p, p+1\},$$
$$\nabla\cdot\boldsymbol{\sigma}_{h,\mathrm{tot}} = \Pi_h^{p'} f,$$
$$\|\boldsymbol{A}^{\frac{1}{2}}\nabla u_h + \boldsymbol{A}^{-\frac{1}{2}}\boldsymbol{\sigma}_{h,\mathrm{tot}}\| \text{ locally minimized.}$$

Construction (Definition 4.5):

1. Run through all finest vertices $\boldsymbol{a} \in \mathcal{V}_h$.
2. Assemble the RTN spaces $\boldsymbol{V}_h^{p'}(\omega_h^{\boldsymbol{a}})$ and $\mathbb{P}_h^{p'}(\omega_h^{\boldsymbol{a}})$, $p' \in \{p, p+1\}$, see (4.13) and Fig. 3, right.
3. Solve the local Neumann mixed finite element problems (4.14) to obtain $\boldsymbol{\sigma}_{h,\mathrm{dis}}^{\boldsymbol{a}} \in \boldsymbol{V}_h^{p'}(\omega_h^{\boldsymbol{a}})$.
4. Combine

$$\boldsymbol{\sigma}_{h,\mathrm{dis}} := \sum_{\boldsymbol{a}\in\mathcal{V}_h} \boldsymbol{\sigma}_{h,\mathrm{dis}}^{\boldsymbol{a}} \in \boldsymbol{V}_h^{p'},$$

   yielding $\nabla\cdot\boldsymbol{\sigma}_{h,\mathrm{dis}} = \Pi_h^{p'} f - r_h$.
5. Obtain $\boldsymbol{\sigma}_{h,\mathrm{alg}}$ following Concept 4.1.
6. Set

$$\boldsymbol{\sigma}_{h,\mathrm{tot}} := \boldsymbol{\sigma}_{h,\mathrm{alg}} + \boldsymbol{\sigma}_{h,\mathrm{dis}}. \tag{4.3}$$

Simplifications:

- Explicit construction avoiding local patchwise problems (4.14): Sec. 8.3 and [70].

Concept 4.2: Total flux reconstruction in $\boldsymbol{H}(\mathrm{div},\Omega)$

4.1.2 Local spaces

Let a mesh level $1 \leq j \leq J$ be fixed, together with a vertex $\boldsymbol{a} \in \mathcal{V}_{j-1}$, i.e., a vertex from the next coarser mesh. The key ingredient for our algebraic residual liftings are local spaces associated with the mesh of level j but defined on the subdomain $\omega_{j-1}^{\boldsymbol{a}}$ of all simplices of level $j-1$ sharing the vertex $\boldsymbol{a}$,

$$\begin{aligned}\boldsymbol{V}_j^p(\omega_{j-1}^{\boldsymbol{a}}) &:= \{\boldsymbol{v}_j \in \boldsymbol{V}_j^p|_{\omega_{j-1}^{\boldsymbol{a}}};\ \boldsymbol{v}_j\cdot\boldsymbol{n}_{\omega_{j-1}^{\boldsymbol{a}}} = 0 \text{ on } \partial\omega_{j-1}^{\boldsymbol{a}}\},\\ \mathbb{P}_j^p(\omega_{j-1}^{\boldsymbol{a}}) &:= \{q_j \in \mathbb{P}_j^p|_{\omega_{j-1}^{\boldsymbol{a}}};\ (q_j,1)_{\omega_{j-1}^{\boldsymbol{a}}} = 0\},\end{aligned} \qquad \boldsymbol{a} \in \mathcal{V}_{j-1}^{\mathrm{int}}, \tag{4.5a}$$

$$\begin{aligned}\boldsymbol{V}_j^p(\omega_{j-1}^{\boldsymbol{a}}) &:= \{\boldsymbol{v}_j \in \boldsymbol{V}_j^p|_{\omega_{j-1}^{\boldsymbol{a}}};\ \boldsymbol{v}_j\cdot\boldsymbol{n}_{\omega_{j-1}^{\boldsymbol{a}}} = 0 \text{ on } \partial\omega_{j-1}^{\boldsymbol{a}} \setminus \partial\Omega\},\\ \mathbb{P}_j^p(\omega_{j-1}^{\boldsymbol{a}}) &:= \mathbb{P}_j^p|_{\omega_{j-1}^{\boldsymbol{a}}},\end{aligned} \qquad \boldsymbol{a} \in \mathcal{V}_{j-1}^{\mathrm{ext}}, \tag{4.5b}$$

where $\boldsymbol{n}_{\omega_{j-1}^{\boldsymbol{a}}}$ stands for the outward unit normal of the domain $\omega_{j-1}^{\boldsymbol{a}}$. The degrees of freedom of the spaces $\boldsymbol{V}_j^p(\omega_{j-1}^{\boldsymbol{a}})$ for an interior vertex with polynomial degree $p = 1$ are illustrated in Fig. 3, left.

4.1.3 Two-level algebraic residual $\boldsymbol{H}(\mathrm{div},\Omega)$-lifting

Let $J = 1$, with coarse mesh $\mathcal{T}_0$ and fine mesh $\mathcal{T}_h = \mathcal{T}_1$. In this two-level setting, our algebraic residual $\boldsymbol{H}(\mathrm{div},\Omega)$-lifting $\boldsymbol{\sigma}_{h,\mathrm{alg}} \in \boldsymbol{V}_h^p$ is based on the mixed finite element problems on each *coarsest patch* $\omega_0^{\boldsymbol{a}}$, $\boldsymbol{a} \in \mathcal{V}_0$. The spaces $\boldsymbol{V}_1^p(\omega_0^{\boldsymbol{a}}) \times \mathbb{P}_1^p(\omega_0^{\boldsymbol{a}})$ associated with fine mesh $\mathcal{T}_1$ are used, see (4.5) and Fig. 3, left, for an illustration. In particular, following (4.5), homogeneous Neumann boundary conditions are prescribed on $\partial\omega_0^{\boldsymbol{a}}$ for interior vertices $\boldsymbol{a} \in \mathcal{V}_0^{\mathrm{int}}$ and on $\partial\omega_0^{\boldsymbol{a}} \setminus \partial\Omega$ for boundary vertices $\boldsymbol{a} \in \mathcal{V}_0^{\mathrm{ext}}$; on $\partial\omega_0^{\boldsymbol{a}} \cap \partial\Omega$, a homogeneous Dirichlet boundary condition is imposed for $\boldsymbol{a} \in \mathcal{V}_0^{\mathrm{ext}}$. The actual construction reads:

Definition 4.1 (Two-level algebraic residual $\boldsymbol{H}(\mathrm{div},\Omega)$-lifting; $J = 1$)**.** *Define*

$$\boldsymbol{\sigma}_{h,\mathrm{alg}} := \sum_{\boldsymbol{a}\in\mathcal{V}_0} \boldsymbol{\sigma}_{1,\mathrm{alg}}^{\boldsymbol{a}}, \tag{4.6}$$

where the vertex contributions are defined as the solution of: find $(\boldsymbol{\sigma}^{\boldsymbol{a}}_{1,\mathrm{alg}}, \gamma^{\boldsymbol{a}}_1) \in \boldsymbol{V}^p_1(\omega^{\boldsymbol{a}}_0) \times \mathbb{P}^p_1(\omega^{\boldsymbol{a}}_0)$ *such that*

$$(\boldsymbol{A}^{-1}\boldsymbol{\sigma}^{\boldsymbol{a}}_{1,\mathrm{alg}}, \boldsymbol{v}_1)_{\omega^{\boldsymbol{a}}_0} - (\gamma^{\boldsymbol{a}}_1, \nabla{\cdot}\boldsymbol{v}_1)_{\omega^{\boldsymbol{a}}_0} = 0 \qquad \forall \boldsymbol{v}_1 \in \boldsymbol{V}^p_1(\omega^{\boldsymbol{a}}_0), \tag{4.7a}$$

$$(\nabla{\cdot}\boldsymbol{\sigma}^{\boldsymbol{a}}_{1,\mathrm{alg}}, q_1)_{\omega^{\boldsymbol{a}}_0} = (r_h\psi^{\boldsymbol{a}}_0 - \boldsymbol{A}\nabla\rho_{0,\mathrm{alg}}{\cdot}\nabla\psi^{\boldsymbol{a}}_0, q_1)_{\omega^{\boldsymbol{a}}_0} \qquad \forall q_1 \in \mathbb{P}^p_1(\omega^{\boldsymbol{a}}_0). \tag{4.7b}$$

Problems (4.7) are well-posed, see, e.g., Brezzi and Fortin [24] or [43, 44] and the references therein. In particular, the Neumann compatibility condition

$$(r_h\psi^{\boldsymbol{a}}_0 - \boldsymbol{A}\nabla\rho_{0,\mathrm{alg}} \cdot \nabla\psi^{\boldsymbol{a}}_0, 1)_{\omega^{\boldsymbol{a}}_0} = 0 \tag{4.8}$$

for all coarsest interior vertices $\boldsymbol{a} \in \mathcal{V}^{\mathrm{int}}_0$ immediately follows from (4.4). Note also that (4.7) are the Euler–Lagrange conditions for the constrained minimization problem

$$\boldsymbol{\sigma}^{\boldsymbol{a}}_{1,\mathrm{alg}} := \arg \min_{\boldsymbol{v}_1 \in \boldsymbol{V}^p_1(\omega^{\boldsymbol{a}}_0),\, \nabla{\cdot}\boldsymbol{v}_1 = \Pi^p_1(r_h\psi^{\boldsymbol{a}}_0 - \boldsymbol{A}\nabla\rho_{0,\mathrm{alg}}\cdot\nabla\psi^{\boldsymbol{a}}_0)} \|\boldsymbol{A}^{-\frac{1}{2}}\boldsymbol{v}_1\|_{\omega^{\boldsymbol{a}}_0}. \tag{4.9}$$

Our construction finds the best local contributions $\boldsymbol{\sigma}^{\boldsymbol{a}}_{1,\mathrm{alg}}$ which lead to the satisfaction of the following crucial divergence constraint:

Lemma 4.2 (Properties of $\boldsymbol{\sigma}_{h,\mathrm{alg}}$; $J = 1$)**.** *The algebraic residual lifting of Definition 4.1 satisfies* $\boldsymbol{\sigma}_{h,\mathrm{alg}} \in \boldsymbol{V}^p_h \subset \boldsymbol{H}(\mathrm{div}, \Omega)$ *and*

$$\nabla{\cdot}\boldsymbol{\sigma}_{h,\mathrm{alg}} = r_h.$$

Proof. All contributions $\boldsymbol{\sigma}^{\boldsymbol{a}}_{1,\mathrm{alg}}$ extended by zero outside of the patches $\omega^{\boldsymbol{a}}_0$ belong to $\boldsymbol{V}^p_h$, so that $\boldsymbol{\sigma}_{h,\mathrm{alg}}$ does so by (4.6) as well. We next use the local divergence constraints (4.7b) in combination with the Neumann compatibility condition (4.8) which gives $\nabla{\cdot}\boldsymbol{\sigma}^{\boldsymbol{a}}_{1,\mathrm{alg}} = \Pi^p_h(r_h\psi^{\boldsymbol{a}}_0 - \boldsymbol{A}\nabla\rho_{0,\mathrm{alg}}{\cdot}\nabla\psi^{\boldsymbol{a}}_0)$. Consequently, the fact that $\psi^{\boldsymbol{a}}_0$, $\boldsymbol{a} \in \mathcal{V}_0$, form a partition of unity and the definition (4.6) lead to

$$\begin{aligned}\nabla{\cdot}\boldsymbol{\sigma}_{h,\mathrm{alg}} &= \sum_{\boldsymbol{a}\in\mathcal{V}_0} \nabla{\cdot}\boldsymbol{\sigma}^{\boldsymbol{a}}_{1,\mathrm{alg}} = \sum_{\boldsymbol{a}\in\mathcal{V}_0} \Pi^p_h(r_h\psi^{\boldsymbol{a}}_0 - \boldsymbol{A}\nabla\rho_{0,\mathrm{alg}}{\cdot}\nabla\psi^{\boldsymbol{a}}_0)\\ &= \Pi^p_h\left(\sum_{\boldsymbol{a}\in\mathcal{V}_0} (r_h\psi^{\boldsymbol{a}}_0 - \boldsymbol{A}\nabla\rho_{0,\mathrm{alg}}{\cdot}\nabla\psi^{\boldsymbol{a}}_0)\right) = \Pi^p_h r_h = r_h,\end{aligned}$$

which finishes the proof. □

4.1.4 Multilevel algebraic residual $\boldsymbol{H}(\mathrm{div}, \Omega)$-lifting

We now extend Definition 4.1 to an arbitrary number of mesh levels. To do so, we exploit the *hierarchical* mesh structure and use a telescopic sum argument:

Definition 4.3 (Algebraic residual $\boldsymbol{H}(\mathrm{div}, \Omega)$-lifting)**.** *Define*

$$\boldsymbol{\sigma}_{h,\mathrm{alg}} := \sum_{j=1}^{J} \sum_{\boldsymbol{a}\in\mathcal{V}_{j-1}} \boldsymbol{\sigma}^{\boldsymbol{a}}_{j,\mathrm{alg}}, \tag{4.10}$$

where the vertex contributions $\boldsymbol{\sigma}^{\boldsymbol{a}}_{j,\mathrm{alg}}$ *on level* $j = 1$ *are given by (4.7) and on all higher levels* $1 < j \le J$ *by: find* $(\boldsymbol{\sigma}^{\boldsymbol{a}}_{j,\mathrm{alg}}, \gamma^{\boldsymbol{a}}_j) \in \boldsymbol{V}^p_j(\omega^{\boldsymbol{a}}_{j-1}) \times \mathbb{P}^p_j(\omega^{\boldsymbol{a}}_{j-1})$ *such that*

$$(\boldsymbol{A}^{-1}\boldsymbol{\sigma}^{\boldsymbol{a}}_{j,\mathrm{alg}}, \boldsymbol{v}_j)_{\omega^{\boldsymbol{a}}_{j-1}} - (\gamma^{\boldsymbol{a}}_j, \nabla{\cdot}\boldsymbol{v}_j)_{\omega^{\boldsymbol{a}}_{j-1}} = 0 \qquad \forall \boldsymbol{v}_j \in \boldsymbol{V}^p_j(\omega^{\boldsymbol{a}}_{j-1}), \tag{4.11a}$$

$$(\nabla{\cdot}\boldsymbol{\sigma}^{\boldsymbol{a}}_{j,\mathrm{alg}}, q_j)_{\omega^{\boldsymbol{a}}_{j-1}} = ((\mathrm{Id} - \Pi^p_{j-1})(r_h\psi^{\boldsymbol{a}}_{j-1}), q_j)_{\omega^{\boldsymbol{a}}_{j-1}} \qquad \forall q_j \in \mathbb{P}^p_j(\omega^{\boldsymbol{a}}_{j-1}). \tag{4.11b}$$

Problems (4.11) are well-posed for all levels $1 < j \le J$ and all vertices $\boldsymbol{a} \in \mathcal{V}_{j-1}$. The Neumann compatibility conditions for $\boldsymbol{a} \in \mathcal{V}^{\mathrm{int}}_{j-1}$, $j > 1$, follow from $\big((\mathrm{Id} - \Pi^p_{j-1})(r_h\psi^{\boldsymbol{a}}_{j-1}), 1\big)_{\omega^{\boldsymbol{a}}_{j-1}} = 0$. In generalization of Lemma 4.2, we now have:

Lemma 4.4 (Properties of $\boldsymbol{\sigma}_{h,\mathrm{alg}}$)**.** *The algebraic residual lifting of Definition 4.3 satisfies* $\boldsymbol{\sigma}_{h,\mathrm{alg}} \in \boldsymbol{V}^p_h \subset \boldsymbol{H}(\mathrm{div}, \Omega)$ *and*

$$\nabla{\cdot}\boldsymbol{\sigma}_{h,\mathrm{alg}} = r_h.$$

Proof. The fact that $\boldsymbol{\sigma}_{h,\mathrm{alg}} \in \boldsymbol{V}_h^p \subset \boldsymbol{H}(\mathrm{div},\Omega)$ is immediate as all the summands $\boldsymbol{\sigma}_{j,\mathrm{alg}}^{\boldsymbol{a}}$ in (4.10) (when extended by zero outside of $\omega_{j-1}^{\boldsymbol{a}}$) belong to $\boldsymbol{V}_h^p \subset \boldsymbol{H}(\mathrm{div},\Omega)$. As for the divergence, redefine for this proof, with an abuse of notation, $\Pi_0^p := 0$. Then, using (4.10), the fact that the hat functions $\psi_{j-1}^{\boldsymbol{a}}$ for vertices $\boldsymbol{a} \in \mathcal{V}_{j-1}$ on level $j-1$ form a partition of unity on the entire domain Ω, the fact that $\Pi_j^p(\mathrm{Id} - \Pi_{j-1}^p) = \Pi_j^p - \Pi_{j-1}^p$, and the local divergence constraint (4.11b), we obtain

$$\begin{aligned}\nabla\cdot\boldsymbol{\sigma}_{h,\mathrm{alg}} &= \sum_{j=1}^{J}\sum_{\boldsymbol{a}\in\mathcal{V}_{j-1}} \nabla\cdot\boldsymbol{\sigma}_{j,\mathrm{alg}}^{\boldsymbol{a}} = \sum_{\boldsymbol{a}\in\mathcal{V}_0} \Pi_1^p(r_h\psi_0^{\boldsymbol{a}} - \boldsymbol{A}\nabla\rho_{0,\mathrm{alg}}\cdot\nabla\psi_0^{\boldsymbol{a}}) + \sum_{j=2}^{J}\sum_{\boldsymbol{a}\in\mathcal{V}_{j-1}} (\Pi_j^p - \Pi_{j-1}^p)(r_h\psi_{j-1}^{\boldsymbol{a}}) \\ &= \sum_{j=1}^{J}(\Pi_j^p - \Pi_{j-1}^p)r_h = \Pi_h^p r_h - \Pi_0^p r_h = r_h.\end{aligned} \tag{4.12}$$

□

4.2 Mass-conservative total flux reconstruction in $\boldsymbol{H}(\mathrm{div},\Omega)$

We start by defining a *discretization flux reconstruction* $\boldsymbol{\sigma}_{h,\mathrm{dis}} \in \boldsymbol{V}_h^{p'}$. We again proceed via solution of local mixed finite element problems, but this time only on the *finest patches* $\omega_h^{\boldsymbol{a}}$ around the *finest mesh vertices* $\boldsymbol{a} \in \mathcal{V}_h$, similarly to [43, Definition 6.9] and [69, Sec. 4.4]. We will in particular employ Raviart–Thomas–Nédélec $\boldsymbol{H}(\mathrm{div},\Omega)$-conforming vector-valued spaces with homogeneous Neumann boundary condition given by

$$\begin{aligned}&\boldsymbol{V}_h^{p'}(\omega_h^{\boldsymbol{a}}) := \{\boldsymbol{v}_h \in \boldsymbol{V}_h^{p'}|_{\omega_h^{\boldsymbol{a}}};\ \boldsymbol{v}_h\cdot\boldsymbol{n}_{\omega_h^{\boldsymbol{a}}} = 0 \text{ on } \partial\omega_h^{\boldsymbol{a}}\},\\ &\mathbb{P}_h^{p'}(\omega_h^{\boldsymbol{a}}) := \{q_h \in \mathbb{P}_h^{p'}|_{\omega_h^{\boldsymbol{a}}};\ (q_h,1)_{\omega_h^{\boldsymbol{a}}} = 0\},\end{aligned} \qquad \boldsymbol{a} \in \mathcal{V}_h^{\mathrm{int}}, \tag{4.13a}$$

$$\begin{aligned}&\boldsymbol{V}_h^{p'}(\omega_h^{\boldsymbol{a}}) := \{\boldsymbol{v}_h \in \boldsymbol{V}_h^{p'}|_{\omega_h^{\boldsymbol{a}}};\ \boldsymbol{v}_h\cdot\boldsymbol{n}_{\omega_h^{\boldsymbol{a}}} = 0 \text{ on } \partial\omega_h^{\boldsymbol{a}}\setminus\partial\Omega\},\\ &\mathbb{P}_h^{p'}(\omega_h^{\boldsymbol{a}}) := \mathbb{P}_h^{p'}|_{\omega_h^{\boldsymbol{a}}},\end{aligned} \qquad \boldsymbol{a} \in \mathcal{V}_h^{\mathrm{ext}}, \tag{4.13b}$$

where, recall, $p' \in \{p, p+1\}$ for a given $p \geq 1$. We refer to Fig. 3, right, for an allustration.

Definition 4.5 (Discretization flux reconstruction)**.** *Define*

$$\boldsymbol{\sigma}_{h,\mathrm{dis}} := \sum_{\boldsymbol{a}\in\mathcal{V}_h} \boldsymbol{\sigma}_{h,\mathrm{dis}}^{\boldsymbol{a}},$$

where the vertex contributions $\boldsymbol{\sigma}_{h,\mathrm{dis}}^{\boldsymbol{a}}$ *are defined as the solution of: find* $(\boldsymbol{\sigma}_{h,\mathrm{dis}}^{\boldsymbol{a}}, \gamma_h^{\boldsymbol{a}}) \in \boldsymbol{V}_h^{p'}(\omega_h^{\boldsymbol{a}}) \times \mathbb{P}_h^{p'}(\omega_h^{\boldsymbol{a}})$ *such that*

$$(\boldsymbol{A}^{-1}\boldsymbol{\sigma}_{h,\mathrm{dis}}^{\boldsymbol{a}}, \boldsymbol{v}_h)_{\omega_h^{\boldsymbol{a}}} - (\gamma_h^{\boldsymbol{a}}, \nabla\cdot\boldsymbol{v}_h)_{\omega_h^{\boldsymbol{a}}} = -(\psi_h^{\boldsymbol{a}}\boldsymbol{A}\nabla u_h, \boldsymbol{v}_h)_{\omega_h^{\boldsymbol{a}}} \qquad \forall \boldsymbol{v}_h \in \boldsymbol{V}_h^{p'}(\omega_h^{\boldsymbol{a}}), \tag{4.14a}$$

$$(\nabla\cdot\boldsymbol{\sigma}_{h,\mathrm{dis}}^{\boldsymbol{a}}, q_h)_{\omega_h^{\boldsymbol{a}}} = (f\psi_h^{\boldsymbol{a}} - \boldsymbol{A}\nabla u_h\cdot\nabla\psi_h^{\boldsymbol{a}} - r_h\psi_h^{\boldsymbol{a}}, q_h)_{\omega_h^{\boldsymbol{a}}} \qquad \forall q_h \in \mathbb{P}_h^{p'}(\omega_h^{\boldsymbol{a}}). \tag{4.14b}$$

The Neumann compatibility condition for (4.14) amounts to

$$(f - r_h, \psi_h^{\boldsymbol{a}})_{\omega_h^{\boldsymbol{a}}} - (\boldsymbol{A}\nabla u_h, \nabla\psi_h^{\boldsymbol{a}})_{\omega_h^{\boldsymbol{a}}} = 0 \qquad \forall \boldsymbol{a} \in \mathcal{V}_h^{\mathrm{int}},$$

and is our assumption (4.1). Similarly as in Lemmas 4.2 and 4.4, we can characterize the divergence of $\boldsymbol{\sigma}_{h,\mathrm{dis}}$ (cf. [43, Lemma 6.12] and [69, Sec. 4.4]):

Lemma 4.6 (Properties of $\boldsymbol{\sigma}_{h,\mathrm{dis}}$)**.** *The discretization flux reconstruction of Definition 4.5 satisfies* $\boldsymbol{\sigma}_{h,\mathrm{dis}} \in \boldsymbol{V}_h^{p'} \subset \boldsymbol{H}(\mathrm{div},\Omega)$ *and*

$$\nabla\cdot\boldsymbol{\sigma}_{h,\mathrm{dis}} = \Pi_h^{p'} f - r_h.$$

Combining Lemmas 4.4 and 4.6, we obtain our first main result showing how to recover mass balance in any situation:

Theorem 4.7 (Mass-conservative total flux reconstruction in $\boldsymbol{H}(\mathrm{div},\Omega)$)**.** *Let* $f \in L^2(\Omega)$, $u_h \in \mathbb{P}_h^p$, $p \geq 1$, $\boldsymbol{A} \in [\mathbb{P}_h^0]^{d\times d}$, *and* $r_h \in \mathbb{P}_h^p$ *be arbitrary but such that the compatibility condition* (4.1) *is satisfied. Let* $\boldsymbol{\sigma}_{h,\mathrm{alg}}$ *and* $\boldsymbol{\sigma}_{h,\mathrm{dis}}$ *be respectively constructed by Definitions 4.3 and 4.5. Then*

$$\boxed{\begin{aligned}\boldsymbol{\sigma}_{h,\mathrm{tot}} := \boldsymbol{\sigma}_{h,\mathrm{alg}} + \boldsymbol{\sigma}_{h,\mathrm{dis}} \in \boldsymbol{V}_h^{p'} \subset \boldsymbol{H}(\mathrm{div},\Omega), \qquad (4.15a)\\ \nabla\cdot\boldsymbol{\sigma}_{h,\mathrm{tot}} = \Pi_h^{p'} f. \qquad (4.15b)\end{aligned}}$$

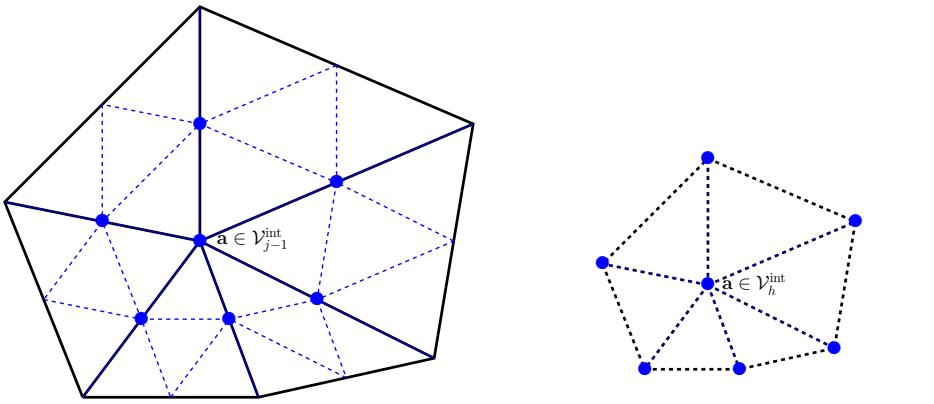

coarse patch $\omega_{j-1}^{\mathbf{a}}$ for $\mathbf{a} \in \mathcal{V}_{j-1}^{\text{int}}$ (full line)
fine mesh $\mathcal{T}_j$ of $\omega_{j-1}^{\mathbf{a}}$ (dashed line)
degrees of freedom of $V_j^p(\omega_{j-1}^{\mathbf{a}})$ (bullets)

fine patch $\omega_h^{\mathbf{a}}$ for $\mathbf{a} \in \mathcal{V}_h^{\text{int}}$ (dashed line)
fine mesh $\mathcal{T}_h$ of $\omega_h^{\mathbf{a}}$ (dashed line)
degrees of freedom of $V_h^p(\omega_h^{\mathbf{a}})$ (bullets)

Figure 4: Degrees of freedom of the local continuous spaces $V_j^p(\omega_{j-1}^{\boldsymbol{a}})$ for the algebraic residual liftings $\rho_{j,\text{alg}}^{\boldsymbol{a}}$, $1 \le j \le J$, (left) and $V_h^p(\omega_h^{\boldsymbol{a}})$ for the total residual liftings $\rho_{h,\text{tot}}^{\boldsymbol{a}}$ (right). Interior vertex $\boldsymbol{a}$, polynomial degree $p = 1$.

5 $H_0^1(\Omega)$-liftings of the algebraic and total residuals

Let $f \in L^2(\Omega)$ be the target divergence, $\boldsymbol{A} \in [\mathbb{P}_h^0]^{d\times d}$ be a diffusion tensor of the medium Ω, and let $u_h \in \mathbb{P}_h^p$, $p \ge 1$, be the (possibly discontinuous) numerical approximation for which r_h is the algebraic residual (no formal link like (4.1) is needed here). We introduce here our hierarchical $H_0^1(\Omega)$-lifting of the algebraic residual in Concept 5.1 and Definition 5.1 and our $H_0^1(\Omega)$-lifting of the total residual in Concept 5.2 and Definition 5.3.

Input:

algebraic residual $r_h \in \mathbb{P}_h^p$, $p \ge 1$,
diffusion tensor $\boldsymbol{A} \in [\mathbb{P}_h^0]^{d\times d}$.

Output:

$$\rho_{h,\text{alg}} \in V_h^p \subset H_0^1(\Omega). \tag{5.1}$$

Construction (Definition 5.1):

1. Solve the coarse problem (4.4).
2. Run through mesh levels $j = 1 \dots J$:
   (a) Run through all coarser vertices $\boldsymbol{a} \in \mathcal{V}_{j-1}$.
   (b) Assemble the continuous spaces $V_j^p(\omega_{j-1}^{\boldsymbol{a}})$ from (5.3), see Fig. 4, left.
   (c) Solve the local Dirichlet conforming finite element problems (5.5) to get $\rho_{j,\text{alg}}^{\boldsymbol{a}} \in V_j^p(\omega_{j-1}^{\boldsymbol{a}})$.
3. Combine

$$\rho_{h,\text{alg}} := \rho_{0,\text{alg}} + \sum_{j=1}^{J} \sum_{\boldsymbol{a}\in\mathcal{V}_{j-1}} w_{\psi_{j-1}^{\boldsymbol{a}}}(\rho_{j,\text{alg}}^{\boldsymbol{a}}),$$

where $w_{\psi_{j-1}^{\boldsymbol{a}}}(\cdot)$ is a weighting by the partition of unity such that $w_{\psi_{j-1}^{\boldsymbol{a}}}(\rho_{j,\text{alg}}^{\boldsymbol{a}}) \in V_j^p(\omega_{j-1}^{\boldsymbol{a}}) \subset V_j^p$.

Simplifications:

- Lowest-degree spaces $V_j^1(\omega_{j-1}^{\boldsymbol{a}})$ instead of $V_j^p(\omega_{j-1}^{\boldsymbol{a}})$ for all $j < J$: Sec. 8.3 and [62].
- Explicit construction avoiding local patchwise problems (5.5): Sec. 8.3.
- Deriving a bound avoiding physical construction of $\rho_{h,\text{alg}}$: possible.

Concept 5.1: Algebraic residual $H_0^1(\Omega)$-lifting

Input:

target divergence $f \in L^2(\Omega)$,
approximation $u_h \in \mathbb{P}_h^p$, $p \ge 1$,
diffusion tensor $\boldsymbol{A} \in [\mathbb{P}_h^0]^{d\times d}$,
algebraic residual $r_h \in \mathbb{P}_h^p$.

Output:

$$\rho_{h,\text{tot}} \in V_h^{p+1} \subset H_0^1(\Omega). \tag{5.2}$$

Construction (Definition 5.3):

1. Run through all finest vertices $\boldsymbol{a} \in \mathcal{V}_h$.
2. Assemble the continuous spaces $V_h^p(\omega_h^{\boldsymbol{a}})$ from (5.7), see Fig. 4, right.
3. Solve the local Neumann conforming finite element problems (5.8) to get $\rho_{h,\text{tot}}^{\boldsymbol{a}} \in V_h^p(\omega_h^{\boldsymbol{a}})$.
4. Combine

$$\rho_{h,\text{tot}} := \sum_{\boldsymbol{a}\in\mathcal{V}_h} \psi_h^{\boldsymbol{a}} \rho_{h,\text{tot}}^{\boldsymbol{a}}.$$

Simplifications:

- Explicit construction avoiding local patchwise problems (5.8): Sec. 8.3.

Concept 5.2: Total residual $H_0^1(\Omega)$-lifting

5.1 Algebraic residual hierarchical $H_0^1(\Omega)$-lifting

The *algebraic residual lifting* $\rho_{h,\mathrm{alg}}$ of Concept 5.1 corresponds to one step multigrid V-cycle with zero pre-smoothing and one post-smoothing via block-Jacobi (additive Schwarz) with respect to patches around vertices. For $1 \leq j \leq J$, set

$$V_j^p(\omega_{j-1}^{\boldsymbol{a}}) := V_j^p|_{\omega_{j-1}^{\boldsymbol{a}}} \cap H_0^1(\omega_{j-1}^{\boldsymbol{a}}) = \{v_h \in H_0^1(\omega_{j-1}^{\boldsymbol{a}}), v_h|_K \in \mathbb{P}^p(K) \quad \forall K \in \mathcal{T}_j \subset \omega_{j-1}^{\boldsymbol{a}}\}, \tag{5.3}$$

see Fig. 4, left; the spaces $V_j^p(\omega_{j-1}^{\boldsymbol{a}})$ are defined on patches around vertices from $\mathcal{V}_{j-1}$, with finer meshes induced by $\mathcal{T}_j$, and with homogeneous Dirichlet boundary conditions imposed.

Definition 5.1 (Algebraic residual $H_0^1(\Omega)$-lifting)**.** *Define*

$$\rho_{h,\mathrm{alg}} := \rho_{0,\mathrm{alg}} + \sum_{j=1}^{J} \rho_{j,\mathrm{alg}} \in V_h^p \subset H_0^1(\Omega), \tag{5.4}$$

where $\rho_{0,\mathrm{alg}}$ *solves* (4.4) *and* $\rho_{j,\mathrm{alg}} := \sum_{\boldsymbol{a}\in\mathcal{V}_{j-1}} w_{\psi_{j-1}^{\boldsymbol{a}}}\big(\rho_{j,\mathrm{alg}}^{\boldsymbol{a}}\big) \in V_j^p$, $1 \leq j \leq J$. *Here the vertex contributions* $\rho_{j,\mathrm{alg}}^{\boldsymbol{a}}$ *on patches* $\omega_{j-1}^{\boldsymbol{a}}$ *are defined as the solution of: find* $\rho_{j,\mathrm{alg}}^{\boldsymbol{a}} \in V_j^p(\omega_{j-1}^{\boldsymbol{a}})$ *such that*

$$(\boldsymbol{A}\nabla\rho_{j,\mathrm{alg}}^{\boldsymbol{a}}, \nabla v_j)_{\omega_{j-1}^{\boldsymbol{a}}} = (r_h, v_j)_{\omega_{j-1}^{\boldsymbol{a}}} - \sum_{i=0}^{j-1} (\boldsymbol{A}\nabla\rho_{i,\mathrm{alg}}, \nabla v_j)_{\omega_{j-1}^{\boldsymbol{a}}} \qquad \forall v_j \in V_j^p(\omega_{j-1}^{\boldsymbol{a}}), \tag{5.5}$$

and $w_{\psi_{j-1}^{\boldsymbol{a}}}(\cdot)$ *stands for weighting a function* $v_h \in V_j^p(\omega_{j-1}^{\boldsymbol{a}})$ *by the hat function* $\psi_{j-1}^{\boldsymbol{a}}$ *as*

$$w_{\psi_{j-1}^{\boldsymbol{a}}}(v_h) \in V_j^p(\omega_{j-1}^{\boldsymbol{a}}), \quad w_{\psi_{j-1}^{\boldsymbol{a}}}(v_h)(\boldsymbol{x}) = \psi_{j-1}^{\boldsymbol{a}}(\boldsymbol{x}) \cdot (v_h)(\boldsymbol{x}), \quad \boldsymbol{x} \text{ Lagrange point of } K \in \mathcal{T}_j, K \subset \omega_{j-1}^{\boldsymbol{a}}.$$

As $w_{\psi_{j-1}^{\boldsymbol{a}}}\big(\rho_{j,\mathrm{alg}}^{\boldsymbol{a}}\big)$ corresponds to multiplication of the Lagrange degrees of freedom by a discrete partition of unity induced by the values of the hat functions $\psi_{j-1}^{\boldsymbol{a}}$, the above procedure more precisely corresponds to applying level-wise the weighted restricted additive Schwarz (RAS) method (see, e.g., [58]) with the domain Ω decomposed into (overlapping) patches $\omega_{j-1}^{\boldsymbol{a}}$.

The following simplification of the construction of Definition 5.1 relies on the finest mesh $\mathcal{T}_J = \mathcal{T}_h$ only. The warning example of Sec. 2.1 shows that its quality can be importantly inferior to that of Definition 5.1.

Remark 5.2 (Algebraic residual $H_0^1(\Omega)$-lifting on the finest mesh $\mathcal{T}_J$ only)**.** *Define the algebraic residual lifting*

$$\underset{\sim}{\rho}_{h,\mathrm{alg}} := \sum_{\boldsymbol{a}\in\mathcal{V}_{J-1}} w_{\psi_{J-1}^{\boldsymbol{a}}}(\underset{\sim}{\rho}_{J,\mathrm{alg}}^{\boldsymbol{a}}) \in V_J^p \subset H_0^1(\Omega),$$

where the vertex contributions $\underset{\sim}{\rho}_{J,\mathrm{alg}}^{\boldsymbol{a}} \in V_J^p(\omega_{J-1}^{\boldsymbol{a}})$ *solve*

$$(\boldsymbol{A}\nabla\underset{\sim}{\rho}_{J,\mathrm{alg}}^{\boldsymbol{a}}, \nabla v_J)_{\omega_{J-1}^{\boldsymbol{a}}} = (r_h, v_J)_{\omega_{J-1}^{\boldsymbol{a}}} \qquad \forall v_J \in V_J^p(\omega_{J-1}^{\boldsymbol{a}}). \tag{5.6}$$

5.2 Total residual $H_0^1(\Omega)$-lifting

For bounding the total error from below, we follow some basic ideas in Bramble [20], Babuška and Strouboulis [10, Sec. 5.1], Repin [74, Sec. 4.1.1], or Ern and Vohralík [44, Sec. 3.3]. In contrast to (5.3), the total residual liftings will only be defined on spaces associated with the finest mesh $\mathcal{T}_h$ and finest mesh patches $\omega_h^{\boldsymbol{a}}$, $\boldsymbol{a} \in \mathcal{V}_h$. The corresponding $H^1(\omega_h^{\boldsymbol{a}})$-conforming scalar-valued spaces are given by

$$V_h^p(\omega_h^{\boldsymbol{a}}) := \{v_h \in H^1(\omega_h^{\boldsymbol{a}}),\, v_h|_K \in \mathbb{P}^p(K) \quad \forall K \in \mathcal{T}_h \subset \omega_h^{\boldsymbol{a}},\, (v_h, 1)_{\omega_h^{\boldsymbol{a}}} = 0\} \qquad \boldsymbol{a} \in \mathcal{V}_h^{\mathrm{int}}, \tag{5.7a}$$

$$V_h^p(\omega_h^{\boldsymbol{a}}) := \{v_h \in H^1(\omega_h^{\boldsymbol{a}}),\, v_h|_K \in \mathbb{P}^p(K) \quad \forall K \in \mathcal{T}_h \subset \omega_h^{\boldsymbol{a}},\, v_h = 0 \text{ on } \partial\omega_h^{\boldsymbol{a}} \cap \partial\Omega\} \qquad \boldsymbol{a} \in \mathcal{V}_h^{\mathrm{ext}}, \tag{5.7b}$$

see Fig. 4, right. The construction reads:

Definition 5.3 (Total residual $H_0^1(\Omega)$-lifting)**.** *Define*

$$\rho_{h,\mathrm{tot}} := \sum_{\boldsymbol{a}\in\mathcal{V}_h} \psi_h^{\boldsymbol{a}} \rho_{h,\mathrm{tot}}^{\boldsymbol{a}} \in V_h^{p+1} \subset H_0^1(\Omega),$$

where the vertex contributions $\rho_{h,\mathrm{tot}}^{\boldsymbol{a}} \in V_h^p(\omega_h^{\boldsymbol{a}})$ *solve*

$$(\boldsymbol{A}\nabla\rho_{h,\mathrm{tot}}^{\boldsymbol{a}}, \nabla v_h)_{\omega_h^{\boldsymbol{a}}} = (f, \psi_h^{\boldsymbol{a}} v_h)_{\omega_h^{\boldsymbol{a}}} - (\boldsymbol{A}\nabla u_h, \nabla(\psi_h^{\boldsymbol{a}} v_h))_{\omega_h^{\boldsymbol{a}}} \qquad \forall v_h \in V_h^p(\omega_h^{\boldsymbol{a}}). \tag{5.8}$$

The local problems (5.8) are associated with homogeneous Neumann data on $\partial\omega_h^{\boldsymbol{a}}$ for interior vertices $\boldsymbol{a} \in \mathcal{V}_h^{\mathrm{int}}$ and with homogeneous Dirichlet–Neumann boundary data for boundary vertices $\boldsymbol{a} \in \mathcal{V}_h^{\mathrm{ext}}$. In the first case, they are well-posed due to the definition (5.7a) of the space $V_h^p(\omega_h^{\boldsymbol{a}})$, where the zero mean value condition is imposed. Even though $\rho_{h,\mathrm{tot}}^{\boldsymbol{a}}$ are in general nonzero on the patch boundary $\omega_h^{\boldsymbol{a}}$, the usage of the hat functions $\psi_h^{\boldsymbol{a}}$ in the definition of $\rho_{h,\mathrm{tot}}$ results in an $H_0^1(\Omega)$-conforming lifting of the total residual.

6 Poisson model problem

In this and the following section, we restrict our attention to the model Poisson problem, its conforming finite element discretization, and the solution of the arising system of linear equations by an arbitrary algebraic solver. We in particular specify the notions of the algebraic and total residuals in this context. With respect to Secs. 4 and 5, we take here $\boldsymbol{A} = \boldsymbol{I}$ for simplicity.

6.1 Poisson model problem

Let $\Omega \subset \mathbb{R}^d$, $1 \le d \le 3$, be an open bounded polytope with a Lipschitz-continuous boundary and let the source term $f \in L^2(\Omega)$. We look for a function $u : \Omega \to \mathbb{R}$ such that

$$-\Delta u = f \qquad \text{in } \Omega, \tag{6.1a}$$

$$u = 0 \qquad \text{on } \partial\Omega. \tag{6.1b}$$

In weak form, problem (6.1) reads: find $u \in H^1_0(\Omega)$ such that

$$(\nabla u, \nabla v) = (f, v) \qquad \forall v \in H^1_0(\Omega). \tag{6.2}$$

For fixed $p \ge 1$, the conforming Galerkin finite element approximation of (6.2) consists in finding $u_h^{\mathrm{ex}} \in V_h^p$ given by (3.2), (3.4) such that

$$(\nabla u_h^{\mathrm{ex}}, \nabla v_h) = (f, v_h) \qquad \forall v_h \in V_h^p. \tag{6.3}$$

Let ψ_h^l, $1 \le l \le N_h$, form a basis of V_h^p. Problem (6.3) is then equivalent to solving a system of linear algebraic equations with a symmetric positive definite matrix: find $\mathrm{U}_h^{\mathrm{ex}} \in \mathbb{R}^{N_h}$ such that

$$\mathbb{A}_h \mathrm{U}_h^{\mathrm{ex}} = \mathrm{F}_h, \tag{6.4}$$

where $(\mathbb{A}_h)_{lm} := (\nabla\psi_h^m, \nabla\psi_h^l)$, $(\mathrm{F}_h)_l := (f, \psi_h^l)$, and $u_h^{\mathrm{ex}} = \sum_{m=1}^{N_h} (\mathrm{U}_h^{\mathrm{ex}})_m \, \psi_h^m$. We note that the algebraic vector $\mathrm{U}_h^{\mathrm{ex}}$ depends on the choice of the basis of V_h^p while $u_h^{\mathrm{ex}} \in V_h^p$ does not.

6.2 Algebraic and total residuals

Let $\mathrm{U}_h \in \mathbb{R}^{N_h}$ be an *arbitrary approximation* to the exact solution $\mathrm{U}_h^{\mathrm{ex}}$ of (6.4), corresponding to

$$u_h = \sum_{m=1}^{N_h} (\mathrm{U}_h)_m \, \psi_h^m \in V_h^p. \tag{6.5}$$

The *algebraic residual vector* is then

$$\mathrm{R}_h := \mathrm{F}_h - \mathbb{A}_h \mathrm{U}_h. \tag{6.6}$$

Following Papež *et al.* [69], we associate with R_h a *discontinuous elementwise polynomial* r_h of degree p, vanishing on the boundary of Ω, i.e., $r_h \in \mathbb{P}_h^p$, $r_h|_{\partial\Omega} = 0$. Consider the Lagrange basis of V_h^p and denote by $\operatorname{supp}\psi_h^l$ the support of the basis function ψ_h^l. Then, for each fixed element $K \in \mathcal{T}_h$, we define $r_h|_K \in \mathbb{P}^p(K)$ by

$$(r_h, \psi_h^l)_K = (\mathrm{R}_h)_l \frac{|K|}{|\operatorname{supp}\psi_h^l|} = \big((f, \psi_h^l) - (\nabla u_h, \nabla\psi_h^l)\big) \frac{|K|}{|\operatorname{supp}\psi_h^l|}, \quad r_h|_{\partial K \cap \partial\Omega} = 0, \tag{6.7}$$

for all basis functions ψ_h^l of the space V_h^p non-vanishing on K. Such r_h obviously satisfies

$$(r_h, \psi_h^l) = \sum_{K \subset \operatorname{supp}\psi_h^l} (r_h, \psi_h^l)_K = (\mathrm{R}_h)_l \sum_{K \subset \operatorname{supp}\psi_h^l} \frac{|K|}{|\operatorname{supp}\psi_h^l|} = (\mathrm{R}_h)_l$$

for all $1 \le l \le N_h$, and the algebraic relation (6.6) yields

$$(r_h, v_h) = (f, v_h) - (\nabla u_h, \nabla v_h) = (\nabla(u_h^{\mathrm{ex}} - u_h), \nabla v_h) \qquad \forall v_h \in V_h^p, \tag{6.8}$$

where we have also employed (6.3). We point out that although r_h is uniquely defined by (6.7), it is not the unique element in $\mathbb{P}_h^p$ which satisfies (6.8). It is also possible to define $r_h \in V_h^p$ directly by (6.8), as in, e.g., [15]. However, this requires the solution of a globally coupled mass system, see also [69, Sec. 5.1], which we want to avoid. A level-wise construction is also possible, see Remark 7.12 below. Note that (6.8) immediately leads to (4.1).

The *total residual* $\mathcal{R}_h$ for $u_h \in V_h^p$ is a functional on $H^1_0(\Omega)$. More precisely, $\mathcal{R}_h \in H^{-1}(\Omega)$ is given by

$$\langle \mathcal{R}_h, v \rangle := (f, v) - (\nabla u_h, \nabla v) \qquad \forall v \in H^1_0(\Omega). \tag{6.9}$$

Note that in contrast to the algebraic residual R_h (respectively its representer r_h) that are both fully at our disposal, we can only access the total residual $\mathcal{R}_h$ via its action on test functions $v \in H^1_0(\Omega)$ via (6.9).

6.3 Motivation for the construction of the algebraic hierarchical liftings

In the concrete setting of Secs. 6.1–6.2, we can explain the motivation behind Definitions 4.3 and 5.1 of the algebraic liftings. Consider for this purpose a hierarchical decomposition of the algebraic error

$$\tilde{\rho}_{h,\mathrm{alg}} := \sum_{j=0}^{J} \tilde{\rho}_{j,\mathrm{alg}} \ \in V_h^p, \tag{6.10a}$$

$$\tilde{\rho}_{0,\mathrm{alg}} \in V_0^1, \qquad (\nabla\tilde{\rho}_{0,\mathrm{alg}}, \nabla v_0) = (r_h, v_0) \qquad \forall v_0 \in V_0^1, \tag{6.10b}$$

$$\tilde{\rho}_{j,\mathrm{alg}} \in V_j^p, \qquad (\nabla\tilde{\rho}_{j,\mathrm{alg}}, \nabla v_j) = (r_h, v_j) - \sum_{i=0}^{j-1} (\nabla\tilde{\rho}_{i,\mathrm{alg}}, \nabla v_j) \qquad \forall v_j \in V_j^p, \quad \forall 1 \le j \le J. \tag{6.10c}$$

We take $\tilde{\rho}_{0,\mathrm{alg}}$ equal to $\rho_{0,\mathrm{alg}}$ of the coarse residual solve (4.4), whereas $\tilde{\rho}_{j,\mathrm{alg}}$, $j \ge 1$, are corrections on increasing mesh levels recursively built from the coarsest-level. From definition (6.10c) with $j = J$, (6.10a), and (6.8), it is obvious that

$$(\nabla\tilde{\rho}_{h,\mathrm{alg}}, \nabla v_h) = (r_h, v_h) = (f, v_h) - (\nabla u_h, \nabla v_h) = (\nabla(u_h^{\mathrm{ex}} - u_h), \nabla v_h) \qquad \forall v_h \in V_h^p,$$

i.e., $\tilde{\rho}_{h,\mathrm{alg}}$ given by (6.10a) is the Riesz representer of the algebraic residual r_h on the finest finite element space V_h^p. It actually satisfies $\tilde{\rho}_{h,\mathrm{alg}} = u_h^{\mathrm{ex}} - u_h$, i.e., $\tilde{\rho}_{h,\mathrm{alg}}$ coincides with the exact algebraic error. Moreover, we find by induction, using the definition of $\tilde{\rho}_{i,\mathrm{alg}}$ and taking in (6.10c) $v_j = \tilde{\rho}_{i,\mathrm{alg}}$, $i < j$, the orthogonality relation

$$(\nabla\tilde{\rho}_{j,\mathrm{alg}}, \nabla\tilde{\rho}_{i,\mathrm{alg}}) = 0 \qquad 0 \le i, j \le J,\ j \ne i. \tag{6.11}$$

Consequently, the algebraic error $\|\nabla(u_h^{\mathrm{ex}} - u_h)\|$ admits the following hierarchical decomposition

$$\|\nabla(u_h^{\mathrm{ex}} - u_h)\|^2 = \|\nabla\tilde{\rho}_{h,\mathrm{alg}}\|^2 = \sum_{j=0}^{J} \|\nabla\tilde{\rho}_{j,\mathrm{alg}}\|^2. \tag{6.12}$$

In our construction (5.5), we restrict (6.10c) to vertex patches in a conforming finite element setting, whereas (4.11) performs a similar restriction in a mixed finite element setting.

7 Algebraic and total error bounds and their efficiency

This section summarizes our main theoretical results for the Poisson model problem (6.1) and its conforming finite element discretization. We stress that all the presented results are valid for *any* $u_h \in V_h^p$, in particular obtained on *any step* of *any algebraic iterative solver* applied to the linear system (6.4). We recall that $u \in H_0^1(\Omega)$ is the weak solution given by (6.2), $u_h^{\mathrm{ex}} \in V_h^p$ its (unavailable) finite element approximation of order p given by (6.3), and $r_h \in \mathbb{P}_h^p$ is the corresponding algebraic residual representer given by (6.7).

7.1 Guaranteed upper and lower error bounds

Relying on the $\boldsymbol{H}(\mathrm{div},\Omega)$*-liftings/reconstructions* of Concepts 4.1 and 4.2 (employed with $\boldsymbol{A} = \boldsymbol{I}$), *upper bounds* on the algebraic and total errors are obtained:

Theorem 7.1 (Guaranteed upper bounds on algebraic and total errors)**.** *Let* $\boldsymbol{\sigma}_{h,\mathrm{alg}}$ *and* $\boldsymbol{\sigma}_{h,\mathrm{dis}}$ *be respectively given by Definitions 4.3 and 4.5, with polynomial degree* $p' \in \{p, p+1\}$ *for the latter. Then*

$$\|\nabla(u_h^{\mathrm{ex}} - u_h)\| \le \|\boldsymbol{\sigma}_{h,\mathrm{alg}}\| =: \overline{\eta}_{\mathrm{alg}} \qquad \textit{(algebraic error upper bound)}, \tag{7.1a}$$

$$\|\nabla(u - u_h)\| \le \|\nabla u_h + \boldsymbol{\sigma}_{h,\mathrm{tot}}\| + \underbrace{\left(\sum_{K\in\mathcal{T}_h} \frac{h_K^2}{\pi^2} \|f - \Pi_h^{p'} f\|_K^2\right)^{\frac{1}{2}}}_{\eta_{\mathrm{osc}}}$$

$$\le \underbrace{\|\nabla u_h + \boldsymbol{\sigma}_{h,\mathrm{dis}}\|}_{\widetilde{\eta}_{\mathrm{dis}}} + \overline{\eta}_{\mathrm{alg}} + \eta_{\mathrm{osc}} =: \overline{\eta} \qquad \textit{(total error upper bound)}. \tag{7.1b}$$

Proof. Using that $(u_h^{\mathrm{ex}} - u_h) \in V_h^p$,

$$\|\nabla(u_h^{\mathrm{ex}} - u_h)\| = \sup_{v_h \in V_h^p,\, \|\nabla v_h\| = 1} (\nabla(u_h^{\mathrm{ex}} - u_h), \nabla v_h). \tag{7.2}$$

Fix $v_h \in V_h^p$ with $\|\nabla v_h\| = 1$. The exact finite element solution definition (6.3), the residual equation (6.8), and the fact that $\nabla\cdot\boldsymbol{\sigma}_{h,\mathrm{alg}} = r_h$ by Lemma 4.4 give

$$(\nabla(u_h^{\mathrm{ex}} - u_h), \nabla v_h) = (f, v_h) - (\nabla u_h, \nabla v_h) = (r_h, v_h) = (\nabla\cdot\boldsymbol{\sigma}_{h,\mathrm{alg}}, v_h) = -(\boldsymbol{\sigma}_{h,\mathrm{alg}}, \nabla v_h),$$

where we have also employed the Green theorem as $\boldsymbol{\sigma}_{h,\mathrm{alg}} \in \boldsymbol{H}(\mathrm{div}, \Omega)$ and $v_h \in H_0^1(\Omega)$. Thus the Cauchy–Schwarz inequality proves (7.1a).

Similarly, as $(u - u_h) \in H_0^1(\Omega)$, there holds

$$\|\nabla(u - u_h)\| = \sup_{v \in H_0^1(\Omega),\, \|\nabla v\| = 1} (\nabla(u - u_h), \nabla v). \tag{7.3}$$

Fix $v \in H_0^1(\Omega)$ with $\|\nabla v\| = 1$. Employing (6.2), adding and subtracting $(\boldsymbol{\sigma}_{h,\mathrm{alg}} + \boldsymbol{\sigma}_{h,\mathrm{dis}}, \nabla v)$, and using the Green theorem, we get

$$(\nabla(u - u_h), \nabla v) = (f, v) - (\nabla u_h, \nabla v) = (f - \nabla\cdot(\boldsymbol{\sigma}_{h,\mathrm{alg}} + \boldsymbol{\sigma}_{h,\mathrm{dis}}), v) - (\boldsymbol{\sigma}_{h,\mathrm{alg}} + \boldsymbol{\sigma}_{h,\mathrm{dis}} + \nabla u_h, \nabla v). \tag{7.4}$$

Recall now the Poincaré inequality

$$\|v - \Pi_h^0 v\|_K \le \frac{h_K}{\pi} \|\nabla v\|_K \qquad \forall K \in \mathcal{T}_h,$$

see [72, 14]. Employing crucially Theorem 4.7 and the Cauchy–Schwarz inequality, the first term of right-hand side of (7.4) can be estimated via

$$(f - \nabla\cdot(\boldsymbol{\sigma}_{h,\mathrm{alg}} + \boldsymbol{\sigma}_{h,\mathrm{dis}}), v) = (f - \Pi_h^{p'} f, v) = \sum_{K \in \mathcal{T}_h} (f - \Pi_h^{p'} f, v - \Pi_h^0 v)_K \le \eta_{\mathrm{osc}} \|\nabla v\| = \eta_{\mathrm{osc}}.$$

Relation (4.3) and the Cauchy–Schwarz and triangle inequalities for the second term then prove (7.1b).

□

Relying on $H_0^1(\Omega)$-*liftings* of Concepts 5.1 and 5.2, we obtain *lower bounds* on the algebraic and total errors:

Theorem 7.2 (Guaranteed lower bounds on algebraic and total errors)**.** *Let $\rho_{h,\mathrm{alg}}$ and $\rho_{h,\mathrm{tot}}$ be respectively given by Definitions 5.1 and 5.3. Then*

$$\|\nabla(u_h^{\mathrm{ex}} - u_h)\| \ge \frac{(r_h, \rho_{h,\mathrm{alg}})}{\|\nabla \rho_{h,\mathrm{alg}}\|} =: \underline{\eta}_{\mathrm{alg}} \qquad \textit{(algebraic error lower bound)}, \tag{7.5a}$$

$$\|\nabla(u - u_h)\| \ge \max\left\{ \underline{\eta}_{\mathrm{alg}}, \frac{\sum_{\boldsymbol{a} \in \mathcal{V}_h} \|\nabla \rho_{h,\mathrm{tot}}^{\boldsymbol{a}}\|_{\omega_h^{\boldsymbol{a}}}^2}{\|\nabla \rho_{h,\mathrm{tot}}\|} \right\} =: \underline{\eta} \qquad \textit{(total error lower bound)}. \tag{7.5b}$$

Proof. To prove the lower bound (7.5a) on the algebraic error, we use the norm characterization (7.2), the exact finite element solution definition (6.3), the fact that $\rho_{h,\mathrm{alg}} \in V_h^p$, and the algebraic residual representer r_h characterization (6.8) to see that

$$\|\nabla(u_h^{\mathrm{ex}} - u_h)\| \ge \frac{(f, \rho_{h,\mathrm{alg}}) - (\nabla u_h, \nabla \rho_{h,\mathrm{alg}})}{\|\nabla \rho_{h,\mathrm{alg}}\|} = \frac{(r_h, \rho_{h,\mathrm{alg}})}{\|\nabla \rho_{h,\mathrm{alg}}\|}.$$

The lower bound (7.5b) follows from the characterization (7.3), (6.2), and the fact that $\rho_{h,\mathrm{alg}}, \rho_{h,\mathrm{tot}} \in H_0^1(\Omega)$. More precisely, for $\rho_{h,\mathrm{tot}}$, we also employ Definition 5.3 as in, e.g., [69, Theorem 2]:

$$\begin{aligned}\|\nabla(u - u_h)\| &\ge \frac{(f, \rho_{h,\mathrm{tot}}) - (\nabla u_h, \nabla \rho_{h,\mathrm{tot}})}{\|\nabla \rho_{h,\mathrm{tot}}\|} \\ &= \frac{\sum_{\boldsymbol{a} \in \mathcal{V}_h} \left((f, \psi_h^{\boldsymbol{a}} \rho_{h,\mathrm{tot}}^{\boldsymbol{a}})_{\omega_h^{\boldsymbol{a}}} - (\nabla u_h, \nabla(\psi_h^{\boldsymbol{a}} \rho_{h,\mathrm{tot}}^{\boldsymbol{a}}))_{\omega_h^{\boldsymbol{a}}} \right)}{\|\nabla \rho_{h,\mathrm{tot}}\|} = \frac{\sum_{\boldsymbol{a} \in \mathcal{V}_h} \|\nabla \rho_{h,\mathrm{tot}}^{\boldsymbol{a}}\|_{\omega_h^{\boldsymbol{a}}}^2}{\|\nabla \rho_{h,\mathrm{tot}}\|}.\end{aligned}$$

□

We will finally estimate the discretization error $\|\nabla(u - u_h^{\mathrm{ex}})\|$, proceeding as in [69, Sec. 6]. We point out that neither u nor u_h^{ex} is known, so that this is the hardest estimate. The Galerkin orthogonality of u_h^{ex}, though, guarantees

$$\|\nabla(u - u_h)\|^2 = \|\nabla(u - u_h^{\mathrm{ex}})\|^2 + \|\nabla(u_h^{\mathrm{ex}} - u_h)\|^2, \tag{7.6}$$

so that we can employ the bounds of Theorems 7.1 and 7.2 to get:

Corollary 7.3 (Guaranteed bounds on the discretization error)**.** *Under the assumptions of Theorems 7.1 and 7.2, there holds*

$$\|\nabla(u - u_h^{\mathrm{ex}})\| \le \sqrt{\overline{\eta}^2 - \underline{\eta}_{\mathrm{alg}}^2} =: \overline{\eta}_{\mathrm{dis}} \qquad \textit{(discretization error upper bound)}, \tag{7.7a}$$

$$\|\nabla(u - u_h^{\mathrm{ex}})\| \ge \sqrt{\underline{\eta}^2 - \overline{\eta}_{\mathrm{alg}}^2} =: \underline{\eta}_{\mathrm{dis}} \qquad \textit{(discretization error lower bound)}, \tag{7.7b}$$

where $\underline{\eta} \ge \overline{\eta}_{\mathrm{alg}}$ is needed in (7.7b).

7.2 Efficiency of the algebraic estimates

The following theorem asserts that our algebraic error upper bound $\overline{\eta}_{\mathrm{alg}} = \|\boldsymbol{\sigma}_{h,\mathrm{alg}}\|$ from (7.1a) does not significantly overestimate the algebraic error $\|\nabla(u_h^{\mathrm{ex}} - u_h)\|$:

Theorem 7.4 (Efficiency of the algebraic upper estimate)**.** *Let $\boldsymbol{\sigma}_{h,\mathrm{alg}}$ be given by Definition 4.3. Then, in addition to (7.1a),*

$$\overline{\eta}_{\mathrm{alg}} \le \overline{C}_{\mathrm{alg}}^{\mathrm{eff}} \|\nabla(u_h^{\mathrm{ex}} - u_h)\|,$$

where $\overline{C}_{\mathrm{alg}}^{\mathrm{eff}}$ is a generic constant only depending on the shape regularity $\kappa_{\mathcal{T}}$ and refinement strength $\iota_{\mathcal{T}}$ of the mesh hierarchy $\{\mathcal{T}_j\}_{0\le j\le J}$, the space dimension d, the polynomial degree p, and the number of mesh levels J.

We postpone the (technical) proof to Appendix A below.

The efficiency of the algebraic lower estimate (respectively its slightly modified construction when the weighted restricted additive Schwarz is replaced by damped Schwarz) has been recently proved in [62, Theorem 5.1]:

Remark 7.5 (Efficiency of the algebraic lower estimate)**.** *Let the Definition 5.1 be modified such that*

$$\rho_{h,\mathrm{alg}} := \rho_{0,\mathrm{alg}} + \sum_{j=1}^{J} \rho_{j,\mathrm{alg}}, \qquad \rho_{j,\mathrm{alg}} := \frac{1}{J(d+1)} \sum_{\boldsymbol{a}\in\mathcal{V}_{j-1}} \rho_{j,\mathrm{alg}}^{\boldsymbol{a}},$$

where $\rho_{j,\mathrm{alg}}^{\boldsymbol{a}}$ solve (5.5). Then, in addition to (7.5a),

$$\underline{\eta}_{\mathrm{alg}} = \frac{(r_h, \rho_{h,\mathrm{alg}})}{\|\nabla \rho_{h,\mathrm{alg}}\|} \ge \underline{C}_{\mathrm{alg}}^{\mathrm{eff}} \|\nabla(u_h^{\mathrm{ex}} - u_h)\|,$$

where $\underline{C}_{\mathrm{alg}}^{\mathrm{eff}}$ is a generic constant depending on the shape regularity $\kappa_{\mathcal{T}}$ and refinement strength $\iota_{\mathcal{T}}$ of the mesh hierarchy $\{\mathcal{T}_j\}_{0\le j\le J}$, the space dimension d, and at most quadratically on the number of mesh levels J.

Please remark that an important difference between Theorem 7.4 and Remark 7.5 is that $\underline{C}_{\mathrm{alg}}^{\mathrm{eff}}$ is p-robust, building on the important result of [79], whereas our current proof shows that $\overline{C}_{\mathrm{alg}}^{\mathrm{eff}}$ can possibly depend on the polynomial degree p (though p-robustness is observed in numerical experiments in Sec. 9 below). Also, the weighted restricted additive Schwarz construction of Definition 5.1 actually behaves better in both the numerical experiments in Sec. 9 as well as in [62, Sec. 6] than that with damping of Remark 7.5, for which the p-robust result is available.

7.3 A safe stopping criterion balancing the algebraic and discretization errors

We believe that a good stopping criterion ensures a balance of the algebraic and discretization *errors* in the sense that

$$\|\nabla(u_h^{\mathrm{ex}} - u_h)\| \leq \gamma \|\nabla(u - u_h^{\mathrm{ex}})\|, \tag{7.8}$$

where γ is a positive user-given real parameter, typically of order 0.1; we remark that (7.8) is equivalent to the requirement that the algebraic error $\|\nabla(u_h^{\mathrm{ex}} - u_h)\|$ is $\gamma/(1+\gamma^2)^{\frac{1}{2}}$-times smaller than the total error $\|\nabla(u-u_h)\|$, see [69, Section 6.3]. In order to ensure this desirable balance and to avoid both over-resolution as well as a *possible too early stopping* of the iterative solver, we propose a *safe* stopping criterion

$$\boxed{\overline{\eta}_{\mathrm{alg}} \leq \gamma\, \underline{\eta}_{\mathrm{dis}} \qquad \text{(global safe stopping criterion)}} \tag{7.9}$$

which immediately implies (7.8) via (7.1a) and (7.7b).

7.4 Efficiency and p-robustness of the total upper estimate

Under the stopping criterion (7.9), we can crucially prove the counterpart to (7.1b) of Theorem 7.1, assessing the maximal theoretical overestimation of the total error $\|\nabla(u-u_h)\|$ by the total estimator $\overline{\eta}$:

Theorem 7.6 (Global efficiency of the total upper estimate)**.** *Let $\boldsymbol{\sigma}_{h,\mathrm{alg}}$ and $\boldsymbol{\sigma}_{h,\mathrm{dis}}$ be respectively given by Definitions 4.3 and 4.5, with polynomial degree $p' = p+1$ for the latter. Let (7.9) hold, without any requirement on the parameter γ. Let finally f be a piecewise polynomial, $f \in \mathbb{P}_h^p$. Then*

$$\boxed{\overline{\eta} = \widetilde{\eta}_{\mathrm{dis}} + \overline{\eta}_{\mathrm{alg}} \leq \overline{C}_{\mathrm{tot}}^{\mathrm{eff}} \|\nabla(u-u_h)\|,} \tag{7.10}$$

where $\overline{C}_{\mathrm{tot}}^{\mathrm{eff}} = (1+\gamma)C$ and where $C = 2(d+1)C_{\mathrm{st}}C_{\mathrm{cont,PF}}$, see (B.2) and (B.3) below, is a generic constant only depending on the shape regularity $\kappa_{\mathcal{T}}$ of the mesh $\mathcal{T}_h$ and the space dimension d.

Please remark that here again, as in Remark 7.5, $\overline{C}_{\mathrm{tot}}^{\mathrm{eff}}$ is independent of the polynomial degree p. The proof builds on the seminal contribution of Braess *et al.* [18, Theorem 7] in two space dimensions, its extension [45, Corollaries 3.3 and 3.6] to three space dimensions, and the treatment of the algebraic term as in [43, 69]. It is technical and we postpone it to Appendix B below.

7.5 Safe local stopping criteria and p-robust local efficiency of the upper total estimate

The stopping criterion (7.9) is global (encompasses the whole domain Ω) and consequently local effects might be missed. To remedy, we can ask that locally, patch by patch around the nodes of the finest mesh $\mathcal{T}_h$, the local algebraic estimators are small enough. Denote $\overline{\eta}_{\mathrm{alg},\omega_h^{\boldsymbol{a}}} := \|\boldsymbol{\sigma}_{h,\mathrm{alg}}\|_{\omega_h^{\boldsymbol{a}}}$, $\boldsymbol{a} \in \mathcal{V}_h$, and let $\gamma_K > 0$, $\forall K \in \mathcal{T}_h$, be fixed real parameters, typically of order 0.1. Then, we can tighten (7.9) to

$$\boxed{\overline{\eta}_{\mathrm{alg},\omega_h^{\boldsymbol{a}}} \leq \min_{K \subset \omega_h^{\boldsymbol{a}}} \frac{\gamma_K}{(1+\gamma_K^2)^{\frac{1}{2}}} \frac{\|\nabla \rho_{h,\mathrm{tot}}^{\boldsymbol{a}}\|_{\omega_h^{\boldsymbol{a}}}}{C_{\mathrm{cont,PF}}} \quad \forall \boldsymbol{a} \in \mathcal{V}_h \qquad \text{(local safe stopping criterion).}} \tag{7.11}$$

These *local criteria* in particular allow to prove the *local efficiency* result, where we express η_* as the sum of elementwise contributions $\eta_{*,K}$, i.e., $\eta_* = \left\{ \sum_{K \in \mathcal{T}_h} (\eta_{*,K})^2 \right\}^{1/2}$:

Theorem 7.7 (Local efficiency of the total upper estimate)**.** *Let $\boldsymbol{\sigma}_{h,\mathrm{alg}}$ and $\boldsymbol{\sigma}_{h,\mathrm{dis}}$ be respectively given by Definitions 4.3 and 4.5, with polynomial degree $p' = p+1$ for the latter. Let (7.11) hold, without any requirements on the parameters γ_K. Let finally f be a piecewise polynomial, $f \in \mathbb{P}_h^p$. Then*

$$\boxed{\widetilde{\eta}_{\mathrm{dis},K} + \overline{\eta}_{\mathrm{alg},K} \leq \overline{C}_{\mathrm{tot},K}^{\mathrm{eff}} \sum_{\boldsymbol{a} \in \mathcal{V}_h,\, \boldsymbol{a} \subset \partial K} \|\nabla(u-u_h)\|_{\omega_h^{\boldsymbol{a}}} \qquad \forall K \in \mathcal{T}_h,} \tag{7.12}$$

where $\overline{C}_{\mathrm{tot},K}^{\mathrm{eff}} = (1+\gamma_K)C$ and where $C = 2C_{\mathrm{st}}C_{\mathrm{cont,PF}}$ is a generic constant only depending on the shape regularity $\kappa_{\mathcal{T}}$ of the mesh $\mathcal{T}_h$ and the space dimension d.

7.6 Remarks

Several remarks and comments on the results of Sections 7.1–7.5 are in order.

Remark 7.8 (Lower bound on the total error)**.** *As shown in [69, Remark 2], for the total lower estimate of (7.5b), there holds*

$$\underline{\eta} \geq \frac{\left(\sum_{\boldsymbol{a}\in\mathcal{V}_h} \|\nabla \rho_{h,\mathrm{tot}}^{\boldsymbol{a}}\|_{\omega_h^{\boldsymbol{a}}}^2\right)^{\frac{1}{2}}}{C_{\mathrm{cont,PF}}\sqrt{d+1}},$$

where $C_{\mathrm{cont,PF}}$ is the constant from inequality (B.2) below. This lower bound on the total error has an ℓ^2 structure with respect to the patches around mesh vertices (can be written as a square root of a sum of squares), but is less precise than $\underline{\eta}$.

Remark 7.9 (Stopping criteria ensuring efficiency of the total estimate but not surely balancing the algebraic and discretization error components)**.** *In some references like [61, 16, 53, 7, 43, 69], an upper bound on the total error distinguishing the algebraic and discretization error indicators in the spirit of (7.1b) has been obtained. Then, the stopping criteria*

$$\overline{\eta}_{\mathrm{alg}} \leq \gamma(\widetilde{\eta}_{\mathrm{dis}} + \eta_{\mathrm{osc}}) \qquad \textit{(global stopping criterion)}, \tag{7.13a}$$

$$\overline{\eta}_{\mathrm{alg},\omega_h^{\boldsymbol{a}}} \leq \min_{K\subset\omega_h^{\boldsymbol{a}}} \gamma_K(\widetilde{\eta}_{\mathrm{dis},K} + \eta_{\mathrm{osc},K}) \quad \forall \boldsymbol{a}\in\mathcal{V}_h \qquad \textit{(local stopping criterion)}, \tag{7.13b}$$

for some real parameters $\gamma > 0$ and $\gamma_K > 0$, $K\in\mathcal{T}_h$, typically of order 0.1, suggest themselves. Note that, though criteria (7.13) typically perform well in practice, they, in contrast to criteria (7.9) or (7.11), do not necessarily ensure the desired balance (7.8). In particular, $\widetilde{\eta}_{\mathrm{dis}}$ is numerically observed but not proven to provide a bound on the discretization error. This, on the other hand, does not preclude the efficiency of the total estimate: if the global stopping criterion (7.13a) is satisfied with parameter γ such that

$$\gamma \leq \frac{1}{2(d+1)C_{\mathrm{st}}C_{\mathrm{cont,PF}}}, \tag{7.14a}$$

then (7.10) still holds true. Similarly, if the local stopping criteria (7.13b) are satisfied with parameters γ_K such that

$$\gamma_K \leq \frac{1}{2(d+1)C_{\mathrm{st}}C_{\mathrm{cont,PF}}} \qquad \forall K\in\mathcal{T}_h, \tag{7.14b}$$

then (7.12) holds true; we refer to Appendix B for the proofs of these two claims. In words, with (7.13) we know how big the total error is, and possibly where is it localized, but we are not sure to know whether the algebraic and discretization errors are already in a good balance (the algebraic error may still dominate).

Remark 7.10 ($\boldsymbol{\sigma}_{h,\mathrm{dis}}$ of polynomial degree $p'=p$)**.** *Let the flux reconstruction $\boldsymbol{\sigma}_{h,\mathrm{dis}}$ of Definition 4.5 be constructed in the space $\boldsymbol{V}_h^{p'}$ with the lower polynomial degree $p'=p$ and let, for simplicity, $f\in\mathbb{P}_h^{p-1}$. Then efficiencies (7.10) and (7.12) still hold with constants $\overline{C}_{\mathrm{tot}}^{\mathrm{eff}} = (d+1)C_{\mathrm{st}}C_{\mathrm{cont,PF}} + \gamma C$ and $\overline{C}_{\mathrm{tot},K}^{\mathrm{eff}} = C_{\mathrm{st}}C_{\mathrm{cont,PF}} + \gamma_K C$ respectively, but the constant C can now theoretically depend on the polynomial degree p, see Appendix B for a proof. The numerical experiments in Sec. 9 are realized with this choice $p'=p$, and no loss of p-robustness is observed in practice.*

Remark 7.11 ($\boldsymbol{H}(\mathrm{div},\Omega)$-liftings with minimal algebraic error resolution)**.** *In [43, Definition 6.9] a different definition for $\boldsymbol{\sigma}_{h,\mathrm{dis}}^{\boldsymbol{a}}$ is used, where $r_h\psi_h^{\boldsymbol{a}}$ in (4.14b) is replaced by the constant $(r_h\psi_h^{\boldsymbol{a}},1)_{\omega_h^{\boldsymbol{a}}}/|\omega_h^{\boldsymbol{a}}|$ and similarly in (4.7b) and (4.11b). Such construction is cheaper and still leads to $\nabla\cdot(\boldsymbol{\sigma}_{h,\mathrm{alg}}+\boldsymbol{\sigma}_{h,\mathrm{dis}}) = \Pi_h^{p'} f$, as in Theorem 4.7, so that the total upper bound (7.1b) of Theorem 7.1 still holds true. However, in such a case, $\nabla\cdot\boldsymbol{\sigma}_{h,\mathrm{alg}} \neq r_h$, and, consequently, there is no algebraic error control in the sense of (7.1a) of Theorem 7.1. Moreover, safe stopping criteria (7.9) or (7.11) cannot be designed. On the other hand, under the stopping criteria (7.13), the global and local efficiencies of the total upper estimate of Theorems 7.6 and 7.7 hold with no need for conditions (7.14), and the choice $p'=p$ is sufficient.*

Remark 7.12 (Level-wise representation and lifting of the algebraic residual)**.** *The representation $r_h\in\mathbb{P}_h^p$ of the algebraic residual in (6.7) is specified on the finest mesh $\mathcal{T}_h$ only. In Definition 4.3, we then employ $\Pi_1^p(r_h\psi_0^{\boldsymbol{a}})$ (minus $\Pi_1^p(\boldsymbol{A}\nabla\rho_{0,\mathrm{alg}}\cdot\nabla\psi_0^{\boldsymbol{a}})$) for $j=1$ and $\Pi_j^p(\mathrm{Id}-\Pi_{j-1}^p)(r_h\psi_{j-1}^{\boldsymbol{a}}) = (\Pi_j^p-\Pi_{j-1}^p)(r_h\psi_{j-1}^{\boldsymbol{a}})$ for $j>1$. This leads to, using the notation $\Pi_0^p=0$, cf. (4.12),*

$$\sum_{j=1}^{J}\sum_{\boldsymbol{a}\in\mathcal{V}_{j-1}} (\Pi_j^p-\Pi_{j-1}^p)(r_h\psi_{j-1}^{\boldsymbol{a}}) = \sum_{j=1}^{J}(\Pi_j^p-\Pi_{j-1}^p)r_h = \Pi_h^p r_h - \Pi_0^p r_h = r_h.$$

In the context of the finite element method (6.3), alternatively, we may repeat (6.7) on each mesh level $1 \le j \le J$, i.e., we may define $r_j \in \mathbb{P}_j^p$ by prescribing on each $K \in \mathcal{T}_j$,

$$(r_j, \psi_j^l)_K = (\mathrm{R}_j)_l \frac{|K|}{|\operatorname{supp} \psi_j^l|} = \big((f, \psi_j^l) - (\nabla u_h, \nabla \psi_j^l)\big) \frac{|K|}{|\operatorname{supp} \psi_j^l|}, \quad r_j|_{\partial K \cap \partial\Omega} = 0, \tag{7.15}$$

where ψ_j^l are the basis functions of level j. In Definition 4.3, we can then employ $\Pi_1^p(r_1 \psi_0^{\boldsymbol{a}})$ (minus $\Pi_1^p(\boldsymbol{A}\nabla\rho_{0,\mathrm{alg}}\cdot\nabla\psi_0^{\boldsymbol{a}})$) for $j = 1$ and $\Pi_j^p((r_j - r_{j-1})\psi_{j-1}^{\boldsymbol{a}})$ for $j > 1$. Denoting $r_0 = 0$, this leads to

$$\sum_{j=1}^{J} \sum_{\boldsymbol{a} \in \mathcal{V}_{j-1}} (\Pi_j^p((r_j - r_{j-1})\psi_{j-1}^{\boldsymbol{a}})) = \sum_{j=1}^{J} (r_j - r_{j-1}) = r_J - r_0 = r_h.$$

With such a construction, the constants C in (A.9) and (A.10) on steps 4 and 5 of the proof of Theorem 7.4 below get independent of J, and consequently, the constant $\overline{C}_{\mathrm{alg}}^{\mathrm{eff}}$ in Theorem 7.4 depends at most linearly on the number of mesh levels J.

8 Implementation, evaluation cost, and cheap equivalent versions

In this section, we briefly comment on the cost of evaluating the developed error estimators and discuss how it can be reduced in comparison to a straightforward implementation of the presented definitions.

8.1 The coarsest level problem

The solution $\rho_{0,\mathrm{alg}}$ of (4.4) requests to solve a linear system with the number of unknowns given by the number of interior vertices of the mesh $\mathcal{T}_0$, which can be considered as negligible. Obtaining the actual piecewise polynomial $\rho_{0,\mathrm{alg}}$ as a function on the finest mesh $\mathcal{T}_h$, however, brings the algorithmic price to the order of one geometric multigrid cycle without any smoothing. Note that the coarsest level solve (4.4) is not necessary at all when the iterative solver itself is a geometric multigrid without any post-smoothing: then $\rho_{0,\mathrm{alg}} = 0$ since any iterate u_h satisfies

$$(f, v_0) - (\nabla u_h, \nabla v_0) = (r_h, v_0) = 0 \qquad \forall v_0 \in V_0^1. \tag{8.1}$$

8.2 Efficient implementation of the proposed estimators

Let $\boldsymbol{\psi}_h^l$, $1 \le l \le \dim(\boldsymbol{V}_h^p)$, denote the basis functions of the Raviart–Thomas–Nédélec space $\boldsymbol{V}_h^p = \boldsymbol{V}_J^p$. Then developing $\boldsymbol{\sigma}_{h,\mathrm{alg}} = \sum_{l=1}^{\dim(\boldsymbol{V}_h^p)} (\mathrm{S}_h)_l \boldsymbol{\psi}_h^l$, the algebraic error estimator $\overline{\eta}_{\mathrm{alg}} = \|\boldsymbol{\sigma}_{h,\mathrm{alg}}\|$ from Theorem 7.1 takes the form

$$\|\boldsymbol{\sigma}_{h,\mathrm{alg}}\|^2 = \mathrm{S}_h^t \mathbb{M}_h \mathrm{S}_h, \tag{8.2}$$

where the global mixed finite element matrix $\mathbb{M}_h$ is given by $(\mathbb{M}_h)_{lm} := (\boldsymbol{\psi}_h^m, \boldsymbol{\psi}_h^l)$. For the coefficients S_h, we see from (4.10) that

$$\mathrm{S}_h = \sum_{j=1}^{J} \sum_{\boldsymbol{a} \in \mathcal{V}_{j-1}} \mathbb{P}_j^J \mathrm{S}_j^{\boldsymbol{a}} \tag{8.3}$$

with an appropriate prolongation matrix $\mathbb{P}_j^J$. These two operations are of optimal complexity, though the passages over different mesh levels via the prolongation matrix $\mathbb{P}_j^J$ again bring the algorithmic price to the order of one geometric multigrid cycle without any smoothing.

The main question is the cost of obtaining the local coefficients $\mathrm{S}_j^{\boldsymbol{a}}$. The key advantage of the problems (4.7), (4.11) which define $\mathrm{S}_j^{\boldsymbol{a}}$ is that they are *local* to the patch $\omega_{j-1}^{\boldsymbol{a}}$ and independent one from each other, enabling a *perfectly scalable parallelization*. Unfortunately, in a direct implementation of (4.7), (4.11), cf. [69, Appendix B], the size of the local matrices is not very small (for lowest-order finite elements $p = 1$ in two space dimensions for example, cf. Fig. 3, left, there are 179 degrees of freedom overall). Though the operations for solving small dense systems are generally cheap on modern computers, it is wise to consider more efficient implementations. In particular, the costs can be reduced importantly by noticing that:

- Using an equivalent implementation of (4.7), (4.11) via *hybridization* (see, e.g., [24, Sec. V.2]) reduces the size of the local matrices; in the above example, there are 84 unknowns in place of 179. On the other hand, the degrees of freedom S_h of the algebraic residual $\boldsymbol{H}(\mathrm{div}, \Omega)$-lifting $\boldsymbol{\sigma}_{h,\mathrm{alg}}$ still need to be obtained to develop (8.2).

p (N_h)	MG iter	algebraic error	eff. index UB	eff. index LB	total error	eff. index UB	eff. index LB	discretization error	eff. index UB	eff. index LB
1 (3.5×10^4)	1	1.2	1.11	1.03^{-1}	1.3	1.46	1.05^{-1}	2.4×10^{-1}	5.85	—
	2	8.0×10^{-2}	1.13	1.04^{-1}	2.5×10^{-1}	1.35	1.05^{-1}		1.39	1.08^{-1}
	3	5.1×10^{-3}	1.15	1.06^{-1}	2.4×10^{-1}	1.06	1.03^{-1}		1.06	1.03^{-1}
2 (1.4×10^5)	1	1.2	1.10	1.00^{-1}	1.2	1.48	1.00^{-1}	2.9×10^{-3}	4.50×10^2	—
	2	1.1×10^{-1}	1.18	1.00^{-1}	1.1×10^{-1}	1.77	1.01^{-1}		5.29×10^1	—
	3	2.8×10^{-3}	1.18	1.01^{-1}	4.1×10^{-3}	1.66	1.19^{-1}		2.10	4.28^{-1}
	4	9.6×10^{-5}	1.20	1.02^{-1}	2.9×10^{-3}	1.05	1.03^{-1}		1.05	1.03^{-1}
3 (3.2×10^5)	1	5.9×10^{-1}	1.09	1.00^{-1}	5.9×10^{-1}	1.33	1.00^{-1}	2.2×10^{-5}	2.36×10^4	—
	3	2.2×10^{-3}	1.19	1.00^{-1}	2.2×10^{-3}	1.75	1.00^{-1}		1.42×10^2	—
	5	1.0×10^{-5}	1.19	1.01^{-1}	2.4×10^{-5}	1.44	1.37^{-1}		1.52	1.70^{-1}
	6	1.4×10^{-6}	1.18	1.01^{-1}	2.2×10^{-5}	1.08	1.12^{-1}		1.08	1.12^{-1}
4 (5.6×10^5)	1	4.5×10^{-1}	1.08	1.00^{-1}	4.5×10^{-1}	1.39	1.00^{-1}	1.5×10^{-7}	2.90×10^6	—
	4	1.2×10^{-4}	1.13	1.00^{-1}	1.2×10^{-4}	1.58	1.00^{-1}		9.64×10^2	—
	7	6.4×10^{-7}	1.11	1.01^{-1}	6.5×10^{-7}	1.53	1.03^{-1}		5.21	—
	10	8.3×10^{-9}	1.12	1.01^{-1}	1.5×10^{-7}	1.06	1.16^{-1}		1.06	1.16^{-1}

Table 1: Sinus problem, multigrid V-cycles: effectivity of the upper (UB) and lower (LB) error bounds

p (N_h)	algebraic error	eff. index UB	eff. index LB	total error	eff. index UB	eff. index LB	discretization error	eff. index UB	eff. index LB
1 (3.5×10^4)	8.7×10^{-4}	1.03	1.01^{-1}	2.4×10^{-1}	1.04	1.03^{-1}	2.4×10^{-1}	1.04	1.03^{-1}
2 (1.4×10^5)	1.9×10^{-5}	1.10	1.01^{-1}	2.9×10^{-3}	1.02	1.02^{-1}	2.9×10^{-3}	1.02	1.02^{-1}
3 (3.2×10^5)	2.6×10^{-6}	1.08	1.00^{-1}	2.2×10^{-5}	1.12	1.13^{-1}	2.2×10^{-5}	1.12	1.14^{-1}
4 (5.6×10^5)	5.1×10^{-8}	1.03	1.00^{-1}	1.6×10^{-7}	1.29	1.38^{-1}	1.5×10^{-7}	1.32	1.47^{-1}

Table 2: Sinus problem, one full multigrid cycle: effectivity of the upper (UB) and lower (LB) error bounds

- The local matrices can be assembled and factorized only *once* in a preparatory step before the iterative solver applied to (6.4) is started. In each iteration, the estimators are then evaluated by forward-backward substitution. This, however, increases importantly the memory requirements.
- On a *structured mesh*, the local matrices associated with (4.7), (4.11) are the *same* for *all interior vertices*. Also, on locally refined unstructured meshes as in [48] or in those created by newest-vertex bisection, only a *handful of different patch geometries* and associated matrices exists, especially in two space dimensions. One then, however, additionally needs to keep track of the different cases.
- Lowest-degree spaces $\boldsymbol{V}_j^0(\omega_{j-1}^{\boldsymbol{a}})$ can be used instead of $\boldsymbol{V}_j^p(\omega_{j-1}^{\boldsymbol{a}})$ for all levels except of J. There is no impact on the presented theory and no noticeable impact on numerical experiments, see [70] for details. On the other hand, the cost on the level J is dominating.

The cost of obtaining $\boldsymbol{\sigma}_{h,\mathrm{dis}}$ is, in turn, smaller since:

- Only the finest mesh $\mathcal{T}_h = \mathcal{T}_J$ and its vertices from the set $\mathcal{V}_h = \mathcal{V}_J$ are employed, there is no run through all mesh levels.
- The sizes of the local matrices are much smaller (42 and 24 instead of the above 179 and 84, respectively, for $p = p' = 1$), as the spaces $\boldsymbol{V}_h^{p'}(\omega_h^{\boldsymbol{a}})$ and $\mathbb{P}_h^{p'}(\omega_h^{\boldsymbol{a}})$ of (4.13) associated with local problems (4.14) are defined on the smaller patches of finest mesh elements only, cf. Fig. 3, right.

Even with the above considerations, the costs may still be important. Thus, avoiding the solutions of the local patchwise problems following [70] that we describe further is appealing.

8.3 Equivalent explicit version without local patchwise problems

Following [38], [59], [85, Sec. 4.3.3], the proof of [18, Theorem 7], [42], or [45, Sec. 6], there are ways to replace the minimizations (4.9), (4.11), and (4.14) by a simplification obtained by a run through the patch of the elements sharing the given vertex, *avoiding the solutions* of the local (high-order) mixed *patchwise*

p (N_h)	PCG iter	algebraic error	eff. index UB	eff. index LB	total error	eff. index UB	eff. index LB	discretization error	eff. index UB	eff. index LB
1 (3.5×10^4)	3	6.4×10^{-2}	1.01	1.00^{-1}	2.5×10^{-1}	1.26	1.06^{-1}	2.4×10^{-1}	1.28	1.07^{-1}
	6	1.3×10^{-2}	1.01	1.00^{-1}	2.4×10^{-1}	1.09	1.03^{-1}		1.09	1.03^{-1}
2 (1.4×10^5)	5	5.2×10^{-2}	1.01	1.00^{-1}	5.2×10^{-2}	1.09	1.00^{-1}	2.9×10^{-3}	7.88	—
	10	5.6×10^{-3}	1.00	1.00^{-1}	6.3×10^{-3}	1.36	1.13^{-1}		2.23	—
	15	1.2×10^{-4}	1.01	1.00^{-1}	2.9×10^{-3}	1.05	1.02^{-1}		1.05	1.02^{-1}
3 (3.2×10^5)	11	4.2×10^{-2}	1.00	1.00^{-1}	4.2×10^{-2}	1.05	1.00^{-1}	2.2×10^{-5}	6.11×10^2	—
	22	6.3×10^{-3}	1.00	1.00^{-1}	6.3×10^{-3}	1.05	1.00^{-1}		9.46×10^1	—
	33	6.7×10^{-5}	1.01	1.00^{-1}	7.0×10^{-5}	1.29	1.05^{-1}		2.76	—
	44	8.0×10^{-7}	1.00	1.00^{-1}	2.2×10^{-5}	1.04	1.10^{-1}		1.04	1.10^{-1}
4 (5.6×10^5)	15	2.6×10^{-2}	1.00	1.00^{-1}	2.6×10^{-2}	1.05	1.00^{-1}	1.5×10^{-7}	5.52×10^4	—
	30	7.0×10^{-4}	1.01	1.00^{-1}	7.0×10^{-4}	1.08	1.00^{-1}		1.88×10^3	—
	45	9.1×10^{-7}	1.00	1.00^{-1}	9.3×10^{-7}	1.16	1.01^{-1}		3.80	—
	60	2.5×10^{-9}	1.01	1.00^{-1}	1.5×10^{-7}	1.02	1.15^{-1}		1.02	1.15^{-1}

Table 3: Sinus problem, PCG iterations: effectivity of the upper (UB) and lower (LB) error bounds

problems, while still maintaining all the results of Sec. 7, in particular the guaranteed constant-free bounds, efficiency, and p-robustness. We present these modifications in detail in [70]; an almost indistinguishable accuracy of the bounds is observed, with an importantly reduced cost. Similar ideas apply to the linear systems (5.5) and (5.8) following [45, Sec. 5], avoiding the solutions of the local high-order primal patchwise problems, with in particular Theorem 7.2 still holding true.

9 Numerical results

We illustrate in this section the performance of our a posteriori error estimates and of the corresponding adaptive stopping criteria from Secs. 6 and 7. We consider the model problem (6.1) with three different choices of the domain $\Omega \subset \mathbb{R}^2$ and of the exact solution u:

$$\begin{aligned}
&\Omega := (-1,1)^2, && u(x,y) := \sin(2\pi x)\sin(2\pi y) && \text{sinus},\\
&\Omega := (0,1)^2, && u(x,y) := x(x-1)y(y-1)\exp\left(-100((x-\tfrac{1}{2})^2-(y-\tfrac{117}{1000})^2)\right) && \text{peak},\\
&\Omega := (-1,1)^2 \setminus [0,1]\times[-1,0], && u(r,\theta) := r^{2/3}\sin(2\theta/3) && \text{L-shape}.
\end{aligned}$$

In the last case, we impose an inhomogeneous Dirichlet boundary condition corresponding to the prescribed exact solution. The additional boundary approximation error is neglected since it is of higher order with respect to the $H^{1/2}(\partial\Omega)$-norm compared to the $H^1(\Omega)$-seminorm on the domain.

We consider the finite element method (6.3) with the polynomial degrees $p = 1, \dots, 4$. For each test problem, we start from an initial Delaunay triangulation of the domain Ω and consider four uniform refinement steps, so that $J = 4$. In each step, each triangle is decomposed into four congruent subtriangles. The arising algebraic systems (6.4) are solved iteratively by three different solvers: 1) a geometric multigrid method (MG) with V(5,0)-cycles, employing 5 Gauss–Seidel pre-smoothing iterations and no post-smoothing; 2) a full multigrid (FMG) method using a single V(3,3)-cycle on each level, with 3 Gauss–Seidel pre- and post-smoothing iterations; 3) a preconditioned conjugate gradient method (PCG) with an incomplete Cholesky preconditioner with the relative drop-off tolerance 10^{-4} (see, e.g., [78, Sec. 10.4]). The multigrid transfer operators are the canonical ones, exploiting the nestedness of the finite element spaces associated with the different mesh levels.

For this work, we use the standard Lagrange bases and mesh-based nestedness only, we do not employ the p-multigrid techniques of, e.g., Pasquetti and Rapetti [71] or Sundar *et al.* [81], or hierarchical bases, see, e.g., Vassilevski [82] and the references therein. Our starting iterate is the zero vector, and we use the stopping criterion (7.13a) with the parameter $\gamma = 0.1$, except for the FMG method with V(3,3)-cycle, for which one single iteration is performed. For the multigrid iteration using V(5,0)-cycles, all our iterates satisfy (up to possible round-off errors in the direct solver on the coarsest level) the coarsest-level orthogonality property (8.1) so that the coarsest level solve (4.4) is not required. This is not the case for the FMG method and the PCG solver. Here, after each iteration, we solve the coarsest-level defect problem (4.4) to construct the Riesz representer $\rho_{0,\mathrm{alg}} \in V_0^p$. The algebraic residual $\boldsymbol{H}(\mathrm{div},\Omega)$-lifting $\boldsymbol{\sigma}_{h,\mathrm{alg}}$ and the discretization flux reconstruction $\boldsymbol{\sigma}_{h,\mathrm{dis}}$ are constructed by Definitions 4.3 and 4.5, respectively, with $p' = p$, and the algebraic and total residual liftings $\rho_{h,\mathrm{alg}}$ and $\rho_{h,\mathrm{tot}}$ are obtained by Definitions 5.1 and 5.3, respectively.

p (N_h)	MG iter	algebraic error	eff. index UB	eff. index LB	total error	eff. index UB	eff. index LB	discretization error	eff. index UB	eff. index LB
1 (9.3×10^3)	1	6.1×10^{-3}	1.13	1.02^{-1}	6.9×10^{-3}	1.61	1.16^{-1}	3.3×10^{-3}	2.84	—
	2	1.9×10^{-4}	1.13	1.03^{-1}	3.3×10^{-3}	1.10	1.03^{-1}		1.10	1.03^{-1}
2 (3.8×10^4)	1	7.5×10^{-3}	1.13	1.00^{-1}	7.5×10^{-3}	1.61	1.00^{-1}	1.1×10^{-4}	8.53×10^{1}	—
	2	4.5×10^{-4}	1.17	1.01^{-1}	4.6×10^{-4}	1.76	1.04^{-1}		6.13	—
	3	8.1×10^{-6}	1.17	1.01^{-1}	1.1×10^{-4}	1.10	1.03^{-1}		1.10	1.03^{-1}
3 (8.5×10^4)	1	4.9×10^{-3}	1.10	1.00^{-1}	4.9×10^{-3}	1.40	1.00^{-1}	2.9×10^{-6}	1.68×10^{3}	—
	3	1.3×10^{-5}	1.18	1.00^{-1}	1.3×10^{-5}	1.75	1.03^{-1}		6.66	—
	5	7.8×10^{-9}	1.17	1.00^{-1}	2.9×10^{-6}	1.01	1.11^{-1}		1.01	1.11^{-1}
4 (1.5×10^5)	1	4.4×10^{-3}	1.09	1.00^{-1}	4.4×10^{-3}	1.44	1.00^{-1}	6.3×10^{-8}	7.28×10^{4}	—
	3	1.8×10^{-5}	1.15	1.00^{-1}	1.8×10^{-5}	1.67	1.00^{-1}		3.72×10^{2}	—
	5	2.4×10^{-8}	1.11	1.00^{-1}	6.8×10^{-8}	1.34	1.35^{-1}		1.38	1.49^{-1}
	6	1.1×10^{-9}	1.11	1.00^{-1}	6.3×10^{-8}	1.02	1.15^{-1}		1.02	1.15^{-1}

Table 4: Peak problem, multigrid V-cycles: effectivity of the upper (UB) and lower (LB) error bounds

p (N_h)	algebraic error	eff. index UB	eff. index LB	total error	eff. index UB	eff. index LB	discretization error	eff. index UB	eff. index LB
1 (9.3×10^3)	1.8×10^{-5}	1.02	1.00^{-1}	3.3×10^{-3}	1.04	1.03^{-1}	3.3×10^{-3}	1.04	1.03^{-1}
2 (3.8×10^4)	1.9×10^{-7}	1.07	1.00^{-1}	1.1×10^{-4}	1.01	1.01^{-1}	1.1×10^{-4}	1.01	1.01^{-1}
3 (8.5×10^4)	2.2×10^{-7}	1.08	1.00^{-1}	2.9×10^{-6}	1.08	1.12^{-1}	2.9×10^{-6}	1.08	1.13^{-1}
4 (1.5×10^5)	9.1×10^{-9}	1.05	1.00^{-1}	6.4×10^{-8}	1.14	1.25^{-1}	6.3×10^{-8}	1.15	1.26^{-1}

Table 5: Peak problem, one full multigrid cycle: effectivity of the upper (UB) and lower (LB) error bounds

Tables 1–8 show the values of the total, algebraic, and discretization errors and the effectivity indices of the upper and lower bounds of the estimators $\overline{\eta}$, $\overline{\eta}_{\mathrm{alg}}$, $\overline{\eta}_{\mathrm{dis}}$, $\underline{\eta}$, $\underline{\eta}_{\mathrm{alg}}$, and $\underline{\eta}_{\mathrm{dis}}$ of Theorems 7.1 and 7.2 and of Corollary 7.3, at specified iterations of the multigrid and conjugate gradient solvers. The effectivity indices for the different terms are computed by

$$\text{effectivity index} := \frac{\text{bound}}{\text{error}}.$$

As for estimating the discretization error, the lower bound $\underline{\eta}_{\mathrm{dis}}$ is not computable in the iterations where the algebraic error is the dominating component of the total one; here the condition $\overline{\eta}_{\mathrm{alg}} \leq \underline{\eta}$ of Corollary 7.3 is not satisfied. Actually, while the algebraic error is the dominating factor, the upper bound $\overline{\eta}_{\mathrm{dis}}$ may not provide a relevant information about the discretization error. Deriving a bound on the discretization error that provides an accurate estimate also for approximations with dominating algebraic error is, to the best of our knowledge, an unresolved issue. However, when the stopping criterion (7.13a) is satisfied, all our upper and lower bounds on all the algebraic, total, and discretization errors are very precise, with effectivity indices always below 1.7. Note finally that in the full multigrid case, the algebraic error is typically reduced to the discretization error within one step. In addition to the presented results, we also tested the accuracy of the approximate discretization error estimator $\widetilde{\eta}_{\mathrm{dis}}$, see (7.1b). In our experiments it actually bounds the discretization error from above and is always smaller than the guaranteed discretization error upper bound $\overline{\eta}_{\mathrm{dis}}$ given in Corollary 7.3, although we have no theoretical proof for this.

In Fig. 5, we plot the discretization and algebraic errors as well as their guaranteed upper and lower bounds, together with the (non-guaranteed) estimator $\widetilde{\eta}_{\mathrm{dis}} = \|\nabla u_h + \boldsymbol{\sigma}_{h,\mathrm{dis}}\|$, for the multigrid V-cycles/conjugate gradient solvers applied to the L-shape problem as in Tables 7 and 9. We highlight there by an arrow the iterations where respectively the safe stopping criterion (7.9) and the alternative stopping criterion (7.13a) stop the iterations. In these examples, there is no important difference, but the rather important over-estimation of the discretization error by $\widetilde{\eta}_{\mathrm{dis}}$ in the first iterations throws a shadow of a doubt on (7.13a). For completeness, the total errors together with their guaranteed upper and lower bounds are plotted in Fig. 6.

The upper bounds (7.1b) and (7.1a) allow estimating the local distribution of the algebraic and total errors. In the numerical experiments, we observe that $\eta_K := \widetilde{\eta}_{\mathrm{dis},K} + \overline{\eta}_{\mathrm{alg},K} + \eta_{\mathrm{osc},K}$ and $\overline{\eta}_{\mathrm{alg},K}$ show an excellent agreement for the local error distribution of the total and algebraic errors, respectively, see Figures 7–12. Note that the local distribution of the algebraic and discretization errors can be very different

p (N_h)	PCG iter	algebraic error	eff. index UB	eff. index LB	total error	eff. index UB	eff. index LB	discretization error	eff. index UB	eff. index LB
1 (9.3×10^3)	2	1.0×10^{-3}	1.01	1.00^{-1}	3.5×10^{-3}	1.29	1.09^{-1}	3.3×10^{-3}	1.32	1.10^{-1}
	4	9.1×10^{-5}	1.02	1.00^{-1}	3.3×10^{-3}	1.07	1.03^{-1}		1.07	1.03^{-1}
2 (3.8×10^4)	4	6.1×10^{-4}	1.01	1.00^{-1}	6.2×10^{-4}	1.20	1.02^{-1}	1.1×10^{-4}	3.81	—
	8	3.2×10^{-6}	1.01	1.00^{-1}	1.1×10^{-4}	1.04	1.01^{-1}		1.04	1.01^{-1}
3 (8.5×10^4)	7	1.1×10^{-3}	1.00	1.00^{-1}	1.1×10^{-3}	1.04	1.00^{-1}	2.9×10^{-6}	1.00×10^2	—
	14	2.2×10^{-5}	1.02	1.00^{-1}	2.2×10^{-5}	1.22	1.01^{-1}		5.41	—
	21	4.8×10^{-8}	1.01	1.00^{-1}	2.9×10^{-6}	1.02	1.11^{-1}		1.02	1.11^{-1}
4 (1.5×10^5)	7	1.1×10^{-3}	1.00	1.00^{-1}	1.1×10^{-3}	1.06	1.00^{-1}	6.3×10^{-8}	5.82×10^3	—
	14	4.9×10^{-5}	1.01	1.00^{-1}	4.9×10^{-5}	1.11	1.00^{-1}		3.81×10^2	—
	21	2.0×10^{-7}	1.01	1.00^{-1}	2.1×10^{-7}	1.28	1.05^{-1}		2.81	—
	28	1.9×10^{-10}	1.01	1.00^{-1}	6.3×10^{-8}	1.01	1.15^{-1}		1.01	1.15^{-1}

Table 6: Peak problem, PCG iterations: effectivity of the upper (UB) and lower (LB) error bounds

p (N_h)	MG iter	algebraic error	eff. index UB	eff. index LB	total error	eff. index UB	eff. index LB	discretization error	eff. index UB	eff. index LB
1 (2.5×10^4)	1	1.4	1.14	1.03^{-1}	1.4	1.61	1.03^{-1}	2.2×10^{-2}	8.31×10^1	—
	2	6.7×10^{-2}	1.14	1.04^{-1}	7.0×10^{-2}	1.61	1.10^{-1}		4.22	—
	3	4.3×10^{-3}	1.16	1.07^{-1}	2.3×10^{-2}	1.37	1.16^{-1}		1.38	1.17^{-1}
	4	4.1×10^{-4}	1.17	1.09^{-1}	2.2×10^{-2}	1.22	1.13^{-1}		1.22	1.13^{-1}
2 (1.0×10^5)	1	2.6	1.19	1.01^{-1}	2.6	1.78	1.01^{-1}	8.9×10^{-3}	4.31×10^2	—
	2	8.9×10^{-2}	1.19	1.01^{-1}	8.9×10^{-2}	1.79	1.01^{-1}		1.49×10^1	—
	3	2.2×10^{-3}	1.18	1.01^{-1}	9.2×10^{-3}	1.55	1.42^{-1}		1.58	1.50^{-1}
	4	8.6×10^{-5}	1.19	1.02^{-1}	8.9×10^{-3}	1.32	1.29^{-1}		1.32	1.29^{-1}
3 (2.3×10^5)	1	2.4	1.19	1.00^{-1}	2.4	1.72	1.00^{-1}	5.3×10^{-3}	6.29×10^2	—
	2	1.1×10^{-1}	1.20	1.00^{-1}	1.1×10^{-1}	1.76	1.00^{-1}		2.92×10^1	—
	3	3.6×10^{-3}	1.18	1.00^{-1}	6.4×10^{-3}	1.89	1.47^{-1}		2.19	6.44^{-1}
	4	1.8×10^{-4}	1.17	1.01^{-1}	5.3×10^{-3}	1.48	1.42^{-1}		1.48	1.42^{-1}
4 (4.0×10^5)	1	2.6	1.18	1.00^{-1}	2.6	1.68	1.00^{-1}	3.8×10^{-3}	9.43×10^2	—
	2	1.3×10^{-1}	1.18	1.00^{-1}	1.3×10^{-1}	1.71	1.00^{-1}		4.93×10^1	—
	3	6.0×10^{-3}	1.16	1.00^{-1}	7.1×10^{-3}	1.87	1.18^{-1}		3.13	—
	4	3.5×10^{-4}	1.13	1.00^{-1}	3.8×10^{-3}	1.57	1.66^{-1}		1.57	1.67^{-1}

Table 7: L-shape problem, multigrid V-cycles: effectivity of the upper (UB) and lower (LB) error bounds

(cf. [68]), see in particular Figures 11–12, where the discretization error is concentrated in the re-entrant corner, whereas the algebraic error is increased in other parts of the domain Ω. Especially in such situations, the local stopping criteria (7.11) and (7.13b) may be very much relevant not to let the total error be locally dominated by the algebraic one, even if the globally measured algebraic error is small, see the discussion in [68, 69].

p (N_h)	algebraic error	eff. index UB	eff. index LB	total error	eff. index UB	eff. index LB	discretization error	eff. index UB	eff. index LB
1 (2.5×10^4)	4.4×10^{-4}	1.11	1.01^{-1}	2.2×10^{-2}	1.22	1.13^{-1}	2.2×10^{-2}	1.22	1.13^{-1}
2 (1.0×10^5)	8.0×10^{-5}	1.12	1.01^{-1}	8.9×10^{-3}	1.32	1.28^{-1}	8.9×10^{-3}	1.32	1.28^{-1}
3 (2.3×10^5)	5.5×10^{-5}	1.09	1.00^{-1}	5.3×10^{-3}	1.45	1.42^{-1}	5.3×10^{-3}	1.45	1.42^{-1}
4 (4.0×10^5)	7.2×10^{-5}	1.08	1.00^{-1}	3.8×10^{-3}	1.49	1.62^{-1}	3.8×10^{-3}	1.49	1.62^{-1}

Table 8: L-shape problem, one full multigrid cycle: effectivity of the upper (UB) and lower (LB) error bounds

p (N_h)	PCG iter	algebraic error	eff. index UB	eff. index LB	total error	eff. index UB	eff. index LB	discretization error	eff. index UB	eff. index LB
1 (2.5×10^4)	4	8.9×10^{-2}	1.02	1.00^{-1}	9.1×10^{-2}	1.26	1.03^{-1}	2.2×10^{-2}	3.35	—
	8	3.8×10^{-4}	1.01	1.00^{-1}	2.2×10^{-2}	1.22	1.12^{-1}		1.22	1.12^{-1}
2 (1.0×10^5)	4	6.2×10^{-1}	1.01	1.00^{-1}	6.2×10^{-1}	1.07	1.00^{-1}	8.9×10^{-3}	2.61×10^{1}	—
	8	6.0×10^{-3}	1.01	1.00^{-1}	1.1×10^{-2}	1.65	1.58^{-1}		1.88	2.86^{-1}
	12	1.9×10^{-4}	1.01	1.00^{-1}	8.9×10^{-3}	1.33	1.28^{-1}		1.33	1.28^{-1}
3 (2.3×10^5)	7	1.0	1.00	1.00^{-1}	1.0	1.05	1.00^{-1}	5.3×10^{-3}	6.29×10^{1}	—
	14	3.1×10^{-2}	1.01	1.00^{-1}	3.1×10^{-2}	1.24	1.01^{-1}		4.48	—
	21	1.7×10^{-3}	1.00	1.00^{-1}	5.6×10^{-3}	1.68	1.48^{-1}		1.74	1.59^{-1}
	28	9.6×10^{-5}	1.00	1.00^{-1}	5.3×10^{-3}	1.46	1.41^{-1}		1.46	1.41^{-1}
4 (4.0×10^5)	7	1.2	1.01	1.00^{-1}	1.2	1.08	1.00^{-1}	3.8×10^{-3}	1.30×10^{2}	—
	14	5.0×10^{-2}	1.01	1.00^{-1}	5.1×10^{-2}	1.14	1.00^{-1}		7.34	—
	21	3.4×10^{-3}	1.00	1.00^{-1}	5.0×10^{-3}	1.77	1.50^{-1}		2.19	—
	28	1.8×10^{-4}	1.01	1.00^{-1}	3.8×10^{-3}	1.52	1.60^{-1}		1.52	1.60^{-1}

Table 9: L-shape problem, PCG iterations: effectivity of the upper (UB) and lower (LB) error bounds

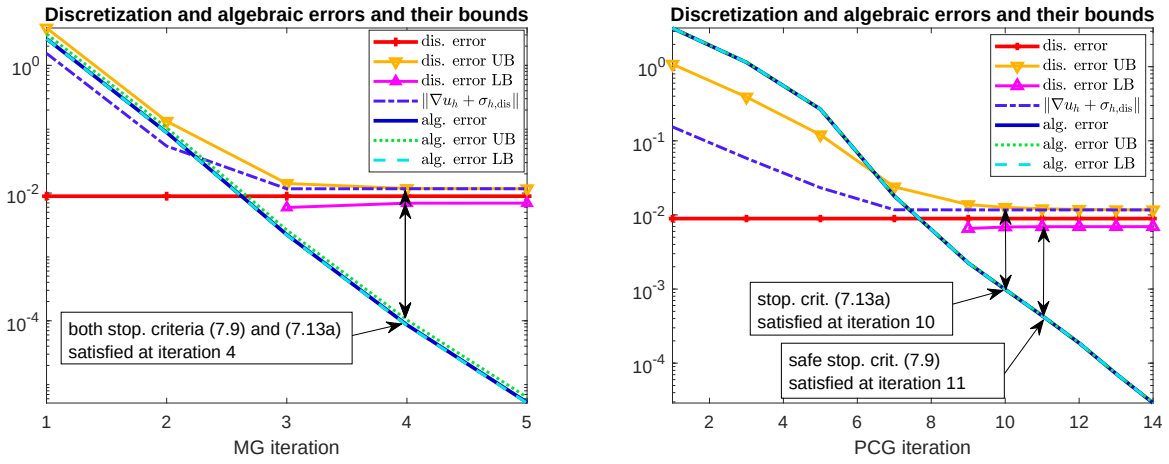

Figure 5: L-shape problem, $p = 2$: discretization and algebraic errors and their upper (UB) and lower (LB) bounds for multigrid V-cycles (left) and PCG (right)

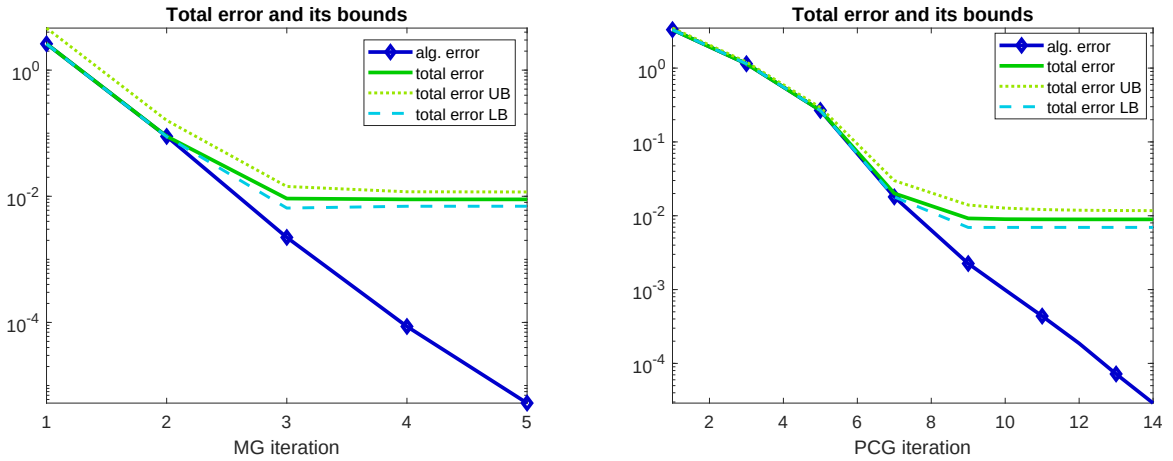

Figure 6: L-shape problem, $p = 2$: total errors and their upper (UB) and lower (LB) bounds for multigrid V-cycles (left) and PCG (right)

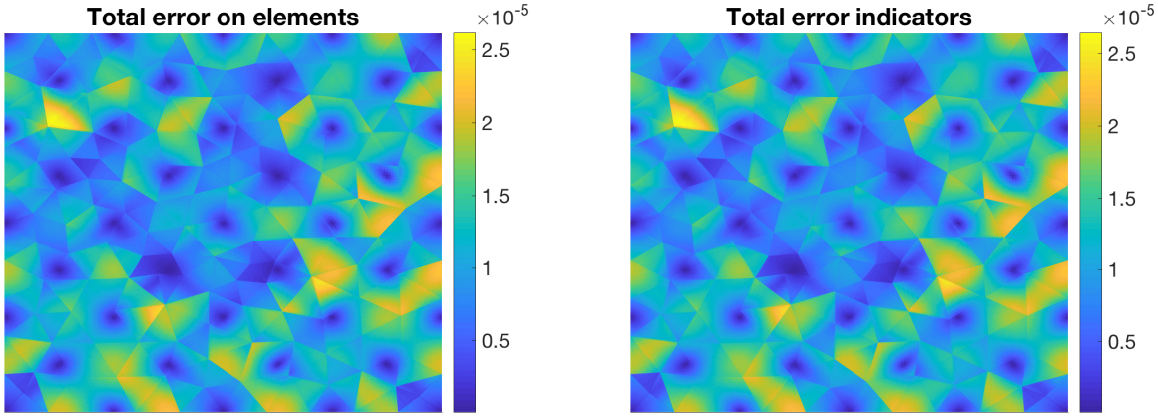

Figure 7: Sinus problem, $p = 2$: elementwise distribution of the total energy error $\|\nabla(u - u_h)\|_K$ (left) and the of local error indicators η_K (right) after one full multigrid cycle

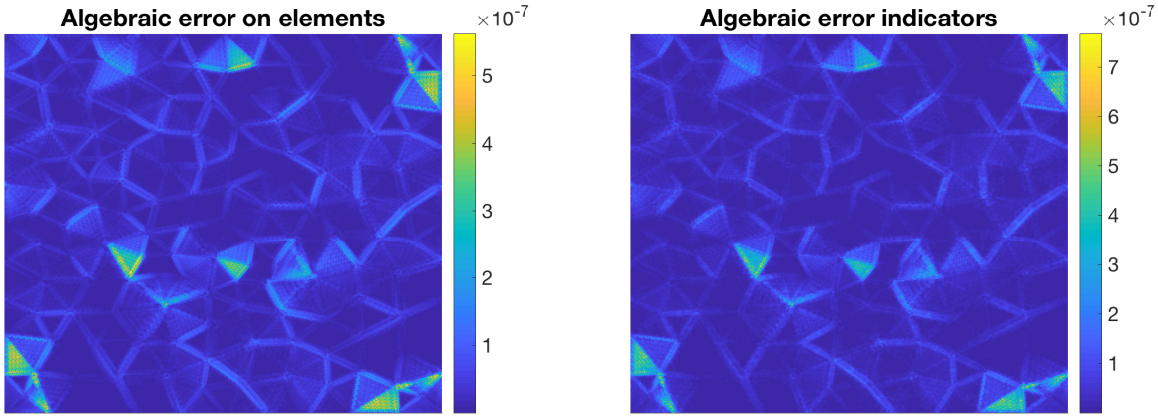

Figure 8: Sinus problem, $p = 2$: elementwise distribution of the algebraic energy error $\|\nabla(u_h^{\mathrm{ex}} - u_h)\|_K$ (left) and of the local error indicators $\overline{\eta}_{\mathrm{alg},K}$ (right) after one full multigrid cycle

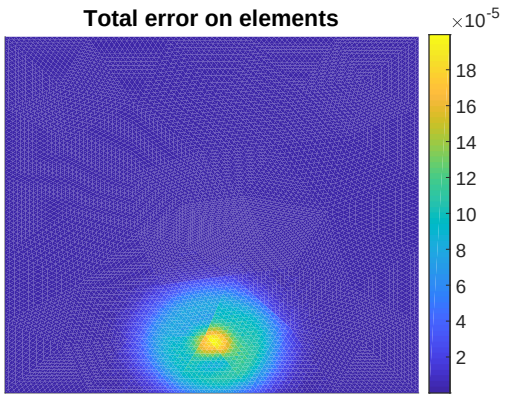

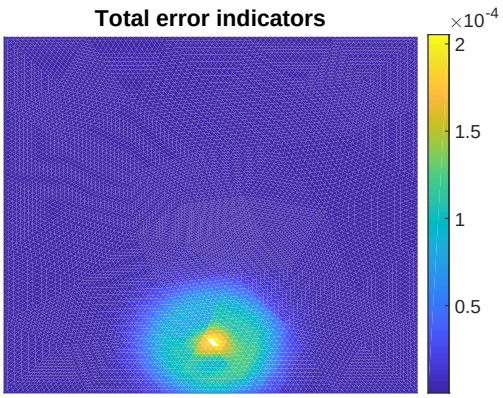

Figure 9: Peak problem, $p = 1$: elementwise distribution of the total energy error $\|\nabla(u - u_h)\|_K$ (left) and of the local error indicators η_K (right) after 2 iterations of the multigrid V-cycle

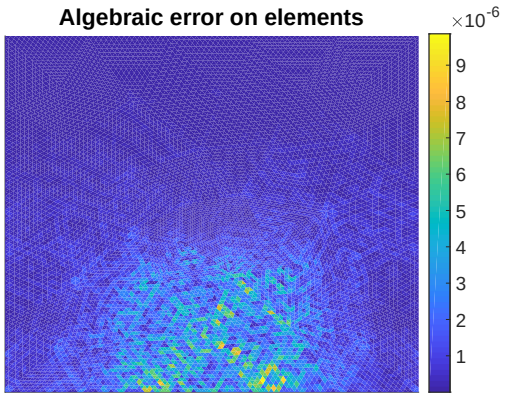

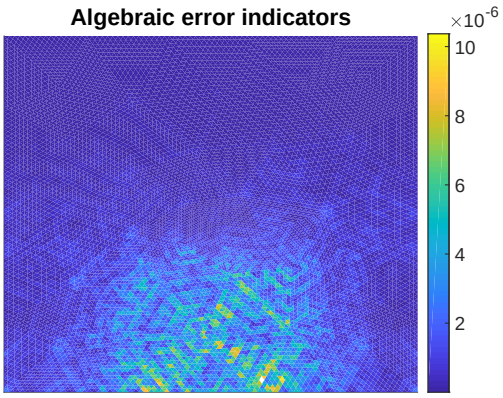

Figure 10: Peak problem, $p = 1$: elementwise distribution of the algebraic energy error $\|\nabla(u_h^{\mathrm{ex}} - u_h)\|_K$ (left) and of the local error indicators $\overline{\eta}_{\mathrm{alg},K}$ (right) after 2 iterations of the multigrid V-cycle

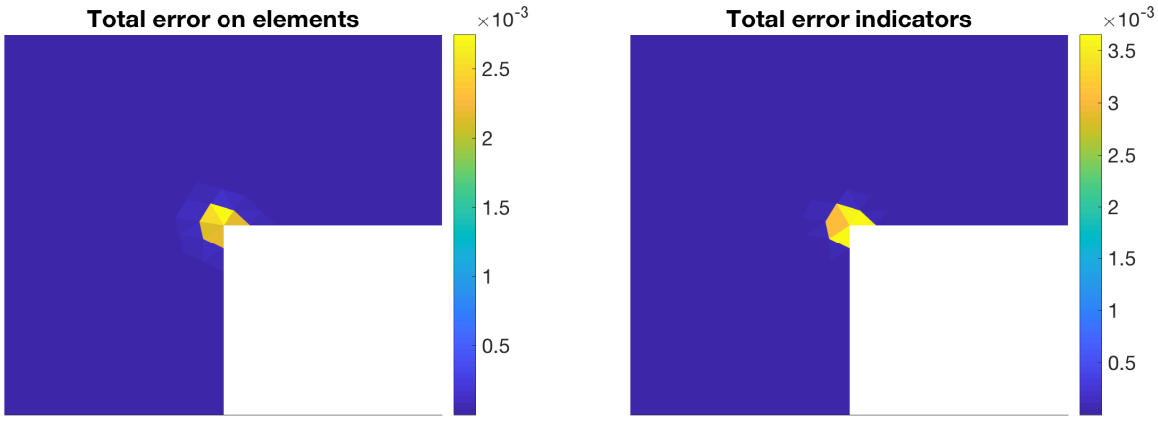

Figure 11: L-shape problem, $p = 3$: elementwise distribution of the total energy error $\|\nabla(u - u_h)\|_K$ (left) and of the local error indicators η_K (right) after 28 PCG iterations. We plot in both figures the part $[-0.1, 0.1] \times [-0.1, 0.1]$ of the discretization domain Ω

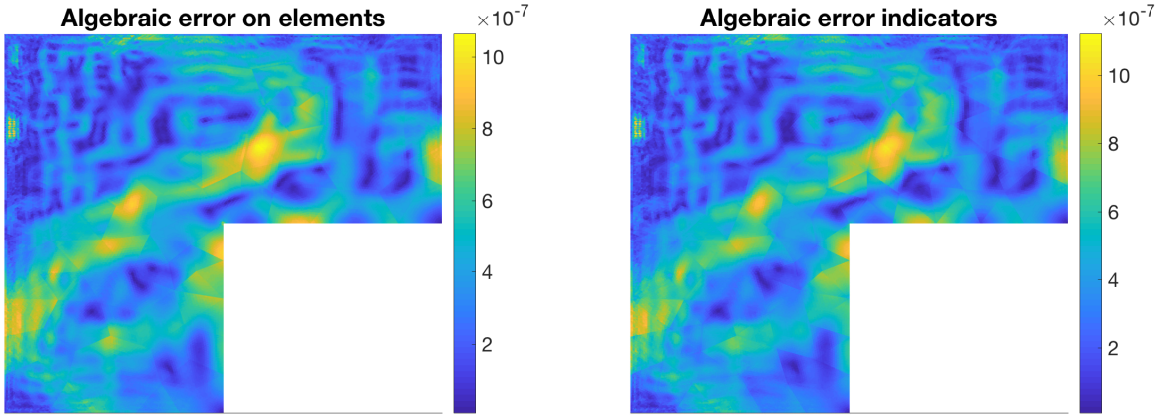

Figure 12: L-shape problem, $p = 3$: elementwise distribution of the algebraic energy error $\|\nabla(u_h^{\mathrm{ex}} - u_h)\|_K$ (left) and of the local error indicators $\overline{\eta}_{\mathrm{alg},K}$ (right) after 28 PCG iterations

10 Conclusion

In the present contribution, we have proposed $\boldsymbol{H}(\mathrm{div})$ and H^1 liftings of given piecewise polynomials over a hierarchy of simplicial meshes, based on a global solve on the coarsest mesh and on local solves on patches of mesh elements around vertices on subsequent mesh levels. In connection with approaches lifting the total residual, two important application arise. First, we were able to design a posteriori error estimators that enable to monitor both the algebraic and the total errors (and consequently also the discretization one) in each iteration of an arbitrary algebraic solver for finite element discretizations of the model Poisson problem. Excellent effectivity indices in numerical experiments are observed, including cases where some classical estimators fail. Second, the $\boldsymbol{H}(\mathrm{div}, \Omega)$-liftings allow to recover mass balance for any problem, any numerical discretization, and any situation.

Several new perspectives are opened by the presented developments. First, our unknown-constant-free approach can significantly reduce the overall cost of iterative solutions of large algebraic systems. Even though a non-negligible effort is spent on the evaluation of the estimators, no (unknown) "safety multiplicative factor" is necessary to ensure reaching the given precision and typically many additional iteration steps and mesh refinements can be saved. Second, as the liftings/reconstructions are *independent* of both the *numerical scheme* and the *algebraic solver*, they open the way for a rigorous "fault control". Note that it is namely immediate to check, for the constructed fields $\boldsymbol{\sigma}_{h,\mathrm{alg}}$ and $\boldsymbol{\sigma}_{h,\mathrm{dis}}$, whether the crucial

property (4.15b) is satisfied exactly/compute the misfit in it. Then even rounding errors and numerical stability issues connected with the computation of the approximate solution u_h can be addressed: indeed, except for the coarse solve, computing the estimators only involves elementwise evaluations of norms of polynomials, whose exactness or confidence interval inclusion can be ensured. In a more distant future, the developed methodology prones for development of integrated solvers with all adaptive algebraic operations like multigrid restriction, prolongation, cycling, and relaxation; with justified stopping criteria; and coupling with adaptive *hp* refinement on the discretization side (here some first results are presented in [36]).

The derivation of the present estimates allows for several simplifications. In particular, it is possible to avoid the solutions of the local (high-order) patchwise problems, while still maintaining all the theoretical results of Sec. 7; this is addressed in [70]. Further simplifications entirely avoiding the liftings/reconstructions and leading in particular to fully algebraic version of the estimates on the algebraic error are likewise possible. They typically introduce various (known) multiplicative constants and decrease the precision of the estimates (sometimes even the guaranteed character is lost), but they bring further radical cuts in the cost of the evaluation of the estimates. Moreover, such estimates are in the form analogous to the estimators based on the stable splittings, which opens door to study their mutual relationships. These developments, which are out of scope of the present manuscript, will be described in detail in a forthcoming contribution.

A Proof of efficiency of the upper algebraic estimate

We show here the efficiency of the upper algebraic estimate $\overline{\eta}_{\mathrm{alg}} = \|\boldsymbol{\sigma}_{h,\mathrm{alg}}\|$ as stated in Theorem 7.4. Recall that $\boldsymbol{\sigma}_{h,\mathrm{alg}}$ is constructed following Definition 4.3 with $\boldsymbol{A} = \boldsymbol{I}$ for $r_h \in \mathbb{P}_h^p$ given elementwise by (6.7).

Proof of Theorem 7.4. The proof proceeds in six steps.

Step 1. It follows immediately from the definition (4.10) of $\boldsymbol{\sigma}_{h,\mathrm{alg}}$ by summing up the local contributions $\boldsymbol{\sigma}_{j,\mathrm{alg}}^{\boldsymbol{a}}$ and from the Cauchy–Schwarz inequality, since any simplex has $(d+1)$ vertices, that

$$\|\boldsymbol{\sigma}_{h,\mathrm{alg}}\|^2 \le J(d+1)\sum_{j=1}^{J}\sum_{\boldsymbol{a}\in\mathcal{V}_{j-1}}\|\boldsymbol{\sigma}_{j,\mathrm{alg}}^{\boldsymbol{a}}\|_{\omega_{j-1}^{\boldsymbol{a}}}^2. \tag{A.1}$$

Step 2. We prove that

$$\|\boldsymbol{\sigma}_{1,\mathrm{alg}}^{\boldsymbol{a}}\|_{\omega_0^{\boldsymbol{a}}} \le h_{\omega_0^{\boldsymbol{a}}} C_{\mathrm{bPF}} C_{\mathrm{eq}} \|\Pi_1^p(r_h\psi_0^{\boldsymbol{a}} - \nabla\rho_{0,\mathrm{alg}}\cdot\nabla\psi_0^{\boldsymbol{a}})\|_{\omega_0^{\boldsymbol{a}}} \tag{A.2a}$$

and

$$\|\boldsymbol{\sigma}_{j,\mathrm{alg}}^{\boldsymbol{a}}\|_{\omega_{j-1}^{\boldsymbol{a}}} \le h_{\omega_{j-1}^{\boldsymbol{a}}} C_{\mathrm{bPF}} C_{\mathrm{eq}} \|\Pi_j^p(\mathrm{Id} - \Pi_{j-1}^p)(r_h\psi_{j-1}^{\boldsymbol{a}})\|_{\omega_{j-1}^{\boldsymbol{a}}}, \quad 1 < j \le J, \tag{A.2b}$$

where $h_{\omega_{j-1}^{\boldsymbol{a}}}$ is the diameter of the patch $\omega_{j-1}^{\boldsymbol{a}}$ and the (computable) constants C_{bPF} and C_{eq} are identified below.

For a fixed $1 \le j \le J$ and $\boldsymbol{a} \in \mathcal{V}_{j-1}$ and $\boldsymbol{A} = \boldsymbol{I}$, take in (4.7) or in (4.11) the test functions $\boldsymbol{v}_j = \boldsymbol{\sigma}_{j,\mathrm{alg}}^{\boldsymbol{a}}$ and $q_j = \gamma_j^{\boldsymbol{a}}$ and sum the two equations to get, using again the compact notation $\Pi_0^p = 0$,

$$\|\boldsymbol{\sigma}_{j,\mathrm{alg}}^{\boldsymbol{a}}\|_{\omega_{j-1}^{\boldsymbol{a}}}^2 = ((\mathrm{Id} - \Pi_{j-1}^p)(r_h\psi_{j-1}^{\boldsymbol{a}} - \nabla\rho_{0,\mathrm{alg}}\cdot\nabla\psi_{j-1}^{\boldsymbol{a}}), \gamma_j^{\boldsymbol{a}})_{\omega_{j-1}^{\boldsymbol{a}}}. \tag{A.3}$$

We will next use the postprocessing by Arnold and Brezzi [9] and Arbogast and Chen [6] of $\gamma_j^{\boldsymbol{a}} \in \mathbb{P}_j^p(\omega_{j-1}^{\boldsymbol{a}})$, a piecewise polynomial of degree p on the mesh $\mathcal{T}_j$ of the patch subdomain $\omega_{j-1}^{\boldsymbol{a}}$, to a higher-order piecewise polynomial $\tilde{\gamma}_j^{\boldsymbol{a}}$ on the mesh $\mathcal{T}_j$ of the patch subdomain $\omega_{j-1}^{\boldsymbol{a}}$ such that

$$\begin{aligned}
\Pi_{\mathbb{P}^p(K)}\tilde{\gamma}_j^{\boldsymbol{a}}|_K &= \gamma_j^{\boldsymbol{a}}|_K && \forall K \in \mathcal{T}_j \subset \omega_{j-1}^{\boldsymbol{a}},\\
\Pi_{\boldsymbol{RTN}_p(K)}(-\nabla\tilde{\gamma}_j^{\boldsymbol{a}})|_K &= \boldsymbol{\sigma}_{j,\mathrm{alg}}^{\boldsymbol{a}}|_K && \forall K \in \mathcal{T}_j \subset \omega_{j-1}^{\boldsymbol{a}},
\end{aligned}$$

where $\boldsymbol{RTN}_p(K) := [\mathbb{P}^p(K)]^d + \mathbb{P}^p(K)\boldsymbol{x}$ is the Raviart–Thomas–Nédélec space on the element K. Then equations (4.7a) and (4.11a) imply that the jumps of $\tilde{\gamma}_j^{\boldsymbol{a}}|_K$ over the interior and Dirichlet boundary faces are orthogonal to face polynomials of degree p, see [9, Section 2] and [6, Section 2]. Note also that $\tilde{\gamma}_j^{\boldsymbol{a}}$ is of mean value zero on $\omega_{j-1}^{\boldsymbol{a}}$ for interior vertices and it vanishes in mean on $\partial\omega_{j-1}^{\boldsymbol{a}} \cap \partial\Omega$ for boundary vertices. Then the broken Poincaré–Friedrichs inequality (see Brenner [23] or Vohralík [83]) gives

$$\|\tilde{\gamma}_j^{\boldsymbol{a}}\|_{\omega_{j-1}^{\boldsymbol{a}}} \le h_{\omega_{j-1}^{\boldsymbol{a}}} C_{\mathrm{bPF}} \|\nabla\tilde{\gamma}_j^{\boldsymbol{a}}\|_{\omega_{j-1}^{\boldsymbol{a}}}, \tag{A.4}$$

where the constant C_{bPF} only depends on the shape regularity $\kappa_{\mathcal{T}}$ of the mesh $\mathcal{T}_j$ and the space dimension d; its computable upper bound (for interior vertices $\boldsymbol{a} \in \mathcal{V}_{j-1}$) is given in [83, Theorem 8.1]. We will also use the norm equivalence result of [84, Lemma 5.4]

$$\|\nabla \tilde{\gamma}_j^{\boldsymbol{a}}\|_{\omega_{j-1}^{\boldsymbol{a}}} \le C_{\mathrm{eq}} \|\boldsymbol{\sigma}_{j,\mathrm{alg}}^{\boldsymbol{a}}\|_{\omega_{j-1}^{\boldsymbol{a}}}, \tag{A.5}$$

where the constant C_{eq} only depends on the shape regularity $\kappa_{\mathcal{T}}$ of $\mathcal{T}_j$, the space dimension d, and the polynomial degree p; $C_{\mathrm{eq}} = 1$ for $p = 0$, and its computable upper bound for $p \ge 1$ can be obtained as in [44, Section 3.3]. The Cauchy–Schwarz inequality in (A.3) with a subsequent application of (A.4) and (A.5) leads to (A.2).

Step 3. For any finest mesh element $K \in \mathcal{T}_h = \mathcal{T}_J$, let $\omega_K := \cup_{\boldsymbol{a} \in \mathcal{V}_h,\, \boldsymbol{a} \subset \partial K} \omega_h^{\boldsymbol{a}}$ denote the domain of all elements sharing a node with K. We prove that

$$h_K \|r_h\|_K \le C \|\nabla(u_h^{\mathrm{ex}} - u_h)\|_{\omega_K} \qquad \forall K \in \mathcal{T}_h, \tag{A.6}$$

where the constant C only depends on the shape regularity $\kappa_{\mathcal{T}}$ of the mesh $\mathcal{T}_h$, on the polynomial degree p, and on the space dimension d.

For this purpose, consider a fixed $K \in \mathcal{T}_h$ and let the set $\mathcal{I}(K)$ contain the indices l of all Lagrange basis functions ψ_h^l of the space V_h^p non-vanishing on K. Then from (6.7), we see

$$r_h|_K = \sum_{m \in \mathcal{I}(K)} (\Phi_K)_m \psi_h^m|_K, \tag{A.7a}$$

$$\Phi_K := \mathbb{G}_K^{-1} \mathrm{R}_K, \tag{A.7b}$$

$$(\mathrm{R}_K)_l := (\mathrm{R}_h)_l \frac{|K|}{|\operatorname{supp} \psi_h^l|}, \quad l \in \mathcal{I}(K), \tag{A.7c}$$

$$(\mathbb{G}_K)_{lm} := (\psi_h^m, \psi_h^l)_K, \quad l, m \in \mathcal{I}(K), \tag{A.7d}$$

$$\|r_h\|_K^2 = \Phi_K^t \mathbb{G}_K \Phi_K = \mathrm{R}_K^t \mathbb{G}_K^{-1} \mathrm{R}_K. \tag{A.7e}$$

Here $\mathbb{G}_K$ is the usual mass matrix of finite elements on the single simplex K, and the vector R_K represents the right-hand sides in (6.7), regrouping the contributions of the finest-level algebraic residual vector R_h to the element K. Note that ω_K corresponds to the union of the supports of the basis functions ψ_h^m, $m \in \mathcal{I}(K)$. Let us introduce the extension $\tilde{r}_h$ and the scaled extension $\hat{r}_h$ of $r_h|_K$ to the element patch ω_K by

$$\tilde{r}_h \in V_h^p|_{\omega_K} \cap H_0^1(\omega_K), \quad \tilde{r}_h := \sum_{m \in \mathcal{I}(K)} (\Phi_K)_m \psi_h^m, \tag{A.8a}$$

$$\hat{r}_h \in V_h^p|_{\omega_K} \cap H_0^1(\omega_K), \quad \hat{r}_h := \sum_{m \in \mathcal{I}(K)} (\Phi_K)_m \frac{|K|}{|\operatorname{supp} \psi_h^m|} \psi_h^m. \tag{A.8b}$$

Then, using (A.7a), (6.7), (6.3), and (A.8b), we see

$$\begin{aligned} \|r_h\|_K^2 &= \sum_{m \in \mathcal{I}(K)} (\Phi_K)_m (r_h, \psi_h^m)_K = \sum_{m \in \mathcal{I}(K)} (\Phi_K)_m (\nabla(u_h^{\mathrm{ex}} - u_h), \nabla \psi_h^m)_{\omega_K} \frac{|K|}{|\operatorname{supp} \psi_h^m|} \\ &= (\nabla(u_h^{\mathrm{ex}} - u_h), \nabla \hat{r}_h)_{\omega_K} \le \|\nabla(u_h^{\mathrm{ex}} - u_h)\|_{\omega_K} \|\nabla \hat{r}_h\|_{\omega_K} \le C h_K^{-1} \|\nabla(u_h^{\mathrm{ex}} - u_h)\|_{\omega_K} \|\hat{r}_h\|_{\omega_K}, \end{aligned}$$

where we have also employed the Cauchy–Schwarz and inverse inequalities; here C is a generic constant only depending on the shape regularity $\kappa_{\mathcal{T}}$ of $\mathcal{T}_h$, p, and d. Let $\mathbb{G}_{\omega_K}$ be the mass matrix of finite elements on the patch ω_K, in extension of (A.7d),

$$(\mathbb{G}_{\omega_K})_{lm} := (\psi_h^m, \psi_h^l)_{\omega_K}, \quad l, m \in \mathcal{I}(K),$$

and let $(\mathbb{N}_{\omega_K})_{ll} := |K|/|\operatorname{supp} \psi_h^l|$ be the diagonal matrix with the scalings $|K|/|\operatorname{supp} \psi_h^l|$. Then, by a basis change via the matrix $\mathbb{N}_{\omega_K}$ and by comparison of the patch mass matrix $\mathbb{G}_{\omega_K}$ to the element mass matrix $\mathbb{G}_K$, we have

$$\|\hat{r}_h\|_{\omega_K}^2 = \Phi_K^t \mathbb{N}_{\omega_K} \mathbb{G}_{\omega_K} \mathbb{N}_{\omega_K} \Phi_K \le C_1 \Phi_K^t \mathbb{G}_{\omega_K} \Phi_K = C_1 \|\tilde{r}_h\|_{\omega_K}^2 \le C_2 \Phi_K^t \mathbb{G}_K \Phi_K = C_2 \|r_h\|_K^2,$$

with constants C_1, C_2 depending $\kappa_{\mathcal{T}}$, p, and d. Thus (A.6) follows.

Step 4. We combine (A.2b) and (A.6) to get, for any $1 < j \le J$,

$$\sum_{\boldsymbol{a} \in \mathcal{V}_{j-1}} \|\boldsymbol{\sigma}_{j,\mathrm{alg}}^{\boldsymbol{a}}\|_{\omega_{j-1}^{\boldsymbol{a}}}^2 \le C_{\mathrm{bPF}}^2 C_{\mathrm{eq}}^2 \sum_{\boldsymbol{a} \in \mathcal{V}_{j-1}} h_{\omega_{j-1}^{\boldsymbol{a}}}^2 \|r_h\|_{\omega_{j-1}^{\boldsymbol{a}}}^2 \le C \|\nabla(u_h^{\mathrm{ex}} - u_h)\|^2, \tag{A.9}$$

where the constant C only depends on the shape regularity $\kappa_{\mathcal{T}}$ and refinement strength $\iota_{\mathcal{T}}$ of the mesh hierarchy $\{\mathcal{T}_j\}_{0\le j\le J}$, on the polynomial degree p, on the space dimension d, and on the number of mesh levels J.

Step 5. We combine (A.2a) and (A.6), giving

$$\begin{aligned}\sum_{\boldsymbol{a}\in\mathcal{V}_0}\|\boldsymbol{\sigma}_{1,\mathrm{alg}}^{\boldsymbol{a}}\|_{\omega_0^{\boldsymbol{a}}}^2 &\le 2C_{\mathrm{bPF}}^2C_{\mathrm{eq}}^2\sum_{\boldsymbol{a}\in\mathcal{V}_0}\big\{h_{\omega_0^{\boldsymbol{a}}}^2\big(\|r_h\|_{\omega_0^{\boldsymbol{a}}}^2+\|\nabla\psi_0^{\boldsymbol{a}}\|_{\infty,\omega_0^{\boldsymbol{a}}}^2\|\nabla\rho_{0,\mathrm{alg}}\|_{\omega_0^{\boldsymbol{a}}}^2\big)\big\}\\ &\le C\|\nabla(u_h^{\mathrm{ex}}-u_h)\|^2,\end{aligned}\tag{A.10}$$

where C again only depends on $\kappa_{\mathcal{T}}$, $\iota_{\mathcal{T}}$, p, d, and J; indeed, for the term $h_{\omega_0^{\boldsymbol{a}}}^2\|r_h\|_{\omega_0^{\boldsymbol{a}}}^2$ we proceed as above in step 4, whereas for $h_{\omega_0^{\boldsymbol{a}}}^2\|\nabla\psi_0^{\boldsymbol{a}}\|_{\infty,\omega_0^{\boldsymbol{a}}}^2\|\nabla\rho_{0,\mathrm{alg}}\|_{\omega_0^{\boldsymbol{a}}}^2$ we use $\|\nabla\psi_0^{\boldsymbol{a}}\|_{\infty,\omega_0^{\boldsymbol{a}}}\le Ch_{\omega_0^{\boldsymbol{a}}}^{-1}$ and

$$\sum_{\boldsymbol{a}\in\mathcal{V}_0}\|\nabla\rho_{0,\mathrm{alg}}\|_{\omega_0^{\boldsymbol{a}}}^2=(d+1)\|\nabla\rho_{0,\mathrm{alg}}\|^2=(d+1)(\nabla(u_h^{\mathrm{ex}}-u_h),\nabla\rho_{0,\mathrm{alg}})\le(d+1)\|\nabla(u_h^{\mathrm{ex}}-u_h)\|^2\tag{A.11}$$

from (4.4) and (6.8).

Step 6. Combining (A.1) with (A.9) and (A.11) leads to the assertion.

□

B Proofs of global and local efficiencies of the upper total estimate

We collect in this appendix the proofs of Theorems 7.6 and 7.7, while also including Remarks 7.9 and 7.10. Let

$$H_*^1(\omega_h^{\boldsymbol{a}}):=\{v\in H^1(\omega_h^{\boldsymbol{a}});\,(v,1)_{\omega_h^{\boldsymbol{a}}}=0\},\qquad \boldsymbol{a}\in\mathcal{V}_h^{\mathrm{int}},\tag{B.1a}$$

$$H_*^1(\omega_h^{\boldsymbol{a}}):=\{v\in H^1(\omega_h^{\boldsymbol{a}});\,v=0\text{ on }\partial\omega_h^{\boldsymbol{a}}\cap\partial\Omega\},\quad \boldsymbol{a}\in\mathcal{V}_h^{\mathrm{ext}}.\tag{B.1b}$$

Standard scaling arguments and the Poincaré–Friedrichs inequality yield

$$\|\nabla(\psi_h^{\boldsymbol{a}}v)\|_{\omega_h^{\boldsymbol{a}}}\le C_{\mathrm{cont,PF}}\|\nabla v\|_{\omega_h^{\boldsymbol{a}}}\qquad\forall v\in H_*^1(\omega_h^{\boldsymbol{a}}),\tag{B.2}$$

where the constant $C_{\mathrm{cont,PF}}$ only depends on the shape regularity $\kappa_{\mathcal{T}}$ of the mesh $\mathcal{T}_h$, see, e.g., [28, Theorem 3.1], [18, Sec. 3], or [44, proof of Lemma 3.12]. A crucial result that we rely on is the stability of the mixed finite element problem (4.14) in the sense that

$$\|\psi_h^{\boldsymbol{a}}\nabla u_h+\boldsymbol{\sigma}_{h,\mathrm{dis}}^{\boldsymbol{a}}\|_{\omega_h^{\boldsymbol{a}}}\le C_{\mathrm{st}}\sup_{v\in H_*^1(\omega_h^{\boldsymbol{a}}),\,\|\nabla v\|_{\omega_h^{\boldsymbol{a}}}=1}\big\{(f-r_h,\psi_h^{\boldsymbol{a}}v)_{\omega_h^{\boldsymbol{a}}}-(\nabla u_h,\nabla(\psi_h^{\boldsymbol{a}}v))_{\omega_h^{\boldsymbol{a}}}\big\},\tag{B.3}$$

for $(f-r_h)\psi_h^{\boldsymbol{a}}\in\mathbb{P}_h^{p'}$ and $\boldsymbol{A}=\boldsymbol{I}$. This result has been proven, in two space dimensions, in Braess *et al.* [18, Theorem 7], and extension to three space dimensions is given in [45, Corollaries 3.3 and 3.6]. Importantly, the constant $C_{\mathrm{st}}>0$ only depends on the shape regularity $\kappa_{\mathcal{T}}$ of the mesh $\mathcal{T}_h$; a computable upper bound on C_{st} is given in [44, Corollary 3.16 and Lemma 3.23].

We start with local efficiency:

Proof of Theorem 7.7, including Remarks 7.9 and 7.10. Let element $K\in\mathcal{T}_h$ be fixed. Definition $\widetilde{\eta}_{\mathrm{dis},K}=\|\nabla u_h+\boldsymbol{\sigma}_{h,\mathrm{dis}}\|_K$, Definition 4.5 of $\boldsymbol{\sigma}_{h,\mathrm{dis}}$, the partition of unity on the simplex K by the hat functions $\psi_h^{\boldsymbol{a}}$ associated with its vertices, and the triangle inequality yield

$$\widetilde{\eta}_{\mathrm{dis},K}=\|\nabla u_h+\boldsymbol{\sigma}_{h,\mathrm{dis}}\|_K=\Big\|\sum_{\boldsymbol{a}\in\mathcal{V}_h,\,\boldsymbol{a}\subset\partial K}\big(\psi_h^{\boldsymbol{a}}\nabla u_h+\boldsymbol{\sigma}_{h,\mathrm{dis}}^{\boldsymbol{a}}\big)\Big\|_K\le\sum_{\boldsymbol{a}\in\mathcal{V}_h,\,\boldsymbol{a}\subset\partial K}\|\psi_h^{\boldsymbol{a}}\nabla u_h+\boldsymbol{\sigma}_{h,\mathrm{dis}}^{\boldsymbol{a}}\|_{\omega_h^{\boldsymbol{a}}}.\tag{B.4}$$

Now, for any vertex $\boldsymbol{a}$ of the simplex K, using the assumptions on the polynomial degree $p'=p+1$, on the datum $f\in\mathbb{P}_h^p$, and crucially the stability bound (B.3),

$$\|\psi_h^{\boldsymbol{a}}\nabla u_h+\boldsymbol{\sigma}_{h,\mathrm{dis}}^{\boldsymbol{a}}\|_{\omega_h^{\boldsymbol{a}}}\le C_{\mathrm{st}}\sup_{v\in H_*^1(\omega_h^{\boldsymbol{a}}),\,\|\nabla v\|_{\omega_h^{\boldsymbol{a}}}=1}\big((\nabla(u-u_h),\nabla(\psi_h^{\boldsymbol{a}}v))_{\omega_h^{\boldsymbol{a}}}+(\boldsymbol{\sigma}_{h,\mathrm{alg}},\nabla(\psi_h^{\boldsymbol{a}}v))_{\omega_h^{\boldsymbol{a}}}\big).$$

Here we have also employed the weak formulation (6.2), the divergence property $\nabla\cdot\boldsymbol{\sigma}_{h,\mathrm{alg}}=r_h$ of Lemma 4.4, and the Green theorem, since $\boldsymbol{\sigma}_{h,\mathrm{alg}}\in\boldsymbol{H}(\mathrm{div},\omega_h^{\boldsymbol{a}})$ and $(\psi_h^{\boldsymbol{a}}v)\in H_0^1(\omega_h^{\boldsymbol{a}})$. Thus, the Cauchy–Schwarz and triangle inequalities together with (B.2) give

$$\|\psi_h^{\boldsymbol{a}}\nabla u_h+\boldsymbol{\sigma}_{h,\mathrm{dis}}^{\boldsymbol{a}}\|_{\omega_h^{\boldsymbol{a}}}\le C_{\mathrm{st}}C_{\mathrm{cont,PF}}\big(\|\nabla(u-u_h)\|_{\omega_h^{\boldsymbol{a}}}+\|\boldsymbol{\sigma}_{h,\mathrm{alg}}\|_{\omega_h^{\boldsymbol{a}}}\big).\tag{B.5}$$

The stopping criterion (7.11) and the bound $\|\nabla\rho^{\boldsymbol{a}}_{h,\mathrm{tot}}\|_{\omega^{\boldsymbol{a}}_h} \le C_{\mathrm{cont,PF}}\|\nabla(u-u_h)\|_{\omega^{\boldsymbol{a}}_h}$ which immediately follows from Definition 5.3 as in [69, proof of Theorem 8] imply

$$\|\boldsymbol{\sigma}_{h,\mathrm{alg}}\|_{\omega^{\boldsymbol{a}}_h} \le \frac{\gamma_K}{(1+\gamma_K^2)^{\frac12}}\|\nabla(u-u_h)\|_{\omega^{\boldsymbol{a}}_h} \le \gamma_K\|\nabla(u-u_h)\|_{\omega^{\boldsymbol{a}}_h}. \tag{B.6}$$

Consequently, (B.5) gives

$$\|\psi^{\boldsymbol{a}}_h\nabla u_h + \boldsymbol{\sigma}^{\boldsymbol{a}}_{h,\mathrm{dis}}\|_{\omega^{\boldsymbol{a}}_h} \le (1+\gamma_K)C_{\mathrm{st}}C_{\mathrm{cont,PF}}\|\nabla(u-u_h)\|_{\omega^{\boldsymbol{a}}_h},$$

and the claim follows from (B.4), $\|\boldsymbol{\sigma}_{h,\mathrm{alg}}\|_K \le \|\boldsymbol{\sigma}_{h,\mathrm{alg}}\|_{\omega^{\boldsymbol{a}}_h}$, (B.6), and the fact that $C_{\mathrm{st}} \ge 1$, $C_{\mathrm{cont,PF}} \ge 1$.

Let us also consider the local stopping criterion (7.13b) of Remark 7.9. Since, by assumption, we have $\eta_{\mathrm{osc}} = 0$, (7.13b) implies

$$\widetilde{\eta}_{\mathrm{dis},K} + \overline{\eta}_{\mathrm{alg},K} \le (1+\gamma_K)\widetilde{\eta}_{\mathrm{dis},K} = (1+\gamma_K)\|\nabla u_h + \boldsymbol{\sigma}_{h,\mathrm{dis}}\|_K \tag{B.7}$$

and

$$\sum_{\boldsymbol{a}\in\mathcal{V}_h,\,\boldsymbol{a}\subset\partial K}\|\boldsymbol{\sigma}_{h,\mathrm{alg}}\|_{\omega^{\boldsymbol{a}}_h} = \sum_{\boldsymbol{a}\in\mathcal{V}_h,\,\boldsymbol{a}\subset\partial K}\overline{\eta}_{\mathrm{alg},\omega^{\boldsymbol{a}}_h} \le (d+1)\gamma_K\widetilde{\eta}_{\mathrm{dis},K},$$

since any simplex has $(d+1)$ vertices. Using (B.4), (B.5), and the above inequalities, we infer

$$(1+\gamma_K)\widetilde{\eta}_{\mathrm{dis},K} \le (1+\gamma_K)C_{\mathrm{st}}C_{\mathrm{cont,PF}}\left(\sum_{\boldsymbol{a}\in\mathcal{V}_h,\,\boldsymbol{a}\subset\partial K}\|\nabla(u-u_h)\|_{\omega^{\boldsymbol{a}}_h} + (d+1)\gamma_K\widetilde{\eta}_{\mathrm{dis},K}\right).$$

Consequently, the requirement on γ_K (7.14b) yields

$$(1+\gamma_K)\widetilde{\eta}_{\mathrm{dis},K} \le 2(1+\gamma_K)C_{\mathrm{st}}C_{\mathrm{cont,PF}}\sum_{\boldsymbol{a}\in\mathcal{V}_h,\,\boldsymbol{a}\subset\partial K}\|\nabla(u-u_h)\|_{\omega^{\boldsymbol{a}}_h},$$

and we conclude (7.12) by (B.7).

Finally, for the sake of completeness, consider Remark 7.10 where $\boldsymbol{\sigma}_{h,\mathrm{dis}}$ of Definition 4.5 is constructed with the smaller polynomial degree $p' = p$. If $f \in \mathbb{P}^{p-1}_h$, then $f\psi^{\boldsymbol{a}}_h \in \mathbb{P}^p_h$, but a trouble arises from the fact that $r_h\psi^{\boldsymbol{a}}_h \notin \mathbb{P}^p_h$. Then, in (B.3), there appears the term

$$\sup_{v\in H^1_*(\omega^{\boldsymbol{a}}_h),\,\|\nabla v\|_{\omega^{\boldsymbol{a}}_h}=1}(\Pi^p_h(\psi^{\boldsymbol{a}}_h r_h), v)_{\omega^{\boldsymbol{a}}_h}.$$

Let $v \in H^1_*(\omega^{\boldsymbol{a}}_h)$ with $\|\nabla v\|_{\omega^{\boldsymbol{a}}_h} = 1$ be fixed. Then

$$(\Pi^p_h(\psi^{\boldsymbol{a}}_h r_h), v)_{\omega^{\boldsymbol{a}}_h} \le \|\Pi^p_h(\psi^{\boldsymbol{a}}_h r_h)\|_{\omega^{\boldsymbol{a}}_h}\|v\|_{\omega^{\boldsymbol{a}}_h} \le C\|\psi^{\boldsymbol{a}}_h r_h\|_{\omega^{\boldsymbol{a}}_h}h_{\omega^{\boldsymbol{a}}_h}\|\nabla v\|_{\omega^{\boldsymbol{a}}_h} \le C\|\nabla\cdot\boldsymbol{\sigma}_{h,\mathrm{alg}}\|_{\omega^{\boldsymbol{a}}_h}h_{\omega^{\boldsymbol{a}}_h} \le C\|\boldsymbol{\sigma}_{h,\mathrm{alg}}\|_{\omega^{\boldsymbol{a}}_h},$$

where the constant C arises from a Poincaré inequality on $\omega^{\boldsymbol{a}}_h$ but also from an inverse inequality, so that it depends on the polynomial degree p. Now (B.6) can be applied and the proof follows. □

Global efficiency is then shown as follows:

Proof of Theorem 7.6, including Remarks 7.9 and 7.10. The proof follows that of Theorem 7.7. The overlap in the construction of $\boldsymbol{\sigma}_{h,\mathrm{dis}}$ by $\boldsymbol{\sigma}^{\boldsymbol{a}}_{h,\mathrm{dis}}$ leads to

$$\|\nabla u_h + \boldsymbol{\sigma}_{h,\mathrm{dis}}\|^2 \le (d+1)\sum_{\boldsymbol{a}\in\mathcal{V}_h}\|\psi^{\boldsymbol{a}}_h\nabla u_h + \boldsymbol{\sigma}^{\boldsymbol{a}}_{h,\mathrm{dis}}\|^2_{\omega^{\boldsymbol{a}}_h},$$

whence (B.5) results in

$$\|\nabla u_h + \boldsymbol{\sigma}_{h,\mathrm{dis}}\|^2 \le (d+1)C^2_{\mathrm{st}}C^2_{\mathrm{cont,PF}}\sum_{\boldsymbol{a}\in\mathcal{V}_h}\left(\|\nabla(u-u_h)\|_{\omega^{\boldsymbol{a}}_h} + \|\boldsymbol{\sigma}_{h,\mathrm{alg}}\|_{\omega^{\boldsymbol{a}}_h}\right)^2,$$

so that

$$\widetilde{\eta}_{\mathrm{dis}} = \|\nabla u_h + \boldsymbol{\sigma}_{h,\mathrm{dis}}\| \le (d+1)C_{\mathrm{st}}C_{\mathrm{cont,PF}}(\|\nabla(u-u_h)\| + \|\boldsymbol{\sigma}_{h,\mathrm{alg}}\|). \tag{B.8}$$

It is immediate, see the discussion in [69, Sec. 6.3], that the safe criterion (7.9) is equivalent to $\overline{\eta}_{\mathrm{alg}} \le \gamma/(1+\gamma^2)^{\frac12}\underline{\eta}$ with $\underline{\eta}$ the guaranteed total error lower bound of Theorem 7.2. Thus, using (7.5b),

$$\overline{\eta}_{\mathrm{alg}} = \|\boldsymbol{\sigma}_{h,\mathrm{alg}}\| \le \frac{\gamma}{(1+\gamma^2)^{\frac12}}\|\nabla(u-u_h)\| \le \gamma\|\nabla(u-u_h)\|, \tag{B.9}$$

and, in combination with (B.8),

$$\widetilde{\eta}_{\mathrm{dis}} = \|\nabla u_h + \boldsymbol{\sigma}_{h,\mathrm{dis}}\| \leq (1+\gamma)(d+1)C_{\mathrm{st}}C_{\mathrm{cont,PF}}\|\nabla(u-u_h)\|,$$

so that the assertion follows by (B.9).

For the case of Remark 7.9, using the global stopping criterion (7.13a), $\eta_{\mathrm{osc}} = 0$, and (B.8),

$$\widetilde{\eta}_{\mathrm{dis}} + \overline{\eta}_{\mathrm{alg}} \leq (1+\gamma)\widetilde{\eta}_{\mathrm{dis}} \leq (1+\gamma)(d+1)C_{\mathrm{st}}C_{\mathrm{cont,PF}}(\|\nabla(u-u_h)\| + \gamma\widetilde{\eta}_{\mathrm{dis}}),$$

and finally (7.14a) leads to

$$(1+\gamma)\widetilde{\eta}_{\mathrm{dis}} \leq 2(1+\gamma)(d+1)C_{\mathrm{st}}C_{\mathrm{cont,PF}}\|\nabla(u-u_h)\|$$

and consequently to the assertion.

Finally, $p' = p$ of Remark 7.10 can be treated as in the proof of Theorem 7.7. □

C Recovering mass balance in a two-phase porous media flow

As we have announced in the introduction, the tools that we develop in Section 4 for the purpose of a posteriori error estimation can actually serve to recover mass balance in any situation. We illustrate this here on the example of finite volume discretizations of immiscible incompressible two-phase flow in porous media.

C.1 Immiscible incompressible two-phase flow in porous media

Let an open bounded polygonal domain $\Omega \subset \mathbb{R}^d$ and a time interval $(0,T)$, $T > 0$, be given. We consider in this appendix an immiscible incompressible two-phase flow in porous media [30, 40, 86] in the form: find the phase saturations s_α and the phase pressures p_α, $\alpha \in \{\mathrm{n},\mathrm{w}\}$, such that

$$\partial_t(\phi s_\alpha) - \nabla\cdot\left(\frac{k_{\mathrm{r},\alpha}(s_{\mathrm{w}})}{\mu_\alpha}\boldsymbol{K}(\nabla p_\alpha + \rho_\alpha \boldsymbol{g})\right) = q_\alpha \qquad \alpha \in \{\mathrm{n},\mathrm{w}\}, \tag{C.1a}$$

$$s_{\mathrm{n}} + s_{\mathrm{w}} = 1, \tag{C.1b}$$

$$p_{\mathrm{n}} - p_{\mathrm{w}} = p_{\mathrm{c}}(s_{\mathrm{w}}). \tag{C.1c}$$

Here the porosity ϕ, the phase viscosities μ_α, the phase densities ρ_α, and the gravity field $\boldsymbol{g}$ are for simplicity constants, whereas the permeability tensor $\boldsymbol{K}$ and the phase sources q_α, $\alpha \in \{\mathrm{n},\mathrm{w}\}$, are piecewise constant with respect to both spatial and temporal meshes; moreover, $k_{\mathrm{r},\alpha}$, $\alpha \in \{\mathrm{n},\mathrm{w}\}$, and p_{c} are given nonlinear functions $\mathbb{R} \to \mathbb{R}$. Define the phase mobilities $\lambda_{\mathrm{r},\alpha}(s_{\mathrm{w}}) := k_{\mathrm{r},\alpha}(s_{\mathrm{w}})/\mu_\alpha$, $\alpha \in \{\mathrm{n},\mathrm{w}\}$. Keeping p_{w} and s_{w} as unknowns while expressing s_{n} as a function of s_{w} from (C.1b) and p_{n} as a function of p_{w} and s_{w} from (C.1c), we arrive at the following equivalent form of (C.1): find $(p_{\mathrm{w}}, s_{\mathrm{w}})$ such that

$$\partial_t(\phi s_{\mathrm{w}}) - \nabla\cdot\big(\lambda_{\mathrm{r,w}}(s_{\mathrm{w}})\boldsymbol{K}(\nabla p_{\mathrm{w}} + \rho_{\mathrm{w}}\boldsymbol{g})\big) = q_{\mathrm{w}}, \tag{C.2a}$$

$$-\partial_t(\phi s_{\mathrm{w}}) - \nabla\cdot\big(\lambda_{\mathrm{r,n}}(s_{\mathrm{w}})\boldsymbol{K}(\nabla(p_{\mathrm{w}} + p_{\mathrm{c}}(s_{\mathrm{w}})) + \rho_{\mathrm{n}}\boldsymbol{g})\big) = q_{\mathrm{n}}. \tag{C.2b}$$

C.2 Fully implicit discretizations

Consider a fully implicit cell-centered finite volume discretization of the immiscible incompressible two-phase flow (C.1). After a spatial and temporal discretization, problem (C.1), or, equivalently, (C.2), leads on each time step n to a system of *nonlinear algebraic equations* of the form, cf. [56] or [86, Section 4.1] and the references therein: find vectors S_{w}^n and P_{w}^n such that

$$\begin{pmatrix} \mathbb{SS}_{\mathrm{w}}^n & \mathbb{SP}_{\mathrm{w}}^n \\ \mathbb{SS}_{\mathrm{n}}^n & \mathbb{SP}_{\mathrm{n}}^n \end{pmatrix} \begin{pmatrix} S_{\mathrm{w}}^n \\ P_{\mathrm{w}}^n \end{pmatrix} = \begin{pmatrix} D_{\mathrm{w}}^n \\ D_{\mathrm{n}}^n \end{pmatrix}. \tag{C.3}$$

A system of *linear algebraic equations* is then obtained on each linearization step k: find vectors $S_{\mathrm{w}}^{n,k}$ and $P_{\mathrm{w}}^{n,k}$ such that

$$\begin{pmatrix} \mathbb{SS}_{\mathrm{w}}^{n,k-1} & \mathbb{SP}_{\mathrm{w}}^{n,k-1} \\ \mathbb{SS}_{\mathrm{n}}^{n,k-1} & \mathbb{SP}_{\mathrm{n}}^{n,k-1} \end{pmatrix} \begin{pmatrix} S_{\mathrm{w}}^{n,k} \\ P_{\mathrm{w}}^{n,k} \end{pmatrix} = \begin{pmatrix} D_{\mathrm{w}}^{n,k-1} \\ D_{\mathrm{n}}^{n,k-1} \end{pmatrix}. \tag{C.4}$$

The point is now that even though cell-centered finite volumes are a *locally conservative* method, local conservation is not present unless (C.3) or at least (C.4) are solved *exactly*. This is hardly achievable in practice, where instead inexact solutions are employed. On each step i of an arbitrary iterative linear solver applied to (C.4), one finally disposes of vectors $S_{\mathrm{w}}^{n,k,i}$ and $P_{\mathrm{w}}^{n,k,i}$ such that

$$\begin{pmatrix} \mathbb{SS}_{\mathrm{w}}^{n,k-1} & \mathbb{SP}_{\mathrm{w}}^{n,k-1} \\ \mathbb{SS}_{\mathrm{n}}^{n,k-1} & \mathbb{SP}_{\mathrm{n}}^{n,k-1} \end{pmatrix} \begin{pmatrix} S_{\mathrm{w}}^{n,k,i} \\ P_{\mathrm{w}}^{n,k,i} \end{pmatrix} = \begin{pmatrix} D_{\mathrm{w}}^{n,k-1} \\ D_{\mathrm{n}}^{n,k-1} \end{pmatrix} - \begin{pmatrix} R_{\mathrm{w}}^{n,k,i} \\ R_{\mathrm{n}}^{n,k,i} \end{pmatrix}, \tag{C.5}$$

where $R_{\mathrm{w}}^{n,k,i}$ and $R_{\mathrm{n}}^{n,k,i}$ are known algebraic residual vectors that can immediately be associated with piecewise constant functions $r_{h,\mathrm{w}}^{n,k,i}, r_{h,\mathrm{n}}^{n,k,i}$ in the present setting.

Applying Concept 4.1, with the lowest polynomial degree $p = 0$, one obtains Raviart–Thomas–Nédélec vector-valued fields $\boldsymbol{\sigma}_{h,\mathrm{alg,w}}^{n,k,i}$ and $\boldsymbol{\sigma}_{h,\mathrm{alg,n}}^{n,k,i}$ such that $\nabla{\cdot}\boldsymbol{\sigma}_{h,\mathrm{alg,w}}^{n,k,i} = r_{h,\mathrm{w}}^{n,k,i}$ and $\nabla{\cdot}\boldsymbol{\sigma}_{h,\mathrm{alg,n}}^{n,k,i} = r_{h,\mathrm{n}}^{n,k,i}$. In the present finite volume setting, we do not need to employ Concept 4.2 and merely combine $\boldsymbol{\sigma}_{h,\mathrm{alg,w}}^{n,k,i}, \boldsymbol{\sigma}_{h,\mathrm{alg,n}}^{n,k,i}$ with the finite volume fluxes directly available from (C.5) to obtain lowest-order Raviart–Thomas–Nédélec total phase fluxes $\boldsymbol{\sigma}_{h,\mathrm{tot,w}}^{n,k,i}$ and $\boldsymbol{\sigma}_{h,\mathrm{tot,n}}^{n,k,i}$ such that

$$\partial_t^n(\phi s_{\alpha,h\tau}^{n,k,i}) + \nabla{\cdot}\boldsymbol{\sigma}_{h,\mathrm{tot},\alpha}^{n,k,i} = q_\alpha^n \qquad \alpha \in \{\mathrm{n},\mathrm{w}\} \tag{C.6}$$

is satisfied pointwise; indeed the availability of $\boldsymbol{\sigma}_{h,\mathrm{alg,w}}^{n,k,i}$ and $\boldsymbol{\sigma}_{h,\mathrm{alg,n}}^{n,k,i}$ such that $\nabla{\cdot}\boldsymbol{\sigma}_{h,\mathrm{alg,w}}^{n,k,i} = r_{h,\mathrm{w}}^{n,k,i}$ and $\nabla{\cdot}\boldsymbol{\sigma}_{h,\mathrm{alg,n}}^{n,k,i} = r_{h,\mathrm{n}}^{n,k,i}$ is the only condition in [86], see equation (4.7) therein, to obtain (C.6), see [86, equation (4.8)]. This is a discrete version of (C.1a) on each temporal step n, each mesh $\mathcal{T}_h$, each linearization step k, and each algebraic solver step i, and it fully remedies on the local mass conservation issue of (C.5). Fig. 13 illustrates this for the example of [86, Section 6.1].

Remark C.1 (General meshes and reconstruction of the face fluxes only)**.** *We would like to stress that Concept 4.1 is not limited to simplicial meshes and can be in the same way used on meshes composed of rectangular parallelepipeds. If one is only interested in the finite volume face fluxes, then, instead of step 2c in Concept 4.1, the same finite volume solver as that used for the discretization (C.3) can be employed for the local problems. This only yields the face fluxes corresponding to the algebraic residual $\boldsymbol{H}(\mathrm{div},\Omega)$-liftings $\boldsymbol{\sigma}_{h,\mathrm{alg,w}}^{n,k,i}$ and $\boldsymbol{\sigma}_{h,\mathrm{alg,n}}^{n,k,i}$; consequently, one only obtains an integral balance in each cell instead of the pointwise expression (C.6). More generally, any locally conservative solver applicable to the given mesh (possibly composed of general polytopes, cf. the recent surveys in Droniou* et al. *[41], Beirão da Veiga* et al. *[17], Cangiani* et al. *[27], Cockburn* et al. *[32], and the references therein) can be used. Then, there is no need to have at disposal an implementation of the Raviart–Thomas–Nédélec spaces, nor one has to construct $\boldsymbol{H}(\mathrm{div},\Omega)$-conforming vector-valued piecewise polynomial fluxes.*

C.3 Iterative coupling/implicit pressure–explicit saturation discretizations

Another popular approach to numerical discretizations of (C.2) consists in keeping (C.2a) and replacing (C.2b) by the sum of (C.2a) and (C.2b), while using a fixed point (Picard) linearization around an available discrete saturation $s_{\mathrm{w},h}^{n,k-1}$. One then arrives at the "iterative coupling" or possibly "implicit pressure–explicit saturation" formulation of (C.1): find p_{w} such that

$$\begin{aligned} &-\nabla{\cdot}\big((\lambda_{\mathrm{r,w}}(s_{\mathrm{w},h}^{n,k-1}) + \lambda_{\mathrm{r,n}}(s_{\mathrm{w},h}^{n,k-1}))\boldsymbol{K}(\nabla p_{\mathrm{w}} + \rho_{\mathrm{w}}\boldsymbol{g})\big) \\ &\quad -\nabla{\cdot}\big(\lambda_{\mathrm{r,n}}(s_{\mathrm{w},h}^{n,k-1})\boldsymbol{K}(\nabla p_{\mathrm{c}}(s_{\mathrm{w},h}^{n,k-1}) + \rho_{\mathrm{n}}\boldsymbol{g} - \rho_{\mathrm{w}}\boldsymbol{g})\big) = q_{\mathrm{w}} + q_{\mathrm{n}}. \end{aligned} \tag{C.7}$$

This is a steady *linear elliptic* problem for the *single unknown* p_{w} on each time step n and iterative coupling step k, with a given symmetric and positive definite diffusion tensor $\boldsymbol{A}^{n,k-1}$ depending on $s_{\mathrm{w},h}^{n,k-1}$. In the context of the vertex-centered spatial discretization, cf. [86, Section 5.1], where $p = 1$, this gives rise to the system of linear algebraic equations (2.2) on each time step n and iterative coupling step k. Applying any iterative solver to (2.2), we have

$$\mathbb{P}_{\mathrm{wn}}^{n,k-1} P_{\mathrm{w}}^{n,k,i} = D_{\mathrm{wn}}^{n,k-1} - R_{\mathrm{wn}}^{n,k,i} \tag{C.8}$$

on each step i, and any local mass conservation is lost. Fortunately, applying Concepts 4.1 and 4.2 (or more generally their extensions of Remark C.1) again enables to restore full local mass balance on each step n, k, i, see Fig. 14.

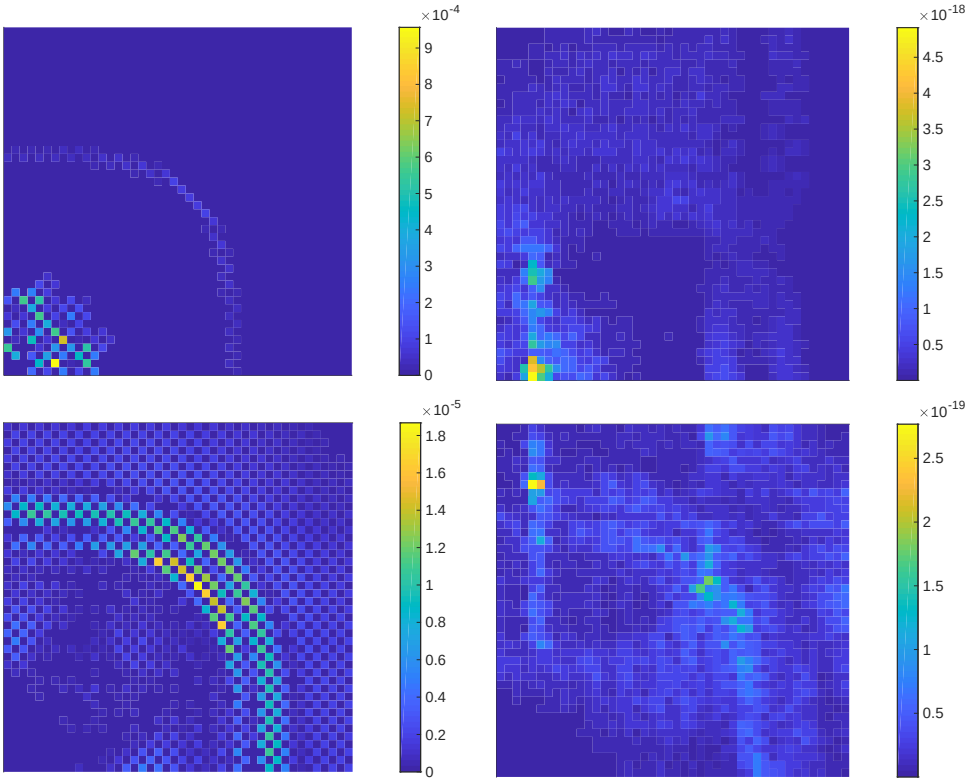

Figure 13: Recovering mass balance on each step (C.5) of a combined temporal/spatial/linearization/algebraic algorithm for numerical approximation of (C.1). Data and setting of [86, Section 6.1], 45×45 uniform mesh, time step 260 (time $2.6 \cdot 10^6$s), first Newton linearization, iteration 195 of GMRes solver with diagonal preconditioning, adaptive stopping criterion [86, (4.13a)] with $\gamma_{\text{alg}} = 0.001$. Original mass balance misfit in each computational cell in m^2s^{-1} (left), corrected mass balance misfit in m^2s^{-1} (right). Water phase (w, top), oil phase (n, bottom). Please note the difference in the scales.

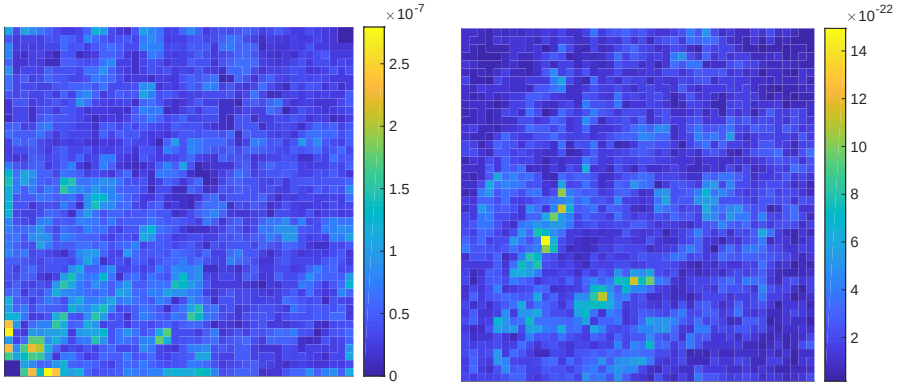

Figure 14: Recovering mass balance on each step (C.8) of a combined temporal/spatial/linearization/algebraic algorithm for numerical approximation of (C.1). Data and setting of [86, Section 6.2], 45×45 uniform mesh, time step 260 (time $2.6 \cdot 10^6$s), first iterative coupling linearization, iteration 171 of the conjugate gradient solver with diagonal preconditioning, adaptive stopping criterion [86, (4.13a)] with $\gamma_{\text{alg}} = 0.001$. Original mass balance misfit in each computational cell in m^2s^{-1} (left), corrected mass balance misfit in m^2s^{-1} (right). Please note the difference in the scales.

References

[1] Agouzal, A., Lipnikov, K., and Vassilevski, Y. Error estimates for a finite element solution of the diffusion equation based on composite norms. *J. Numer. Math.* **17** (2009), 77–95. https://doi.org/10.1515/JNUM.2009.006.

[2] Ahmed, E., Ali Hassan, S., Japhet, C., Kern, M., and Vohralík, M. A posteriori error estimates and stopping criteria for space-time domain decomposition for two-phase flow between different rock types. *SMAI J. Comput. Math.* **5** (2019), 195–227. https://doi.org/10.5802/smai-jcm.47.

[3] Ainsworth, M. A framework for obtaining guaranteed error bounds for finite element approximations. *J. Comput. Appl. Math.* **234** (2010), 2618–2632. http://dx.doi.org/10.1016/j.cam.2010.01.037.

[4] Ali Hassan, S., Japhet, C., Kern, M., and Vohralík, M. A posteriori stopping criteria for optimized Schwarz domain decomposition algorithms in mixed formulations. *Comput. Methods Appl. Math.* **18** (2018), 495–519. https://doi.org/10.1515/cmam-2018-0010.

[5] Alonso Rodríguez, A., and Valli, A. Finite element potentials. *Appl. Numer. Math.* **95** (2015), 2–14. https://doi.org/10.1016/j.apnum.2014.05.014.

[6] Arbogast, T., and Chen, Z. On the implementation of mixed methods as nonconforming methods for second-order elliptic problems. *Math. Comp.* **64** (1995), 943–972. https://doi.org/10.2307/2153478.

[7] Arioli, M., Georgoulis, E. H., and Loghin, D. Stopping criteria for adaptive finite element solvers. *SIAM J. Sci. Comput.* **35** (2013), A1537–A1559. http://dx.doi.org/10.1137/120867421.

[8] Arioli, M., Loghin, D., and Wathen, A. J. Stopping criteria for iterations in finite element methods. *Numer. Math.* **99** (2005), 381–410. http://dx.doi.org/10.1007/s00211-004-0568-z.

[9] Arnold, D. N., and Brezzi, F. Mixed and nonconforming finite element methods: implementation, postprocessing and error estimates. *RAIRO Modél. Math. Anal. Numér.* **19** (1985), 7–32. https://doi.org/10.1051/m2an/1985190100071.

[10] Babuška, I., and Strouboulis, T. *The finite element method and its reliability*. Numerical Mathematics and Scientific Computation. The Clarendon Press Oxford University Press, New York, 2001.

[11] Bai, D., and Brandt, A. Local mesh refinement multilevel techniques. *SIAM J. Sci. Statist. Comput.* **8** (1987), 109–134. http://dx.doi.org/10.1137/0908025.

[12] Bank, R. E., and Sherman, A. H. An adaptive, multilevel method for elliptic boundary value problems. *Computing* **26** (1981), 91–105. http://dx.doi.org/10.1007/BF02241777.

[13] Bank, R. E., and Smith, R. K. A posteriori error estimates based on hierarchical bases. *SIAM J. Numer. Anal.* **30** (1993), 921–935. http://dx.doi.org/10.1137/0730048.

[14] Bebendorf, M. A note on the Poincaré inequality for convex domains. *Z. Anal. Anwendungen* **22** (2003), 751–756. http://dx.doi.org/10.4171/ZAA/1170.

[15] Becker, R., Johnson, C., and Rannacher, R. Adaptive error control for multigrid finite element methods. *Computing* **55** (1995), 271–288. http://dx.doi.org/10.1007/BF02238483.

[16] Becker, R., and Mao, S. Convergence and quasi-optimal complexity of a simple adaptive finite element method. *M2AN Math. Model. Numer. Anal.* **43** (2009), 1203–1219. http://dx.doi.org/10.1051/m2an/2009036.

[17] Beirão da Veiga, L., Brezzi, F., Marini, L. D., and Russo, A. Mixed virtual element methods for general second order elliptic problems on polygonal meshes. *ESAIM Math. Model. Numer. Anal.* **50** (2016), 727–747. http://dx.doi.org/10.1051/m2an/2015067.

[18] Braess, D., Pillwein, V., and Schöberl, J. Equilibrated residual error estimates are p-robust. *Comput. Methods Appl. Mech. Engrg.* **198** (2009), 1189–1197. http://dx.doi.org/10.1016/j.cma.2008.12.010.

[19] Braess, D., and Schöberl, J. Equilibrated residual error estimator for edge elements. *Math. Comp.* **77** (2008), 651–672. http://dx.doi.org/10.1090/S0025-5718-07-02080-7.

[20] Bramble, J. H. *Multigrid methods*, vol. **294** of *Pitman Research Notes in Mathematics Series*. Longman Scientific & Technical, Harlow; copublished in the United States with John Wiley & Sons, Inc., New York, 1993.

[21] Brandt, A. Multi-level adaptive solutions to boundary-value problems. *Math. Comp.* **31** (1977), 333–390.

[22] Brandt, A., and Livne, O. E. Revised edition of the 1984 original [MR0772748]. *Multigrid techniques—1984 guide with applications to fluid dynamics*, vol. **67** of *Classics in Applied Mathematics*. Society for Industrial and Applied Mathematics (SIAM), Philadelphia, PA, 2011. https://doi.org/10.1137/1.9781611970753.

[23] Brenner, S. C. Poincaré-Friedrichs inequalities for piecewise H^1 functions. *SIAM J. Numer. Anal.* **41** (2003), 306–324. https://doi.org/10.1137/S0036142902401311.

[24] Brezzi, F., and Fortin, M. *Mixed and hybrid finite element methods*, vol. **15** of *Springer Series in Computational Mathematics*. Springer-Verlag, New York, 1991. http://dx.doi.org/10.1007/978-1-4612-3172-1.

[25] Cancès, C., Pop, I. S., and Vohralík, M. An a posteriori error estimate for vertex-centered finite volume discretizations of immiscible incompressible two-phase flow. *Math. Comp.* **83** (2014), 153–188. http://dx.doi.org/10.1090/S0025-5718-2013-02723-8.

[26] Cancès, E., Dusson, G., Maday, Y., Stamm, B., and Vohralík, M. Guaranteed and robust a posteriori bounds for Laplace eigenvalues and eigenvectors: conforming approximations. *SIAM J. Numer. Anal.* **55** (2017), 2228–2254. http://dx.doi.org/10.1137/15M1038633.

[27] Cangiani, A., Georgoulis, E. H., and Houston, P. *hp*-version discontinuous Galerkin methods on polygonal and polyhedral meshes. *Math. Models Methods Appl. Sci.* **24** (2014), 2009–2041. http://dx.doi.org/10.1142/S0218202514500146.

[28] Carstensen, C., and Funken, S. A. Fully reliable localized error control in the FEM. *SIAM J. Sci. Comput.* **21** (1999/00), 1465–1484. http://dx.doi.org/10.1137/S1064827597327486.

[29] Chen, L., Nochetto, R. H., and Xu, J. Optimal multilevel methods for graded bisection grids. *Numer. Math.* **120** (2012), 1–34. http://dx.doi.org/10.1007/s00211-011-0401-4.

[30] Chen, Z. Pure and Applied Mathematics, Vol. 65. *Multiphase flows in porous media*. Academic Press [A subsidiary of Harcourt Brace Jovanovich, Publishers], New York-London, 1995.

[31] Chippada, S., Dawson, C. N., Martínez, M. L., and Wheeler, M. F. A projection method for constructing a mass conservative velocity field. *Comput. Methods Appl. Mech. Engrg.* **157** (1998), 1–10. https://doi.org/10.1016/S0045-7825(98)80001-7.

[32] Cockburn, B., Di Pietro, D. A., and Ern, A. Bridging the hybrid high-order and hybridizable discontinuous Galerkin methods. *ESAIM Math. Model. Numer. Anal.* **50** (2016), 635–650. http://dx.doi.org/10.1051/m2an/2015051.

[33] Cockburn, B., Gopalakrishnan, J., and Wang, H. Locally conservative fluxes for the continuous Galerkin method. *SIAM J. Numer. Anal.* **45** (2007), 1742–1776. https://doi.org/10.1137/060666305.

[34] Dabaghi, J., Martin, V., and Vohralík, M. Adaptive inexact semismooth Newton methods for the contact problem between two membranes. *J. Sci. Comput.* **84** (2020), 28. https://doi.org/10.1007/s10915-020-01264-3.

[35] Dabaghi, J., Martin, V., and Vohralík, M. A posteriori estimates distinguishing the error components and adaptive stopping criteria for numerical approximations of parabolic variational inequalities. *Comput. Methods Appl. Mech. Engrg.* **367** (2020), 113105. https://doi.org/10.1016/j.cma.2020.113105.

[36] Daniel, P., Ern, A., and Vohralík, M. An adaptive *hp*-refinement strategy with inexact solvers and computable guaranteed bound on the error reduction factor. *Comput. Methods Appl. Mech. Engrg.* **359** (2020), 112607. https://doi.org/10.1016/j.cma.2019.112607.

[37] Dawson, C., Sun, S., and Wheeler, M. F. Compatible algorithms for coupled flow and transport. *Comput. Methods Appl. Mech. Engrg.* **193** (2004), 2565–2580. https://doi.org/10.1016/j.cma.2003.12.059.

[38] Destuynder, P., and Métivet, B. Explicit error bounds in a conforming finite element method. *Math. Comp.* **68** (1999), 1379–1396. http://dx.doi.org/10.1090/S0025-5718-99-01093-5.

[39] Di Pietro, D. A., Flauraud, E., Vohralík, M., and Yousef, S. A posteriori error estimates, stopping criteria, and adaptivity for multiphase compositional Darcy flows in porous media. *J. Comput. Phys.* **276** (2014), 163–187. http://dx.doi.org/10.1016/j.jcp.2014.06.061.

[40] Douglas, Jr., J., Ewing, R. E., and Wheeler, M. F. The approximation of the pressure by a mixed method in the simulation of miscible displacement. *RAIRO Anal. Numér.* **17** (1983), 17–33.

[41] Droniou, J., Eymard, R., and Herbin, R. Gradient schemes: generic tools for the numerical analysis of diffusion equations. *ESAIM Math. Model. Numer. Anal.* **50** (2016), 749–781. http://dx.doi.org/10.1051/m2an/2015079.

[42] Ern, A., Smears, I., and Vohralík, M. Discrete p-robust $\boldsymbol{H}(\mathrm{div})$-liftings and a posteriori estimates for elliptic problems with H^{-1} source terms. *Calcolo* **54** (2017), 1009–1025. https://doi.org/10.1007/s10092-017-0217-4.

[43] Ern, A., and Vohralík, M. Adaptive inexact Newton methods with a posteriori stopping criteria for nonlinear diffusion PDEs. *SIAM J. Sci. Comput.* **35** (2013), A1761–A1791. http://dx.doi.org/10.1137/120896918.

[44] Ern, A., and Vohralík, M. Polynomial-degree-robust a posteriori estimates in a unified setting for conforming, nonconforming, discontinuous Galerkin, and mixed discretizations. *SIAM J. Numer. Anal.* **53** (2015), 1058–1081. http://dx.doi.org/10.1137/130950100.

[45] Ern, A., and Vohralík, M. Stable broken H^1 and $\boldsymbol{H}(\mathrm{div})$ polynomial extensions for polynomial-degree-robust potential and flux reconstruction in three space dimensions. *Math. Comp.* **89** (2020), 551–594. http://dx.doi.org/10.1090/mcom/3482.

[46] Ewing, R. E., and Wang, J. Analysis of multilevel decomposition iterative methods for mixed finite element methods. *RAIRO Modél. Math. Anal. Numér.* **28** (1994), 377–398. https://doi.org/10.1051/m2an/1994280403771.

[47] Falgout, R. D., and Jones, J. E. Multigrid on massively parallel architectures. In *Multigrid methods, VI (Gent, 1999)*, vol. **14** of *Lect. Notes Comput. Sci. Eng.* Springer, Berlin, 2000, pp. 101–107. http://dx.doi.org/10.1007/978-3-642-58312-4_13.

[48] Gmeiner, B., Rüde, U., Stengel, H., Waluga, C., and Wohlmuth, B. Performance and scalability of hierarchical hybrid multigrid solvers for Stokes systems. *SIAM J. Sci. Comput.* **37** (2015), C143–C168. http://dx.doi.org/10.1137/130941353.

[49] Griebel, M., and Oswald, P. On the abstract theory of additive and multiplicative Schwarz algorithms. *Numer. Math.* **70** (1995), 163–180. http://dx.doi.org/10.1007/s002110050115.

[50] Hackbusch, W. *Multigrid methods and applications*, vol. **4** of *Springer Series in Computational Mathematics*. Springer-Verlag, Berlin, 1985.

[51] Hiptmair, R., Wu, H., and Zheng, W. Uniform convergence of adaptive multigrid methods for elliptic problems and Maxwell's equations. *Numer. Math. Theory Methods Appl.* **5** (2012), 297–332. http://dx.doi.org/10.4208/nmtma.2012.m1128.

[52] Janssen, B., and Kanschat, G. Adaptive multilevel methods with local smoothing for H^1- and H^{curl}-conforming high order finite element methods. *SIAM J. Sci. Comput.* **33** (2011), 2095–2114. http://dx.doi.org/10.1137/090778523.

[53] Jiránek, P., Strakoš, Z., and Vohralík, M. A posteriori error estimates including algebraic error and stopping criteria for iterative solvers. *SIAM J. Sci. Comput.* **32** (2010), 1567–1590. http://dx.doi.org/10.1137/08073706X.

[54] Keilegavlen, E., and Nordbotten, J. M. Inexact linear solvers for control volume discretizations in porous media. *Comput. Geosci.* **19** (2015), 159–176. https://doi.org/10.1007/s10596-014-9453-8.

[55] Kopteva, N. Fully computable a posteriori error estimator using anisotropic flux equilibration on anisotropic meshes. ArXiv Preprint 1704.04404, https://arxiv.org/abs/1704.04404, 2017.

[56] Lacroix, S., Vassilevski, Y., Wheeler, J., and Wheeler, M. Iterative solution methods for modeling multiphase flow in porous media fully implicitly. *SIAM J. Sci. Comput.* **25** (2003), 905–926. http://dx.doi.org/10.1137/S106482750240443X.

[57] Liesen, J., and Strakoš, Z. *Krylov Subspace Methods. Principles and Analysis.* Numerical Mathematics and Scientific Computation. Oxford University Press, Oxford, United Kingdom, 2013.

[58] Loisel, S., Nabben, R., and Szyld, D. B. On hybrid multigrid-Schwarz algorithms. *J. Sci. Comput.* **36** (2008), 165–175. https://doi.org/10.1007/s10915-007-9183-3.

[59] Luce, R., and Wohlmuth, B. I. A local a posteriori error estimator based on equilibrated fluxes. *SIAM J. Numer. Anal.* **42** (2004), 1394–1414. http://dx.doi.org/10.1137/S0036142903433790.

[60] Mallik, G., Vohralík, M., and Yousef, S. Goal-oriented a posteriori error estimation for conforming and nonconforming approximations with inexact solvers. *J. Comput. Appl. Math.* **366** (2020), 112367. https://doi.org/10.1016/j.cam.2019.112367.

[61] Meidner, D., Rannacher, R., and Vihharev, J. Goal-oriented error control of the iterative solution of finite element equations. *J. Numer. Math.* **17** (2009), 143–172. http://dx.doi.org/10.1515/JNUM.2009.009.

[62] Miraçi, A., Papež, J., and Vohralík, M. A multilevel algebraic error estimator and the corresponding iterative solver with p-robust behavior. *SIAM J. Numer. Anal.* (2020). DOI 10.1137/19M1275929, http://dx.doi.org/10.1137/19M1275929.

[63] Nicaise, S., Witowski, K., and Wohlmuth, B. I. An a posteriori error estimator for the Lamé equation based on equilibrated fluxes. *IMA J. Numer. Anal.* **28** (2008), 331–353. http://dx.doi.org/10.1093/imanum/drm008.

[64] Notay, Y., and Napov, A. A massively parallel solver for discrete Poisson-like problems. *J. Comput. Phys.* **281** (2015), 237–250. http://dx.doi.org/10.1016/j.jcp.2014.10.043.

[65] Olshanskii, M. A., and Tyrtyshnikov, E. E. Theory and applications. *Iterative methods for linear systems.* Society for Industrial and Applied Mathematics, Philadelphia, PA, 2014. http://dx.doi.org/10.1137/1.9781611973464.

[66] Oswald, P. Theory and applications. *Multilevel finite element approximation.* Teubner Skripten zur Numerik. [Teubner Scripts on Numerical Mathematics]. B. G. Teubner, Stuttgart, 1994. http://dx.doi.org/10.1007/978-3-322-91215-2.

[67] Oswald, P. Stable subspace splittings for Sobolev spaces and domain decomposition algorithms. In *Domain decomposition methods in scientific and engineering computing (University Park, PA, 1993)*, vol. **180** of *Contemp. Math.* Amer. Math. Soc., Providence, RI, 1994, pp. 87–98. http://dx.doi.org/10.1090/conm/180/01959.

[68] Papež, J., Liesen, J., and Strakoš, Z. Distribution of the discretization and algebraic error in numerical solution of partial differential equations. *Linear Algebra Appl.* **449** (2014), 89–114. http://dx.doi.org/10.1016/j.laa.2014.02.009.

[69] Papež, J., Strakoš, Z., and Vohralík, M. Estimating and localizing the algebraic and total numerical errors using flux reconstructions. *Numer. Math.* **138** (2018), 681–721. https://doi.org/10.1007/s00211-017-0915-5.

[70] Papež, J., and Vohralík, M. Inexpensive guaranteed and efficient upper bounds on the algebraic error in finite element discretizations. HAL Preprint 02422851, submitted for publication, https://hal.inria.fr/hal-02422851, 2020.

[71] Pasquetti, R., and Rapetti, F. Spectral element methods on simplicial meshes. In *Spectral and high order methods for partial differential equations—ICOSAHOM 2012*, vol. **95** of *Lect. Notes Comput. Sci. Eng.* Springer, Cham, 2014, pp. 37–55. http://dx.doi.org/10.1007/978-3-319-01601-6_3.

[72] Payne, L. E., and Weinberger, H. F. An optimal Poincaré inequality for convex domains. *Arch. Rational Mech. Anal.* **5** (1960), 286–292.

[73] Prager, W., and Synge, J. L. Approximations in elasticity based on the concept of function space. *Quart. Appl. Math.* **5** (1947), 241–269.

[74] Repin, S. *A posteriori estimates for partial differential equations*, vol. **4** of *Radon Series on Computational and Applied Mathematics*. Walter de Gruyter GmbH & Co. KG, Berlin, 2008. http://dx.doi.org/10.1515/9783110203042.

[75] Rüde, U. Fully adaptive multigrid methods. *SIAM J. Numer. Anal.* **30** (1993), 230–248.

[76] Rüde, U. *Mathematical and computational techniques for multilevel adaptive methods*, vol. **13** of *Frontiers in Applied Mathematics*. Society for Industrial and Applied Mathematics (SIAM), Philadelphia, PA, 1993. http://dx.doi.org/10.1137/1.9781611970968.

[77] Rüde, U. Error estimates based on stable splittings. In *Domain decomposition methods in scientific and engineering computing (University Park, PA, 1993)*, vol. **180** of *Contemp. Math.* Amer. Math. Soc., Providence, RI, 1994, pp. 111–118.

[78] Saad, Y. *Iterative methods for sparse linear systems*, second ed. Society for Industrial and Applied Mathematics, Philadelphia, PA, 2003.

[79] Schöberl, J., Melenk, J. M., Pechstein, C., and Zaglmayr, S. Additive Schwarz preconditioning for p-version triangular and tetrahedral finite elements. *IMA J. Numer. Anal.* **28** (2008), 1–24. http://dx.doi.org/10.1093/imanum/drl046.

[80] Sun, S., and Wheeler, M. F. Projections of velocity data for the compatibility with transport. *Comput. Methods Appl. Mech. Engrg.* **195** (2006), 653–673. https://doi.org/10.1016/j.cma.2005.02.011.

[81] Sundar, H., Stadler, G., and Biros, G. Comparison of multigrid algorithms for high-order continuous finite element discretizations. *Numer. Linear Algebra Appl.* **22** (2015), 664–680. http://dx.doi.org/10.1002/nla.1979.

[82] Vassilevski, P. S. Matrix-based analysis and algorithms for solving finite element equations. *Multilevel block factorization preconditioners*. Springer, New York, 2008.

[83] Vohralík, M. On the discrete Poincaré–Friedrichs inequalities for nonconforming approximations of the Sobolev space H^1. *Numer. Funct. Anal. Optim.* **26** (2005), 925–952. http://dx.doi.org/10.1080/01630560500444533.

[84] Vohralík, M. Unified primal formulation-based a priori and a posteriori error analysis of mixed finite element methods. *Math. Comp.* **79** (2010), 2001–2032. http://dx.doi.org/10.1090/S0025-5718-2010-02375-0.

[85] Vohralík, M. Guaranteed and fully robust a posteriori error estimates for conforming discretizations of diffusion problems with discontinuous coefficients. *J. Sci. Comput.* **46** (2011), 397–438. http://dx.doi.org/10.1007/s10915-010-9410-1.

[86] Vohralík, M., and Wheeler, M. F. A posteriori error estimates, stopping criteria, and adaptivity for two-phase flows. *Comput. Geosci.* **17** (2013), 789–812. http://dx.doi.org/10.1007/s10596-013-9356-0.

[87] Vohralík, M., and Yousef, S. A simple a posteriori estimate on general polytopal meshes with applications to complex porous media flows. *Comput. Methods Appl. Mech. Engrg.* **331** (2018), 728–760. https://doi.org/10.1016/j.cma.2017.11.027.

[88] Wu, H., and Chen, Z. Uniform convergence of multigrid V-cycle on adaptively refined finite element meshes for second order elliptic problems. *Sci. China Ser. A* **49** (2006), 1405–1429. http://dx.doi.org/10.1007/s11425-006-2005-5.

[89] Xu, J., Chen, L., and Nochetto, R. H. Optimal multilevel methods for $H(\mathrm{grad})$, $H(\mathrm{curl})$, and $H(\mathrm{div})$ systems on graded and unstructured grids. In *Multiscale, nonlinear and adaptive approximation*. Springer, Berlin, 2009, pp. 599–659. http://dx.doi.org/10.1007/978-3-642-03413-8_14.

[90] Yang, U. M. Parallel algebraic multigrid methods—high performance preconditioners. In *Numerical solution of partial differential equations on parallel computers*, vol. **51** of *Lect. Notes Comput. Sci. Eng.* Springer, Berlin, 2006, pp. 209–236. http://dx.doi.org/10.1007/3-540-31619-1_6.